



universität
wien

DISSERTATION / DOCTORAL THESIS

Titel der Dissertation /Title of the Doctoral Thesis

„Macroporous high performance polymers“

verfasst von / submitted by

Dmitrii Rusakov

angestrebter akademischer Grad / in partial fulfilment of the requirements for the degree of

Doktor der Naturwissenschaften (Dr. rer. nat.)

Wien, 2022 / Vienna 2022

Studienkennzahl lt. Studienblatt /
degree programme code as it appears on the student
record sheet:

UA 796 605 419

Dissertationsgebiet lt. Studienblatt /
field of study as it appears on the student record sheet:

Chemie

Betreut von / Supervisor:

Univ.-Prof. Dr. Dipl.-Chem. Alexander Bismarck

ABSTRACT

Among common engineering materials, polymers are the most used because of their low densities in comparison with traditional materials, low production costs and good mechanical properties. Porous high performance polymers are materials that combine excellent mechanical properties, outstanding chemical stability with light-weight and high surface area. Moreover, the main disadvantage of high performance polymers – their cost, can be reduced by introducing porosity, while retaining good mechanical and chemical stability. My PhD thesis aimed to develop, test and optimise a universal method for the production of bulk porous high performance polymers with tailored properties. A modified thermally induced phase separation (TIPS) was developed and tested on semi-crystalline (polyetheretherketone and polyetherketoneketone) and amorphous (polyetherimide) polymers. The process parameters, such as solvent choice, polymer concentration and heating/cooling profile were studied and their influence on the morphological, physical and mechanical properties of the resulting porous polymers, such as porosity, foam density, pore structure, specific surface area, mechanical properties in compression and degree of crystallinity, were investigated. It was found that among the investigated high boiling solvents, 4-phenylphenol was most suitable for polyetheretherketone and 9-fluorenone for polyetherketoneketone. Two types of solid-liquid demixing occurred during the TIPS process. The type of solid-liquid demixing depended on the solvent melting point and polymer concentration. The resulting porous polymers possessed a high pore anisotropy when solvent solidification occurred prior to polymer gelation during demixing. However, when solvent solidification occurred after polymer gelation, the resulting pore morphology was homogeneous and isotropic. Adjusting the polymer concentration in the selected process solvent allows for control of the foam porosity, density and the mechanical properties of the resulting porous polymer; an increased polymer concentration resulted in higher foam densities and mechanical properties. The process cooling rate did not have a significant influence on the properties of the produced porous polymers, with the exception of rapid cooling rate (10 °C/min) which caused the formation of cracks within the porous polymers due to thermal residual stresses. The crystallinity of the porous semi-crystalline polymers produced by solution processing was higher than that typically obtained when crystallised from the melt. The produced porous polyetheretherketone and polyetherketoneketone possessed comparable porosities and foam densities as materials described in the literature but significantly higher mechanical properties.

ZUSAMMENFASSUNG

Im Vergleich zu anderen technischen Materialien werden Polymere vor allem wegen ihrer geringen Dichte, niedrigen Produktionskosten und guten mechanischen Eigenschaften verwendet. Poröse Hochleistungspolymere sind Materialien, die hervorragende mechanische Eigenschaften und chemische Stabilität mit geringem Gewicht und großer Oberfläche vereinen. Darüber hinaus kann der Hauptnachteil von Hochleistungspolymeren – ihre Kosten – durch das Erzeugen von Porosität reduziert werden, während gute mechanische und chemische Stabilität erhalten bleibt. Ziel dieser Arbeit war es, ein universelles Verfahren zur Herstellung von porösen Hochleistungspolymeren mit maßgeschneiderten Eigenschaften zu entwickeln, zu testen und zu optimieren. Dazu wurde eine modifizierte thermisch induzierte Phasentrennung entwickelt und an teilkristallinen (Polyetheretherketon und Polyetherketonketon) und amorphen (Polyetherimid) Polymeren getestet. Prozessparameter wie die Wahl des Lösungsmittels, Polymerkonzentration sowie Heiz- und Kühlprofil wurden variiert und in weiterer Folge ihr Einfluss auf die Porosität, Porenstruktur, Schaumdichte, spezifische Oberfläche, Kristallisationsgrad und mechanischen Eigenschaften der porösen Polymere untersucht. Es wurde festgestellt, dass unter den verwendeten hochsiedenden Lösungsmitteln 4-Phenylphenol am besten für Polyetheretherketon und 9-Fluorenon für Polyetherketonketon geeignet ist. Während des TIPS-Prozesses traten zwei Arten von fest-flüssig-Entmischung auf. Die Art der Entmischung hing vor allem vom Schmelzpunkt des Lösungsmittels und der Polymerkonzentration ab. Trat während des Entmischens die Lösungsmittelverfestigung vor der Polymergelierung auf, besaßen die daraus resultierenden porösen Polymere eine hohe Poreanisotropie. Wenn die Lösungsmittelverfestigung hingegen nach der Polymergelierung auftrat, besaßen die daraus resultierenden porösen Polymere eine homogene und isotrope Poremorphologie. Das Einstellen der Polymerkonzentration in dem ausgewählten Prozesslösungsmittel ermöglicht die Steuerung der Porosität, Dichte und der mechanischen Eigenschaften der porösen Polymere. Eine erhöhte Polymerkonzentration führte zu höheren Schaumdichten und besseren mechanischen Eigenschaften. Die Prozessabkühlgeschwindigkeit hatte keinen wesentlichen Einfluss auf die Eigenschaften der erzeugten porösen Polymere. Eine Ausnahme stellte nur die höchste Abkühlgeschwindigkeit von 10 °C/min, da es aufgrund thermischer Restspannungen zur Rissbildung innerhalb der porösen Polymere führte. Die Kristallinität der aus Lösung hergestellten porösen teilkristallinen Polymere war höher als jene, die aus der Schmelze kristallisiert wurden. Die hergestellten porösen Polymere besaßen vergleichbare Porositäten und Schaumdichten wie bereits beschriebene Materialien, zeichneten sich aber durch deutlich bessere mechanische Eigenschaften aus.

Acknowledgement

I would like to express my heartfelt gratitude to Prof. Alexander Bismarck for allowing me to finish my PhD with him and for leading me through scientific difficulties. He has been a supervisor who always found solutions to troubles and encouraged me.

I would also want to express my sincere thanks to Dr. Angelika Menner for her scientific and organisational advice. She helped me a lot to understand the way of scientific writing. I would also like to thank Dr. Florian Spieckermann, Dr. Harald Wilhelm and Innozenz Steffny for their contributions to my research and the Austrian Science Fund (FWF) for the financial support.

I would like to thank Dr. Andreas Mautner and Dr. Qixiang Jiang for being willing to discuss scientific challenges, giving advice and guiding me. I would especially like to thank Dr. Marta Fortea Verdejo, Mag. Kathrin Weiland, Dr. Mitchell Jones, and all other members of our research group for all their support, encouraging and making me feel at home. I am grateful for the help of all BSc, MSc and exchange students (Alice Charton, Manon Goubet, Daniel Langerreiter, Lisa Panzenböck, Anto Pulko, Julie Seidelmannová, Seo Hee Son and Hanna Trzesniowski) for their contribution to my thesis and their support while working with me.

Furthermore, I would also like to acknowledge to Assoc.Prof. Falk Liebner, Prof. Antje Potthast and Prof. Thomas Rosenau for giving me the possibility to work in another amazing scientific group. I would like to express my gratitude to Dr. Irina Sulaeva, Mag. Nadine Kohlhuber, Dr. Ivan Sumerskii, Dr. Grigory Zinovyev and all other members of NAWARO group for their warm welcome, support and the will to help me in a new scientific field. I would especially like to thank Christiane Gollner, who was always ready to help with administrative issues.

Most importantly, I would like to express my sincere appreciation to my parents, who always believed in me and gave me invaluable support. Without their love and belief in me, I would never be able to finish my PhD. I would also like to deeply thank my old and new friends, and especially Liza F. for encouraging and supporting me.

List of Scientific Publications

Publication 1: Rusakov, D., Menner, A., Bismarck, A., High-Performance Polymer Foams by Thermally Induced Phase Separation, *Macromolecular Rapid Communications* **41** (2020), 2000110. DOI: 10.1002/marc.202000110

D.R. experimental design, visualisation, data collection and analysis, drafting the manuscript: A.M. conceptualisation, supervision, revision of draft, funding acquisition: A.B. conceptualisation, methodology, supervision, manuscript draft revision, editing and proofing, funding acquisition.

Publication 2: Rusakov, D., Menner, A., Spieckermann, F., Wilhelm, H., Bismarck, A., Morphology and properties of foamed high crystallinity PEEK prepared by high temperature thermally induced phase separation, *Journal of Applied Polymer Science* **139** (2021), 51423. DOI: 10.1002/app.51423

D.R. experimental design, visualisation, data collection and analysis, drafting the manuscript: A.M. conceptualisation, supervision, revision of draft, funding acquisition: F.S. data collection and analysis, revision of draft: H.W. data analysis, revision of draft: A.B. conceptualisation, methodology, supervision, manuscript draft revision, editing and proofing, funding acquisition.

Publication 3: Rusakov, D., Steffny, I., Spieckermann, F., Menner, A., Bismarck, A., High porosity poly (ether ketone ketone): Influence of solvents on foam properties, submitted 2022.

D.R. experimental design, visualisation, data collection and analysis, drafting the manuscript: I.S. data collection and analysis, revision of draft: F.S. data analysis, revision of draft: A.M. conceptualisation, supervision, revision of draft, funding acquisition: A.B. conceptualisation, methodology, supervision, manuscript draft revision, editing and proofing, funding acquisition.

Oral presentations and papers at conferences:

Rusakov, D., Menner, A., Bismarck, A., High Porosity Macroporous Polyetheretherketone. 1st International conference of Advanced Polymer Materials and Nanocomposites (ANM2017). Aveiro, 2017.

Rusakov, D., Menner, A., Bismarck, A., High porosity Polyetherketoneketone. Danube Vltava Sava Polymer Meeting (DVSPM), Vienna, 2017.

Menner, A., Rusakov, D., Bismarck, A., High performance polymer foams: How to push lots of air into PEEK, PEKK and TPI. 256th National Meeting and Exposition of the American-Chemical-Society (ACS) - Nanoscience, Nanotechnology and Beyond. Boston, 2018.

Menner, A., Rusakov, D., Bismarck, A., Pushing lot`s of air into PEEK and PEKK. 18th European Conference on Composite Materials (ECCM18). Athens, 2018.

Rusakov, D., Menner, A., Bismarck, A., Foaming what can`t be foamed: macroporous Polyimides. 18th European Conference on Composite Materials (ECCM18). Athens, 2018.

Abstracts.....	I
Zusammenfassung.....	II
Acknowledgement.....	III
List of Scientific Publications.....	IV
Table of Contents.....	V
List of Abbreviations and Symbols.....	VI
List of Figures.....	VII
List of Tables.....	XI
Chapter 1. Introduction.....	1
1.1. Scope of the thesis.....	4
1.2. Structure of the thesis.....	4
Chapter 2. Background.....	5
2.1. Introduction to porous polymers, also called polymer foams.....	5
2.2. High Performance Polymers: A brief Introduction.....	13
2.3. Polyetherimide: Synthesis, Properties and Applications.....	15
2.4. Polyetheretherketone: Synthesis, Properties and Applications.....	18
2.5. Polyetherketoneketone: Synthesis, Properties and Applications.....	23
2.6. Thermally Induced Phase Separation.....	25
Chapter 3. Experimental.....	30
3.1. Materials and methods.....	30
3.2. Characterisation of (porous) high performance polymers.....	30
3.2.1. Density (absolute and foam) and porosity.....	30
3.2.2. Pore morphology.....	31
3.2.3. Mechanical (compression) properties.....	33
3.2.4. Thermal properties and degree of crystallinity.....	33
Chapter 4. Results and discussion.....	35
4.1. High-Temperature Thermally Induced Phase Separation.....	35
4.1.1. Experimental Setup.....	35
4.1.2. Preparation of porous high performance polymer.....	36
4.1.3. Solid-liquid demixing during the HT-TIPS process.....	37
4.2. Solvent selection for production of porous PEI, PEEK and PEKK.....	38
4.3. Influence of polymer concentration on properties of porous PEEK and PEKK.....	44
4.3.1. Properties of porous PEEK.....	44
4.3.2. Properties of porous PEKK.....	46
4.4. Influence of cooling rate on morphology of porous PEEK and PEKK.....	48
4.5. Influence of cooling rate on degree of crystallinity of porous PEEK and PEKK.....	50
Chapter 5. Overall Conclusions.....	51
5.1. Conclusion.....	51
5.2. Outlook for future work.....	52
References.....	54
Publication 1.....	63
Publication 2.....	74
Publication 3.....	94

List of Abbreviations and Symbols:

2D – Two-dimensional, flat film or surface

3D – Three-dimensional

4PPH – 4-Phenylphenol

9FN – 9-Fluorenone

BET – Brunauer–Emmett–Teller theory

BJH – Barrett-Joyner-Halenda theory

DPK – Diphenyl ketone

DPS – Diphenyl sulfone

DSC – Differential scanning calorimetry

E – Young`s modulus

HDT – Heat deflection temperature or heat distortion temperature

HPP(s) – High performance polymer(s)

HT-TIPS – High temperature thermally induced phase separation

ISO – International Organization for Standardization

LOI – Limiting oxygen index

T_b – Boiling temperature

T_g – Glass transition temperature

T_m – Melting temperature

TIPS – Thermally induced phase separation

PEEK – Polyetheretherketone

PEI – Polyethylenimine

PEKK – Polyetherketoneketone

PAEK(s) – Polyaryletherketone(s)

SEM – Scanning electron microscopy

σ – Tensile or compression strength

χ – Degree of crystallinity

List of Figures:

Fig. 1: Polymeric materials pyramid as a function of continuous operation temperature, Figure adapted from thyssenkrupp Engineered Plastics, High Performance Plastics (Link in: https://www.onlineplastics.com/products/high-performance-plastics-c-1_192.html#1-YToxOntzOjQ6lmdyaWQiO2k6MDt9 accessed on: 14.11.21).

Fig. 2: Typical Ashby chart showing the Young's modulus as a function of density for various materials classes allowing for the comparison of metals, ceramics, composites, natural materials, polymers and elastomers, as well as foams. This chart highlights the fact that acceptable Young's moduli, as a measure of the mechanical stiffness, can be maintained upon introduction of porosity into materials (Link in: <http://en.51shape.com/?p=2240>, accessed on 24.11.21).

Fig. 3: Gas bubble coalescence observed by optical microscopy in porous PEEK produced by foam injection moulding (Copied from [22] with permission from Springer).

Fig. 4: Young moduli (left) and compressive strength (right) as a function of density of commercially available foams and porous materials [35] (Figure modified from Gibson, L. J., and M. F. Ashby. "Cellular Solids: Structure and Properties" 2nd ed. Cambridge University Press, © 1997. Figures courtesy of Lorna Gibson and Cambridge University Press).

Fig. 5: Schematic process representation of bio-based polyurethane foam production as example of a chemical blowing process (Link in: www.sciencedirect.com/science/article/pii/S0926669019308921, accessed on: 07.12.2021, open access under the terms and conditions of the Creative Commons Attribution (CC BY) license).

Fig. 6: Schematic representation of a physical blowing process. (Link in: <https://www.mdpi.com/1420-3049/25/15/3408/htm>, accessed on: 07.12.2021, open access under the terms and conditions of the Creative Commons Attribution (CC BY) license).

Fig. 7: Phenolic foam panel (with subsequent carbonisation) prepared by mechanical frothing [49]. (Link in: <https://www.sciencedirect.com/science/article/pii/S0264127519300954>, accessed on 24.11.21, open access under the terms and conditions of the Creative Commons Attribution (CC BY) license).

Fig. 8: Schematic of polymer foaming processes. (Copied from: Standau T., Altstädt V. (2019) Foams. In: Karger-Kocsis J., Bárány T. (eds) Polypropylene Handbook. Springer, Cham. Link in: https://doi.org/10.1007/978-3-030-12903-3_10, with permission from Springer).

Fig. 9: Schematic of preparation of porous polymers by emulsion templating [62] (Link in: <https://www.frontiersin.org/articles/10.3389/fbioe.2020.00875/full>, accessed on: 07.12.2021, open access under the terms and conditions of the Creative Commons Attribution (CC BY) license).

Fig. 10: Shear moduli (log) as function of temperature of amorphous and semi-crystalline polymers showing the forming region of both polymers highlighting the narrow process temperature window of semi-crystalline polymers [68] (Link in: <https://www.sciencedirect.com/science/article/pii/B9780815515456000053>, accessed on: 23.12.2021, with permission from Elsevier).

Fig. 11: Macroporous PTFE obtained from Pickering water-in-hexane emulsion; (a) is photo of a net-shaped w/o emulsion stabilized by colloidal polymer particles, (b) the same emulsion after drying and (c) sintering. [69] This series of photos clearly shows dramatic shrinkage of the emulsion templated green foam body during processing into a porous high performance polymer (Modified image from link: <https://www.sciencedirect.com/science/article/abs/pii/S0032386109004297>, accessed on: 23.12.2021, with permission from Elsevier).

Fig. 12: Structural formulas for selected amorphous (PSU, PES, PBI) and semi-crystalline (PPS, PAI) high performance polymers showing the common chemical features of these polymers.

Fig. 13: Amorphous and semicrystalline polymers temperature-to-mechanical performance plot at the various polymer state (L. van den Berg, Development of 2nd Generation Proteinous Bioplastics, Master thesis, The University of Waikato, 2009 Link: https://www.researchgate.net/publication/44195198_Development_of_2nd_Generation_Proteinous_Bioplastics accessed on 26.11.21).

Fig. 14a: The first step reaction between 4-nitrophthalimide and bisphenol A disodium salt.

Fig. 14b: The second step reaction between tetracarboxylic dianhydride and m-phenylene diamine.

Fig. 15a: The electrophilic PEEK synthesis route (final step, without end-capping reaction).

Fig. 15b: The nucleophilic PEEK synthesis route (final step).

Fig. 16: Schematic of porogen leaching process for the production of porous PEEK [148]. (Link in: <https://link.springer.com/article/10.1007/s40204-019-00123-1>, accessed on 07.12.2021, open access under the terms of the Creative Commons Attribution 4.0 International License).

Fig. 17: Picture of the morphology of “surface-porous” PEEK [147]. (Link in: <https://www.sciencedirect.com/science/article/abs/pii/S1742706114005248>, accessed on: 13.12.2021, with permission from Elsevier).

Fig. 18: Schematic of fabrication of porous PEEK using the solvent exchange process [74]. (Link in: <https://www.sciencedirect.com/science/article/abs/pii/S0032386119301971>, accessed on: 13.12.2021, with permission from Elsevier).

Fig. 19: Schematic of the electrophilic route of PEKK synthesis.

Fig. 20: Schematic of the production of porous PEKK (with subsequent surface treatment) preparation via compression moulding and porogen leaching [161]. (Link in: <https://pubs.acs.org/doi/10.1021/acsbiomaterials.6b00103>, accessed on: 08.12.2021, open access under the terms and conditions of the Creative Commons Attribution (CC BY) license).

Fig. 21: Examples of applications of porous polymer products made using the TIPS process: schematic representation (A) of artificial scaffolds for tissue engineering [69] (Link in: <https://www.intechopen.com/chapters/23660>, accessed on 16.12.2021, open access under the terms and conditions of the Creative Commons Attribution (CC BY) license); cross-sectional (B) and general view (C) of hollow fibre membranes for gas-liquid separation [169] (Link in:

<https://www.mdpi.com/2079-6439/6/4/76/html>, accessed on: 16.12.2021, open access under the terms and conditions of the Creative Commons Attribution (CC BY) license).

Fig. 22: Schematic phase diagram of a polymer-solvent system. The polymer fraction is plotted as a function of temperature (left image): C is the critical point. Schematic of phase demixing and the resulting pore morphology: A→B is the spinodal decomposition; D→P the nucleation and growth of the polymer-poor phase at a polymer fraction below the critical point; E→R nucleation and growth of the polymer-rich phase occurring at a polymer fraction above the critical point (right image). (Copied and modified from [171] with permission of Elsevier Books).

Fig. 23: Characteristic images of tissue engineering scaffolds made from poly(lactic-co-glycolic acid) (PLGA): (a) cross-section of microtubular structure of the PLGA scaffold and (b) vertical section, as well as a PLGA scaffold with an isotropic pore structure (c) cross-section and (d) vertical section [177]. (Link in: <https://www.sciencedirect.com/science/article/abs/pii/S0142961206004728>, accessed on 16.12.2021, with permission from Elsevier).

Fig. 24: Adsorption/desorption isotherm exemplarily shown for porous PEEK produced by HT-TIPS.

Fig. 25: Illustration of the determination of compression (crush) strength and Young's modulus from a strain-stress curve.

Fig. 26: Illustration of the evaluation of the degree of crystallinity from the melting peak(s) on DSC curve.

Fig. 27: HT-TIPS setup. On the left figure: glass vessel (1), thermometer (2), 50 mL glass beaker with polymer/solvent solution (3), high temperature hose connectors (4). On the right: pipes connected to tap water (5), Huber Unistat T305W HT thermostat with PILOT ONE control unit (6).

Fig. 28: Schematic representation of the fabrication of porous HPP samples using HT-TIPS process. The heating/cooling profile of 20 wt.% of PEEK in 4PPH with a cooling rate of 1°C/min was used as process example.

Fig. 29: Chemical structure of the selected solvents, where A is 4-phenylphenol, B is 9-fluorenone, C is diphenyl sulfone and D is diphenyl ketone.

Fig. 30: Photos of fracture surfaces of cylindrical porous PEI samples obtained from 4PPH (row A) and from 9FN (row B) solutions with PEI concentrations of 10 (1), 20 (2) and 30 (3) wt.%.

Fig. 31: Photos of fracture surfaces of porous PEI samples obtained from DPK (row A) and from DPS (row B) solutions with concentrations of 10 (1) and 20 (2) wt.%. Note it was impossible to dissolve more PEI in those solvents.

Fig. 32: Photographs showing the process issues during HT-TIPS of PEEK in DPS: A) Green laser pointer does not pass through a 10 wt.% PEEK in DPS solution indicating an inhomogeneous polymer solution and solvent recondensation on the beaker walls above the solution level and B) resulting porous PEEK sample obtained from 10 wt.% PEEK in DPS solution was fragile and exhibited a non-homogeneous pore structure.

Fig. 33: The resulting porous PEKK shrunk inside a cylindrical mould (A) and fracture surface (B) of the same sample, which was obtained from 10 wt.% PEKK in DPK solution. SEM images of the porous PEKK at magnifications of 1000x (C) and 3000x (D).

Fig. 34: Photos and SEM images of porous PEKK samples obtained from PEKK in DPS solutions with concentrations of 10 (row A) and 20 (row B) wt.%; SEM images obtained at magnifications of 500x (A2, B2) and 2000x (A3, B3).

Fig. 35: Elastic moduli of our porous PEEK obtained from 4PPH solutions, using various cooling rates and polymer concentrations compared with literature data [74]. (Link in: <https://onlinelibrary.wiley.com/doi/full/10.1002/app.51423>, accessed on: 07.01.2022, open access under the terms and conditions of the Creative Commons Attribution (CC BY) license)

Fig. 36: Elastic modulus (A) and crush strength (B) of porous PEKK produced from 20 wt.% PEKK in 4PPH and 9FN using cooling rates $\beta = 0.5$ and $1^\circ\text{C}/\text{min}$ as a function of porosity and compared with literature data [163].

Fig. 37: Photographs (left) and SEM images (right) of porous PEEK samples produced from 4PPH solutions, produced by HT-TIPS from 5 wt.% (row A), 10 wt.% (row B), 15 wt.% (row C) and 20 wt.% (row D) at cooling rates β of 1) $0.5^\circ\text{C}/\text{min}$, 2) $1^\circ\text{C}/\text{min}$, 3) $2^\circ\text{C}/\text{min}$ and 4) $10^\circ\text{C}/\text{min}$.

Fig. 38: Photographs (left) and SEM images (right) of porous PEKK samples produced from 4PPH (row A and B) and from 9FN (row C and D) solutions, produced by HT-TIPS from 10 wt.% (row A and C) and 20 wt.% (row B and D) at cooling rates β of 1) $0.5^\circ\text{C}/\text{min}$, 2) $1^\circ\text{C}/\text{min}$, 3) $2^\circ\text{C}/\text{min}$ and 4) $10^\circ\text{C}/\text{min}$.

List of Tables:

Table 1: Glass (T_g) and melting temperature (T_m), Young's modulus (E) and tensile strength (σ), and degree of crystallinity (χ) of PEKK (Arkema KEPTSAN®) as a function of the T/I ratio.

Table 2: Clear point solution temperatures for PEEK, PEKK and PEI as function of polymer concentration and solvent nature.

Table 3: Clear solution and cloud points for PEI in 4PPH, 9FN, DPK and DPS solutions.

Table 4: Skeletal ρ_s and foam ρ_f density, porosity P , surface area A_s , elastic modulus E and crush strength σ of porous PEEK samples produced from 4PPH solutions.

Table 5: Skeletal ρ_s and foam ρ_f density, porosity P , surface area A_s , elastic modulus E and crush strength σ of porous PEKK samples produced from 4PPH and 9FN solutions.

Table 6: Degree of crystallinity χ of porous PEEK and PEKK produced from 4PPH and 9FN solutions containing various amounts of polymer using cooling rates of 0.5 – 10 °C/min calculated from the heat of melting (first heating run) and crystallisation (first cooling run) as measured using standard DSC. χ determined from the first heating run represents the polymer crystallinity for materials crystallised from solution while χ obtained from the cooling run represents that of melt crystallised polymers.

Chapter 1. Introduction

Polymer materials have taken a significant place among other engineering materials. The story of the polymers started in the 19th century and is still not over. Polymers have found a wide range of applications, ranging from nanoscale particles and thin membranes to big construction blocks and materials. Modern times required the production of new high-strength, safe and inexpensive polymer materials. Thermoplastic polymers are commonly classified into amorphous and semi-crystalline and in addition following their thermomechanical properties (**Fig. 1**). The polymers are grouped according to their continuous usage temperature (also continuous service temperature) into classes, ranging from standard or commodity to high performance polymers (HPPs).

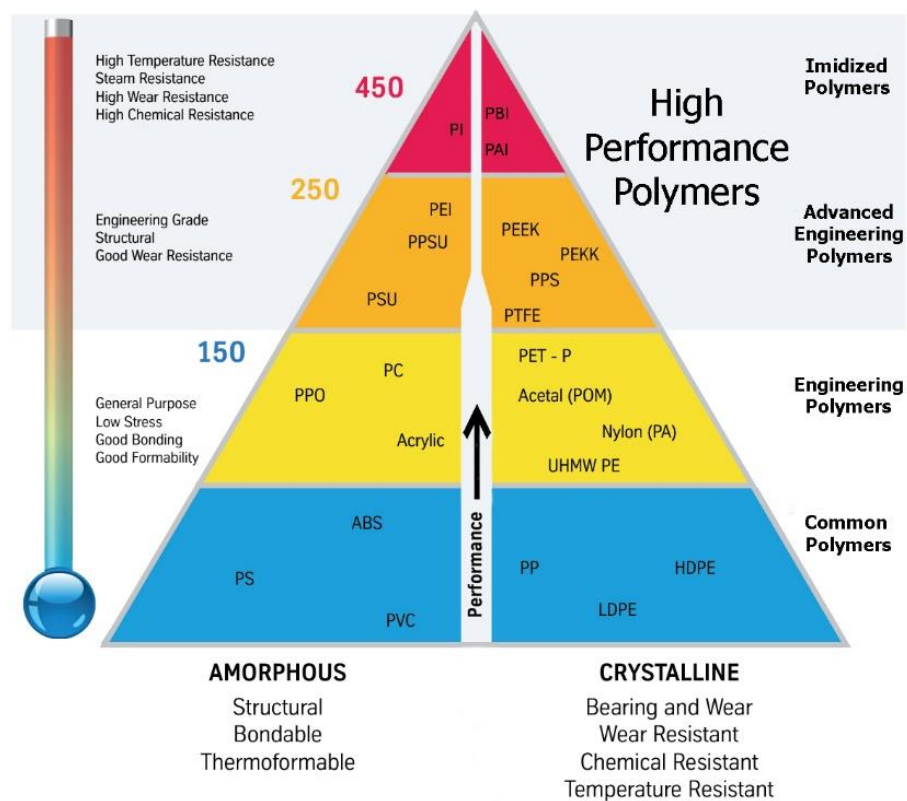


Fig. 1: Polymeric materials pyramid as a function of continuous operation temperature, Figure adapted from thyssenkrupp Engineered Plastics, High Performance Plastics (Link in: https://www.onlineplastics.com/products/high-performance-plastics-c-1_192.html#1-YToxOntzOjQ6ImdyYWQiO2k6MDt9 accessed on: 14.11.21).

In general, HPPs possess outstanding mechanical, thermal and chemical stability in comparison to all standard or engineering polymers. The weight-to-strength ratio of HPPs allows to use them as a replacement for the traditional materials, such as metals, in the places where weight carries a penalty, for instance in the aerospace industry. Their low density, high thermal stability, limiting oxygen index (LOI), and dielectric properties render them ideal materials for air- and spacecraft interior applications. High thermal and mechanical stability allows to use of HPPs as high-load

bearings, gears or fittings to replace metals or ceramics [1, 2]. Further promising applications of HPPs are scaffolds for tissue engineering and implants, because of their chemical and bio-inertness [3, 4]. However, the biggest disadvantage of HPPs is their high price. A possibility to maximise their advantages while reducing the price of structures is to produce porous high-performance polymers.

Porous polymers or foams are materials that contain dispersed gas (or liquid) inside with well-defined boundaries between dispersed and continuous phases. In comparison with non-porous bulk polymers, the porous variant has a lower weight, higher surface area, better thermal and sound insulation properties. On the other hand, porous polymers have lower mechanical properties in comparison with non-porous bulk polymers. Nevertheless, porous polymers have another significant advantage – decreasing the material amount which is required to produce a certain volume while simultaneously maintaining the intrinsic polymer properties, such as chemical and thermal stability. In the case of HPPs, the introduction of porosity allows for the production of (ultra) light-weight, chemically and thermally stable materials with an acceptable mechanical property profile (**Fig. 2**) [5-7].

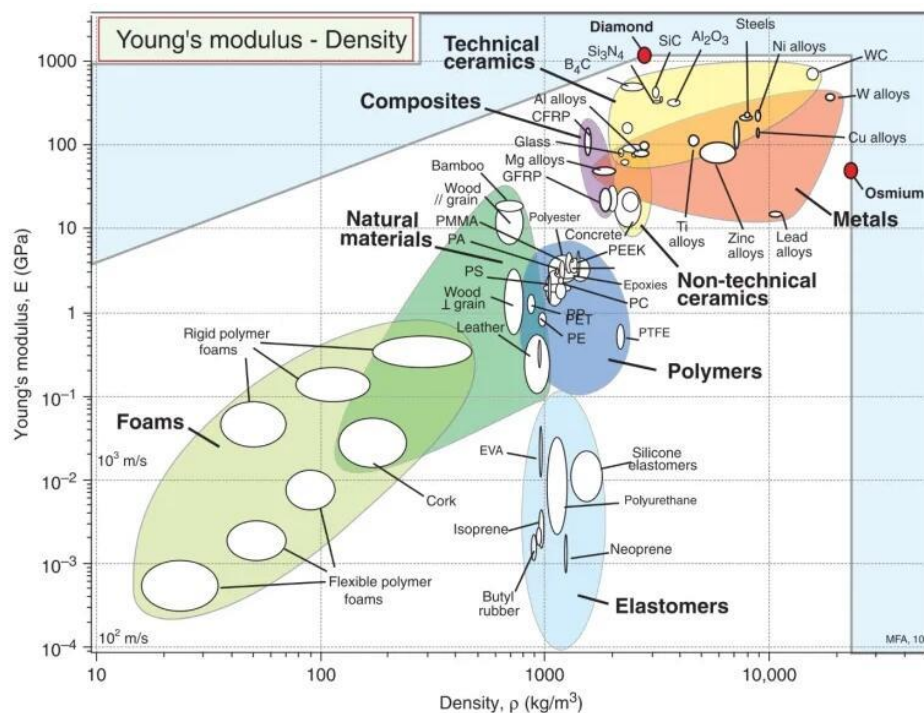


Fig. 2: Typical Ashby chart showing the Young's modulus as a function of density for various materials classes allowing for the comparison of metals, ceramics, composites, natural materials, polymers and elastomers, as well as foams. This chart highlights the fact that acceptable Young's moduli, as a measure of the mechanical stiffness, can be maintained upon introduction of porosity into materials (Link in: <http://en.51shape.com/?p=2240>, accessed on 24.11.21).

Polymer foams are commonly produced by physical or chemical blowing. Physical blowing agents are gases or low boiling point liquids, which are introduced into the polymer without chemical interaction. Commonly, the blowing agent (e.g. carbon dioxide) is dissolved in the polymer melt under high pressure and/or elevated temperature. Then, a pressure drop occurs which results in the formation and expansion of gas bubbles creating a porous structure. In chemical blowing, gas formation occurs by a chemical reaction or thermal decomposition of the blowing agent [8, 9]. Various other methods have been developed to produce porous polymers, such as particles leaching [10], solvent casting [11], various gelation technics [12], electrospinning [13], emulsion templating [14] and more recently also additive manufacturing techniques [15]. All these methods are well applicable for common and engineering polymers. However, in the case of the HPPs, high energy consumption and special apparatus are required. Particulate leaching, gas blowing and additive manufacturing methods for the production of porous HPP require process temperatures above the glass transition or melting point [16-18]. The solvents resistance of HPPs causes significant trouble to prepare HPP solutions required as a precursor for electrospinning, solvent casting and gelation methods [19-21]. In addition, the presence of a stiff and rigid crystalline phase (for semi-crystalline HPP) causes additional issues for homogeneous gas or liquid phase dispersion in the continuous polymer phase (see **Fig. 3**). In the other words – their main advantages are also leading to their disadvantages when aiming to produce porous high-performance polymers.

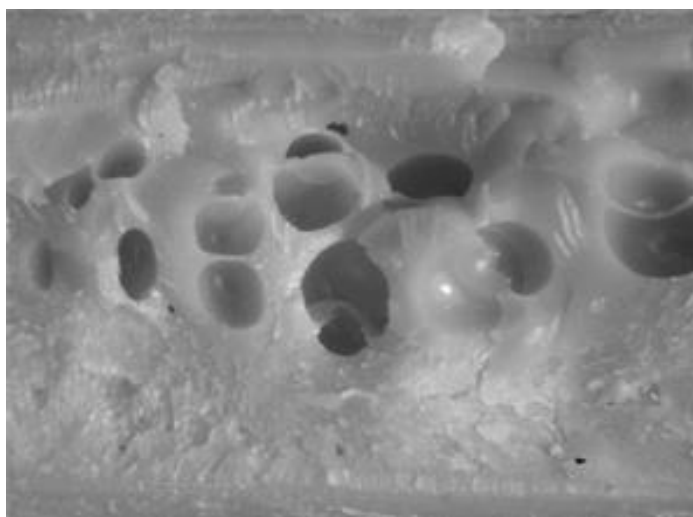


Fig. 3: Gas bubble coalescence observed by optical microscopy in porous PEEK produced by foam injection moulding (Copied from [22] with permission from Springer).

1.1. Scope of the thesis

The aim of my thesis was the development of a thermally induced phase separation (TIPS) process as a universal method for the production of monolithic high performance polymer foams with tailored porosity, i.e. density, and thus mechanical properties. Polyetheretherketone (PEEK), polyetherketoneketone (PEKK) and polyetherimide (PEI) were selected as common examples for semi-crystalline and amorphous high-performance polymers for the realisation of macroporous bulk materials with a porosity exceeding 70% and tailored mechanical properties using the developed TIPS method.

To achieve the aim the following objectives will be addressed:

- i) to identify suitable solvent(s) to dissolve the selected polymers with concentrations of at least 10 wt.% the polymers
- ii) to develop a suitable TIPS method to process HPP solutions into monolithic porous polymers
- iii) to optimise the TIPS process with respect to polymer concentration, dissolving times and temperatures, cooling rates, the extraction of solvent and drying procedure of the foam precursor
- iv) to identify the influence of process parameters on properties of the resulting porous polymers, such as bulk (affected by the degree of crystallinity) and foam density, porosity, surface area and pore morphology, as well as compression properties.

1.2. Structure of the thesis

Following this brief introduction, my thesis will be structured as follows: initially, I will review the background and state-of-the-art in **Chapter 2**. Following the literature review, the materials used and applied characterisation methods will be described in **Chapter 3**. In **Chapter 4** I will introduce the developed high temperature thermally induced phase separation process (HT-TIPS) and summarise and discuss the major findings, which will be contrasted with the state-of-the-art. Initially, I focused on the identification of a universal solvent for the selected HPPs. Some possible solvents were already described in the literature and successfully used in various applications. All of these solvents are inert, aprotic and have high boiling temperatures, which renders them suitable to dissolve HPPs. Among the tested solvents were diphenyl sulfone (DPS), diphenyl ketone (DPK) and 9-fluorenone (9FN). However, I found that 4-phenylphenol (4PPH) was the most versatile solvent. 4PPH is an inert aprotic solvent with a melting temperature of 167°C and

a high boiling point of 321°C. 4PPH is soluble in acetone and ethanol, which allows for 4PPH extraction from porous polymer precursors produced using HT-TIPS. Furthermore, it was possible to dissolve all selected polymers in 4PPH with mass concentrations up to 20 wt.% at temperatures below excessive solvent evaporation (**Publication 1**). The HT-TIPS process was optimised and the influence of process parameters, such as polymer concentration, dissolution time and temperature as well as cooling rate, were investigated. The minimal dissolution temperature and time had to be identified for each polymer. This is crucial because higher temperatures and dissolution times than necessary for full polymer dissolution results in additional costs and solvent loss during HT-TIPS. The polymer in solvent concentration is the primary factor controlling the porosity and foam density of porous HPPs, while the cooling rate influences the phase separation process and pore morphology (**Publication 2 and 3**). Solvent extraction and drying do not have a significant effect on resulting porous samples, with the exception of PEKK in 9FN solutions (**Publication 3**). 9FN was used as the solvent for PEKK and it could be shown that porous PEKK obtained from PEKK in 9FN solutions demonstrated better mechanical and surface properties than porous PEKK obtained from 4PPH solution (**Publication 3**).

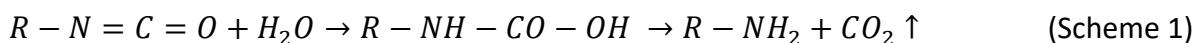
All resulting porous HPPs were characterised using various analytical methods. The skeletal density was measured by gas-replacement pycnometry, foam density by dry powder displacement method and porosity was calculated from these two experimental values. Surface area and pore size distribution were investigated via BET and BJH methods, respectively, with additional surface inspection using SEM. Thermal properties and the degree of crystallinity was characterised by DSC and Flash-DSC. The compression properties were measured adapting the standard ISO 844:2001 (**Publication 2 and 3**).

Chapter 2. Background

2.1. Introduction to porous polymers, also called polymer foams

Among other polymer materials, there are materials that contain a large number of bubbles, holes or caverns inside the polymer matrix. These polymeric materials are called porous polymers or polymer foams. In comparison with original bulk polymers, foams have a much lower density and yet sufficient strength, as well as providing better heat and sound insulation properties. Such unique property combination allows for the use of polymer foams in a wide range of applications, such as automobiles, furniture, packaging materials, in bio-medical applications, sports

volume of inert gas during a chemical reaction (**Scheme 1**) or thermal decomposition (**Scheme 2**).



Inorganic or organic chemical blowing agents are compounded into the polymer melt and release a gas (typically nitrogen, hydrogen or carbon dioxide) by thermal composition at specific temperatures [38]. Gas can also be released during a chemical reaction between monomers and water, such as the reaction between water and isocyanate during foamed polyurethane production (**Fig. 5**) [39]. The blowing agents can be divided by activation mechanism in endothermic and exothermic ones [40]. Endothermic blowing agents consume heat during the decomposition reaction, which allows to control the gas production by temperature. Exothermic blowing agents are producing heat and gas during their decomposition reaction which cannot be stopped by simple cooling since an insulating foam is being produced. Inorganic blowing agents have limited applications in polymer processing and are mainly represented by various carbonates or nitrates. Organic blowing agents are more popular and release nitrogen or CO₂ during decomposition. Commonly used are various azo-, nitroso- and sulfonyl- compounds [41]. Chemical blowing agents are more expensive than physical ones.

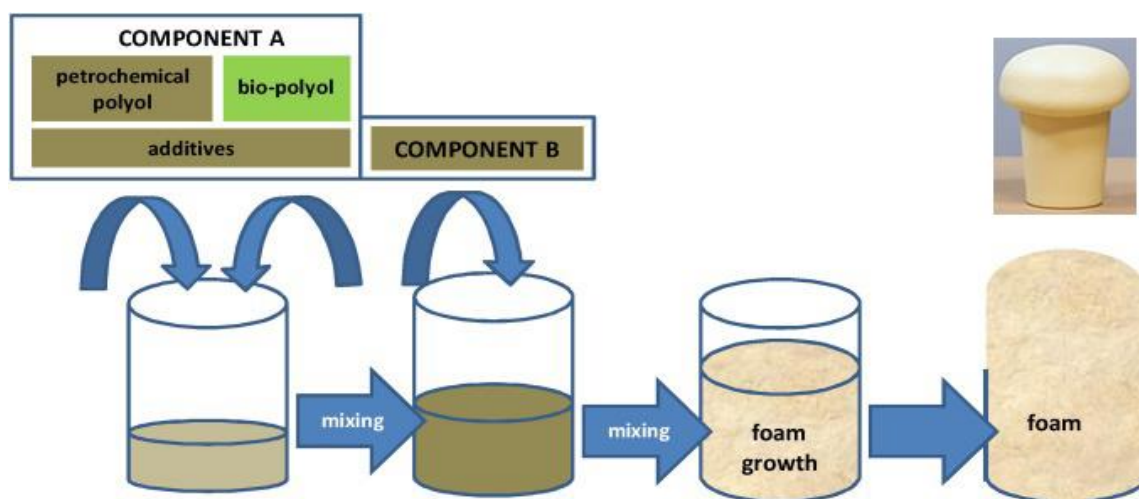


Fig. 5: Schematic process representation of bio-based polyurethane foam production as example of a chemical blowing process (Link in: www.sciencedirect.com/science/article/pii/S0926669019308921, accessed on: 07.12.2021, open access under the terms and conditions of the Creative Commons Attribution (CC BY) license).

In contrast to chemical blowing, physical blowing typically involves the introduction of low-boiling liquids or inert gas into the polymer matrix at evaluated pressure and temperature.

Nowadays, the most common physical blowing agents are inert gases, which are dissolving into a molten polymer under high pressure and then expand by pressure drop (**Fig. 6**) [42].

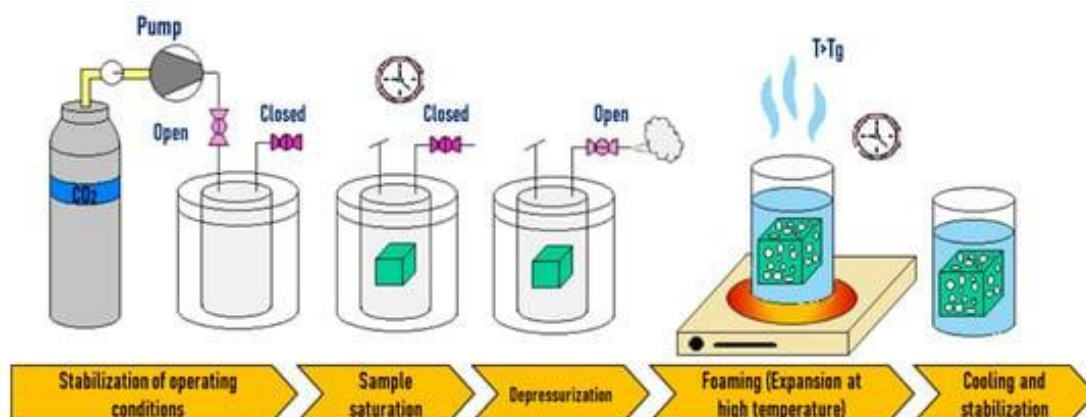


Fig. 6: Schematic representation of a physical blowing process. (Link in: <https://www.mdpi.com/1420-3049/25/15/3408/htm>, accessed on: 07.12.2021, open access under the terms and conditions of the Creative Commons Attribution (CC BY) license).

Another possibility is to utilise supercritical carbon dioxide, which allows for gas saturation to take place at temperatures below the polymer melting point [43]. One more notable physical foaming method is the introduction of hollow beads or expandable spheres into the polymer matrix as inert density decreasing additives [44]. Porous polymers produced by this method are called syntactic foams [45]. Physical blowing is a relatively simple process for the production of porous polymers. It is also pollution-free if no low boiling point organic fluids are being used [46, 47]. However, special apparatus is required and the process can be very high energy consuming.

A special case to introduce gas into a (pre)polymer is mechanical frothing [48]; gas is mechanically whipped into a liquid monomer, resin or water containing polymer particles to produce a stable froth or cream [49, 50]. During frothing the gas phase bubbles are dispersed into the liquid phase and kinetically stabilized by their viscosity. To increase the froth stability, surfactants or viscosity modifiers can be added to the liquid phase [51]. Subsequent polymerisation/solidification results in the formation of macroporous polymer foams. Mechanical frothing is a relatively simple, inexpensive and porogen-free process, which does not require costly special equipment and is well-suitable mainly for thermoset polymers (**Fig. 7**).

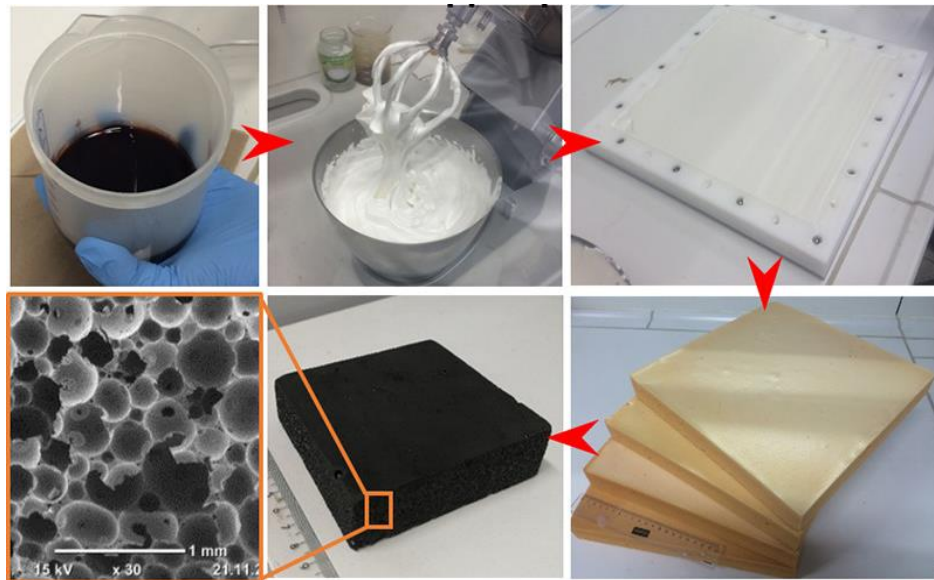


Fig. 7: Phenolic foam panel (with subsequent carbonisation) prepared by mechanical frothing [49]. (Link in: <https://www.sciencedirect.com/science/article/pii/S0264127519300954>, accessed on 24.11.21, open access under the terms and conditions of the Creative Commons Attribution (CC BY) license).

Polymer foaming processes involving the chemical, physical or mechanical introduction of gases commonly consists of three steps [52, 53]: gas bubble formation, gas bubble expansion and polymer solidification. In the first step, the gas phase is dissolving and saturating the polymer phase under specific conditions (usually elevated temperature and pressure). When the gas concentration in the polymer reaches saturation, gas microbubbles start agglomerating and form nuclei for gas bubbles expansion. During the bubble expansion phase, gas bubbles grow driven by internal gas pressure. There are several main factors which influence the bubble expansion process: melt viscosity, polymer (melt) surface tension, gas diffusivity, process temperature and pressure. The melt viscosity is the crucial factor for bubble formation because it is limiting the bubble diameter and expansion rate. During polymer solidification, gas bubbles are stabilized in a solid polymer phase (**Fig. 8**). Due to gas bubble growth, their surface area increases and they become unstable. Increasing the melt viscosity, for instance by cooling, is a common way of foam stabilization preventing bubble coalesce or collapse. Increasing the viscoelasticity of the polymer phase (by cooling) or solidification due to polycondensation or polyaddition (of monomers forming thermosetting polymers) prevents gas bubbles escaping from the foamed material.

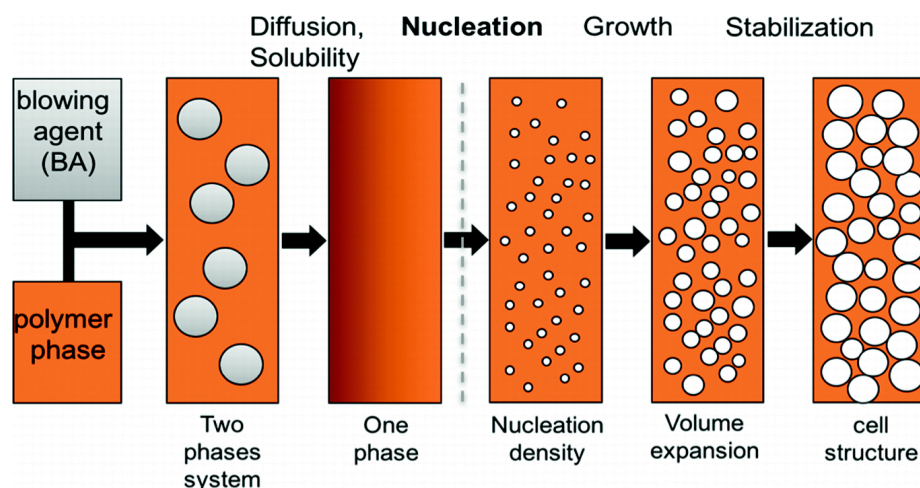


Fig. 8: Schematic of polymer foaming processes. (Copied from: Standau T., Altstädt V. (2019) *Foams*. In: Karger-Kocsis J., Bárány T. (eds) *Polypropylene Handbook*. Springer, Cham. Link in: https://doi.org/10.1007/978-3-030-12903-3_10, with permission from Springer).

There are several commonly used industrial foaming processes: extrusion, injection moulding, reaction injection moulding, mould pressing and free-foaming (in the case of polyurethanes). During extrusion foaming, the polymer and foaming agent are mixed inside an extruder at elevated temperature and the resulting foamed material is extruded into a mould for shaping. In foam injection moulding, foaming takes place inside a mould where the polymer saturated with a gas phase (under elevated pressure and temperature) when the pressure is reduced resulting in the formation and expansion of gas bubbles. Afterwards, the mould is cooled solidifying the foam resulting in the final porous product. Reaction injection moulding is quite similar to the injection moulding process, with a few differences – liquid resin pre-mixed with a blowing agent is injected into the mould under high pressure, followed by curing and foaming inside the mould also under high pressure. Reaction injection moulding processes are more suitable for thermosets than thermoplastic polymers. Foam mould pressing is quite simple; prepared foamable polymer beads or pellets are placed inside a mould, pressed and formed while the polymer expands to produce the porous product. Free foaming is another simple and versatile process, in which the foam components are mixed in an open mould, the reaction mixture expands during the chemical reaction between the components forming free rising foam. This process is mainly applicable for thermoset polymers, for example in polyurethane foam production [54].

Phase separation or phase inversion is another group of methods to prepare porous polymers. In the polymer phase separation method, the polymer dope or solution separates into polymer-rich and polymer-poor phases, while a porous polymer is obtained from the polymer-rich phase

after solvent removal. By varying the process parameters such as polymer concentration, process heating and cooling rates, solvent nature, etc. the properties of the resulting porous product can be controlled [55]. Phase separation methods are mainly used for the production of porous membranes or thin films and are not commonly used to produce monolithic porous polymers. There are several phase separation methods:

- TIPS processes utilise the temperature-dependent polymer solubility [56];
- non-solvent induced phase separation or immersion precipitation processes, in which polymer precipitation from polymer-in-solvent dope or solution occurs due to immersion in a non-solvent, which is caused by lowering the solvent quality [57];
- vapour induced phase separation processes, where the polymer dope or solution is exposed to a non-solvent vapour which initiates polymer phase separation [58];
- and air-casting methods, when solvent evaporation from polymer dope or solution leads to a decreased polymer solubility resulting in polymer precipitation [59].

Another notable method to prepare porous polymers is emulsion templating. An emulsion prepared from two immiscible liquids, where one of them is a dispersed phase (usually water) and the other is the continuous phase (for example, monomers with additives) is polymerised or solidified. The removal of the dispersed phase results in a porous polymer whose structure is determined by the morphology of the emulsion template (**Fig. 9**). The porosity and pore morphology can be controlled by tuning the emulsion phase ratio, adding surfactants or colloidal particles. Templating methods are relatively simple and mainly used to prepare macroporous polymers by polymerisation of monomers [60-62].

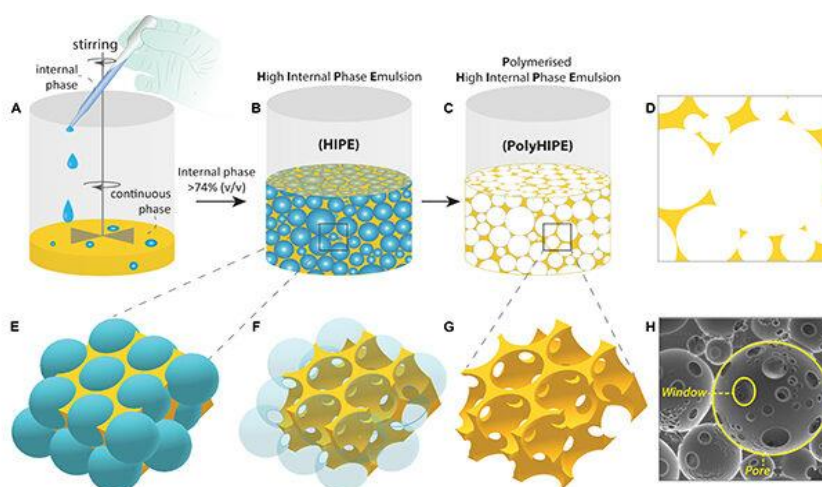


Fig. 9: Schematic of preparation of porous polymers by emulsion templating [62] (Link in: <https://www.frontiersin.org/articles/10.3389/fbioe.2020.00875/full>, accessed on: 07.12.2021, open access under the terms and conditions of the Creative Commons Attribution (CC BY) license).

Porous HPPs (but especially semi-crystalline HPPs), however, cannot easily be produced using the methods described above or the processes are associated with significant difficulties. While amorphous HPP foams can be produced via gas blowing or phase separation methods [63-66], semi-crystalline HPPs has a much smaller processing range in which gas blowing is possible (**Fig. 10**). As mentioned above, the crystalline phase stays rigid below melting and only becomes a viscous liquid above the melting temperature. In the liquid state, semi-crystalline HPPs undergo a significant viscosity drop and the melt strength reduces; both are crucial factors to stabilize gas bubbles in the polymer melt. Below the melting point, the polymer viscosity and strength are very high and, therefore, gas bubbles cannot overcome the resistance of the rigid polymer phase making it impossible to produce a foamed structure. On the other hand, at temperatures above the melting point, gas bubbles do coalesce (**Fig. 3**) because of the low melt strength/viscosity of semi-crystalline HPPs [22, 67].

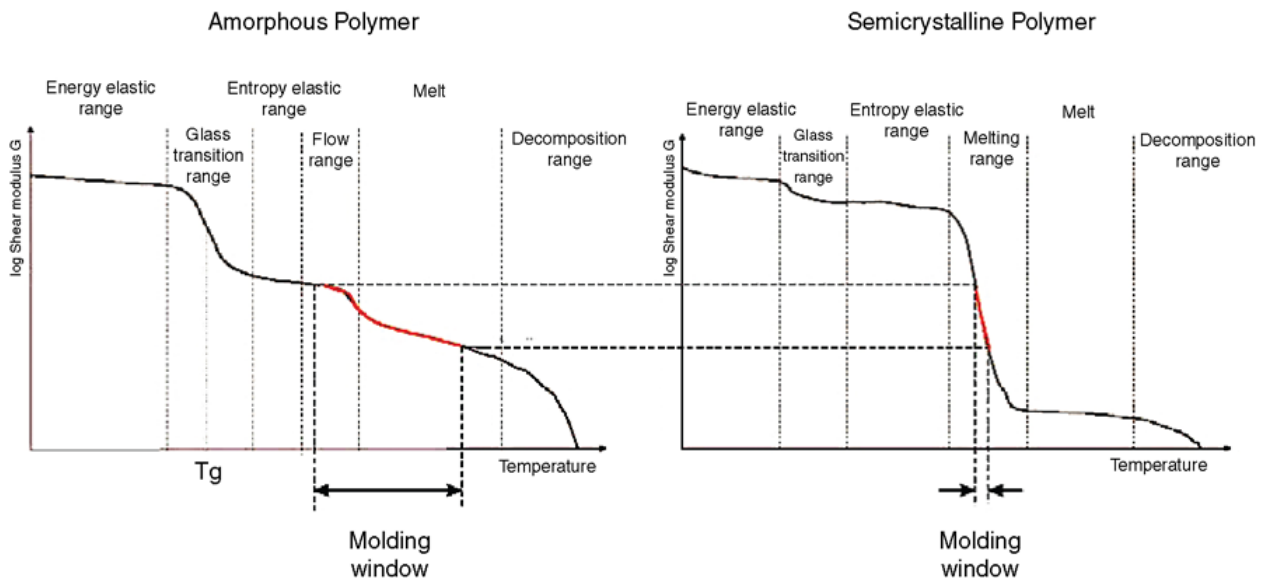


Fig. 10: Shear moduli (log) as function of temperature of amorphous and semi-crystalline polymers showing the forming region of both polymers highlighting the narrow process temperature window of semi-crystalline polymers [68] (Link in: <https://www.sciencedirect.com/science/article/pii/B9780815515456000053>, accessed on: 23.12.2021, with permission from Elsevier).

Synthesis of HPPs directly in emulsion templates is extremely difficult because of the evolved synthesis route (**Fig. 14a-b, 15a-b**) involving high temperature solvents and elevated temperatures seriously limiting the choice of immiscible liquids for the dispersed phase. However, a possible approach to utilize emulsion templating for HPPs is to prepare HPP particle-stabilized (also called Pickering) emulsions. Removal of the liquid phases by drying leaves a green body of HPP particles, which after sintering results in a produce porous polymer having the

structure of the emulsion template. However, this process is accompanied by significant shrinkage of both emulsion templates and green body (**Fig. 11**) [50, 69].

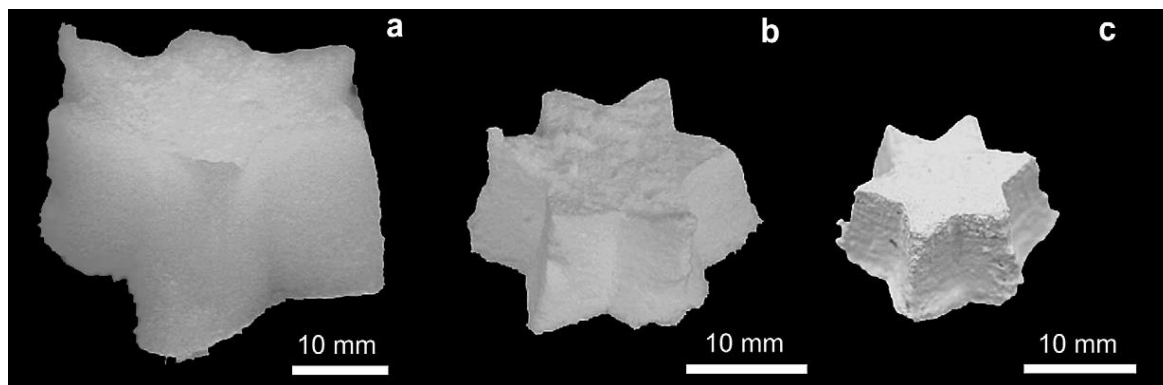


Fig. 11: Macroporous PTFE obtained from Pickering water-in-hexane emulsion; (a) is photo of a net-shaped w/o emulsion stabilized by colloidal polymer particles, (b) the same emulsion after drying and (c) sintering. [69] This series of photos clearly shows dramatic shrinkage of the emulsion templated green foam body during processing into a porous high performance polymer (Modified image from link: <https://www.sciencedirect.com/science/article/abs/pii/S0032386109004297>, accessed on: 23.12.2021, with permission from Elsevier).

Phase separation methods are widely used to produce porous polymer films and membranes, as well as bulk porous polymers, which were frequently used as scaffolds for tissue engineering applications [70]. However, only recently it was shown that porous monolithic semi-crystalline HPPs can be produced by means of phase separation methods using specific solvents and/or processes [71-75].

2.2. High-Performance Polymers: A brief Introduction

High-performance polymers are a group of synthetic polymers that outperforms common or engineering polymers. One of the main characteristics of all high-performance polymers is their high continuous-use temperature (above 150°C). The high service temperature is directly related to the chemical structure of HPPs, which provides outstanding mechanical, thermal and chemical stability (see **Fig. 12**). Common HPP structural features are [76-78]:

- Aromatic rings in the polymer backbone and/or
- Mechanically rigid and oxidative stable groups (-C=O, -O- and -C-F) and/or
- Presence of mainly aromatic C-H then aliphatic C-H groups.

In general, HPPs can be divided into two main groups: 1) amorphous polymers, such as polyetherimides (PEI), polysulphones (PSU), polyphenylenesulphones (PPSU), polyethersulfone (PES), polybenzimidazoles (PBI), polyimides (PI); 2) and semi-crystalline, such as

polyaryleneetherketones (for example polyetheretherketone (PEEK), polyetherketoneketone (PEKK)), fluoropolymers (polytetrafluoroethylene (PTFE or Teflon)) and polyvinylidene difluoride (PVDF)), polyamide-imides (PAI), and polyphenylene sulphide (PPS). Sometimes imidized polymers (PAI, PBI and PI) are clustered into an individual group, which is located above high-performance polymers and called ultra-performance polymers (see **Fig. 1**). The imidized polymers have very specific property combinations, such as dramatically high continuous use temperatures and lack of a melting point. At the same time, they possess significant processing issues and weak chemical resistance to boiling water, strong alkalis, bases and amines [79-81].

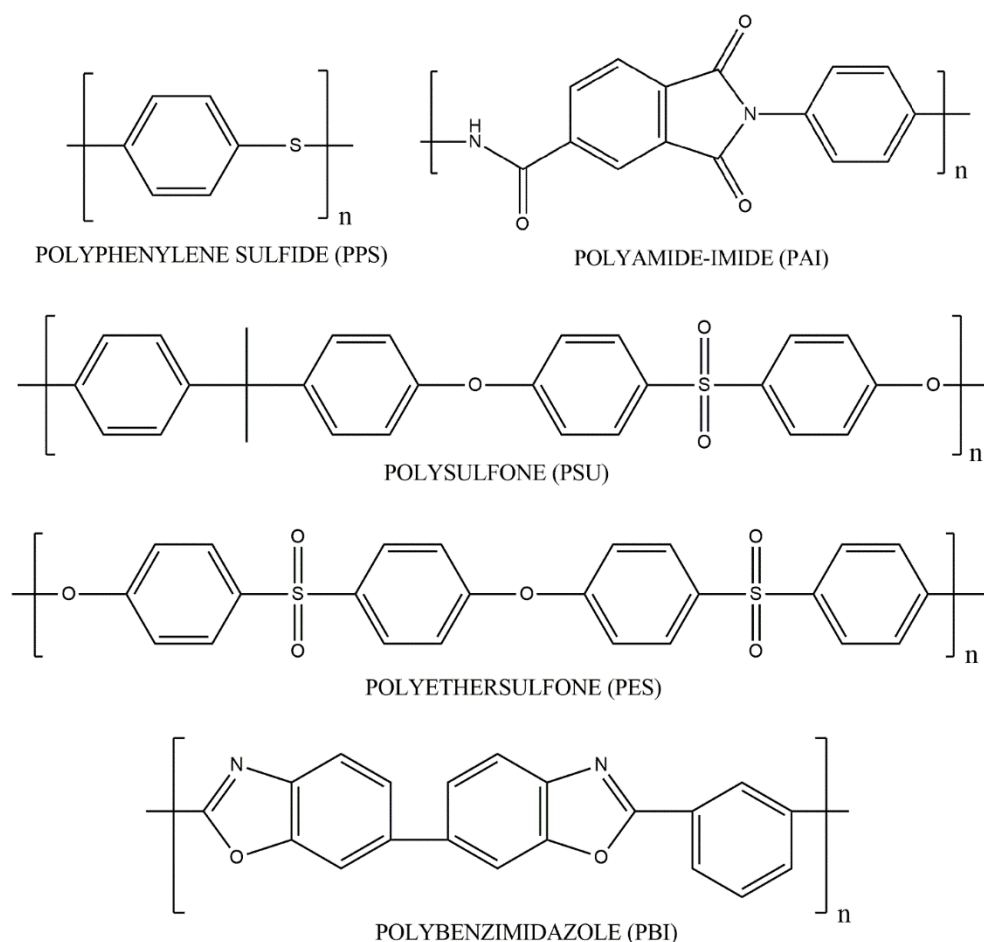


Fig. 12: Structural formulas for selected amorphous (PSU, PES, PBI) and semi-crystalline (PPS, PAI) high performance polymers showing the common chemical features of these polymers.

The thermal stability of HPPs can be characterised by their glass transition (T_g), melting (T_m) and heat deflection (HDT) temperatures. The glass transition temperature is related to polymer chains mobility and at temperatures exceeding T_g , chains lose rigidity and transfer to the viscous state. In the case of the fully amorphous HPPs, this is the maximum usage temperature because above T_g amorphous HPPs lose their mechanical stability. At the temperature significantly above T_g amorphous HPP, without a crystalline phase, will start to thermally degrade and decompose

[82]. When semi-crystalline HPPs are heated to temperatures above the glass transition temperature they undergo just a minor mechanical performance loss (**Fig. 13**), which is related to the presence of the crystalline phase reinforcing the viscous polymer phase. Only when the temperature reaches T_m of the crystalline phase, semi-crystalline HPPs start to flow and lose mechanical performance [83]. The HDT is a characteristic of the mechanical stability of a polymer under stress at elevated temperatures. For amorphous HPPs, HDT is near T_g , whereas for semi-crystalline HPPs, it is between T_g and T_m and is strongly dependent on the degree of crystallinity and crystalline structure [84, 85].

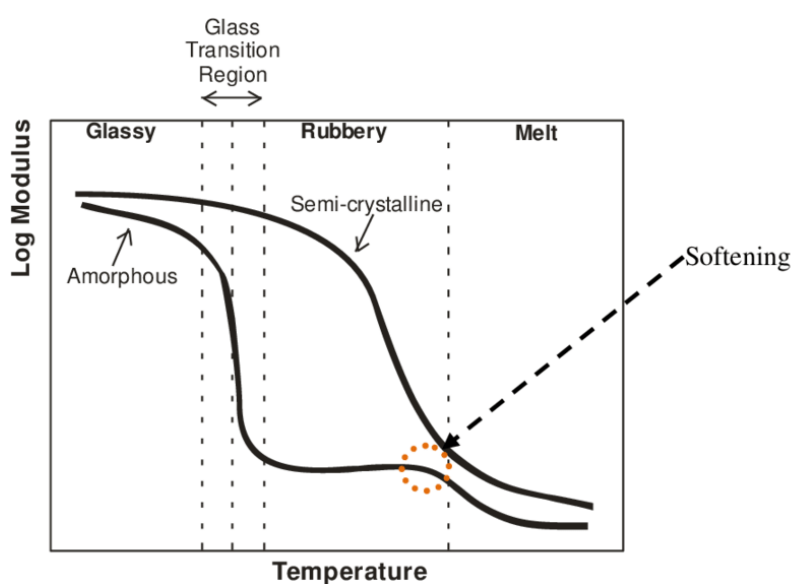


Fig. 13: Amorphous and semicrystalline polymers temperature-to-mechanical performance plot at the various polymer state (L. van den Berg, *Development of 2nd Generation Proteinous Bioplastics*, Master thesis, The University of Waikato, 2009 Link: https://www.researchgate.net/publication/44195198_Development_of_2nd_Generation_Proteinous_Bioplastics accessed on 26.11.21, accessed on 13.01.2022).

2.3. Polyetherimide: Synthesis, Properties, and Applications

One notable polymer among the imidized family is polyetherimide, which was invented by a team headed by Wirth in the 1970s and was introduced into the market under the trade name Ultem® by General Electrics in 1982 [86]. In comparison with other imidized HPPs, PEI has a more flexible ether linkage, which disrupts the ordering of polymer chains and prevents the formation of a rigid crystalline structure. As result, PEI possesses a lower processing temperature than traditional polyimides with the retention of most of the other properties [87, 88].

One of the most common commercially available unfilled PEI resins is Ultem 1000. It is an amorphous, transparent thermoplastic material with density of 1270 - 1280 kg/m³, compression and tensile strength of around 150 and 110-115 MPa, respectively, and high compression (3.4

GPa) and tensile (3.5 GPa) moduli and an elongation to break of 80%. The T_g of the Ultem 1000 is 217°C with HDT in the range of 200-210°C. Furthermore, Ultem 1000 has good dielectric properties over a wide temperature and frequency range and a high LOI of 47 [89-91]. However, PEI has chemical resistance to most common solvents and acids but is unstable in strong alkaline, amine and ammonia environment. In addition, it can be dissolved in various aprotic polar solvents, such as dimethyl formamide, chloroform, dimethyl acetamide and N-methyl pyrrolidone [92, 93].

Common to the synthesis of polyimides is the ring-opening reaction between diamine and dianhydride to produce polyamide acid, which after water removal leads to polyimide formation. In this step, high boiling solvents to dissolve the monomers and high reaction temperatures are required. The resulting polyimide is difficult to process because of its incredibly rigid polymer backbone, outstanding high glass transition, which limits the availability of polyimides [94]. The key feature in PEI synthesis is the use of bisphenol-A based dianhydrides, obtained via the reaction between the nitro group in phthalimide and difunctional imide salt (**Fig. 14a**). Then, the resulting product reacts with diamine (m-phenylene in the PEI case) to create polyamide acid (**Fig. 14b**). In the final step, water removal by heating leads to the formation of PEI. PEI has at least three flexible linkages – two ether links and one isopropylidene group, which imparts its amorphous nature [81, 86].

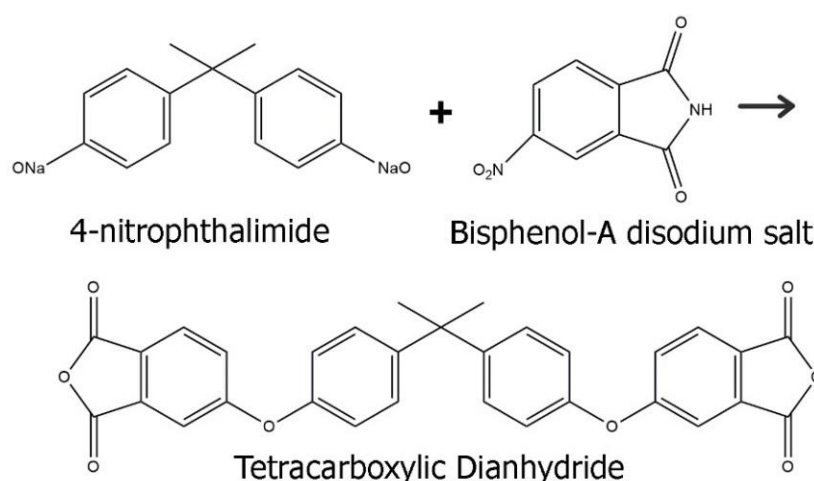


Fig. 14a: The first step reaction between 4-nitrophthalimide and bisphenol A disodium salt.

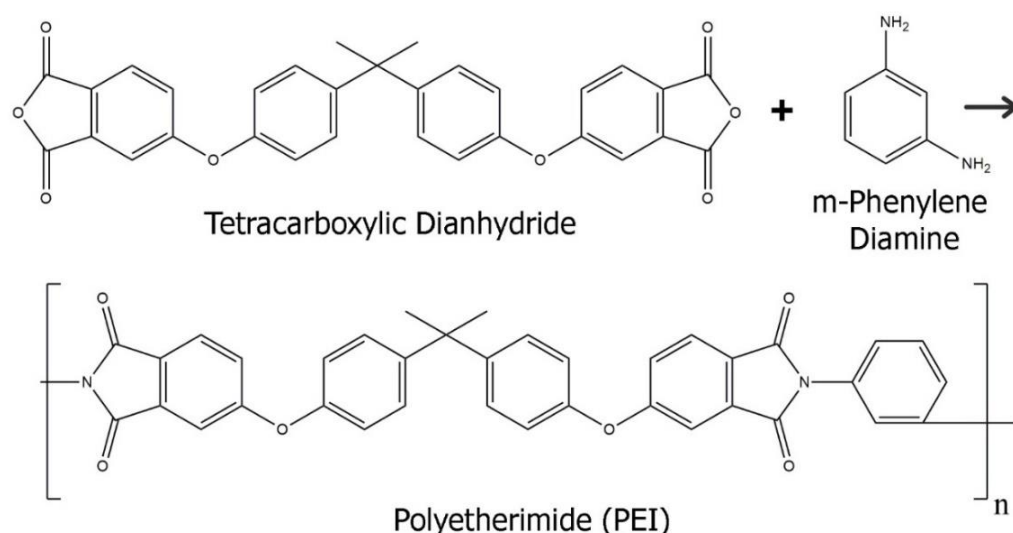


Fig. 14b: The second step reaction between tetracarboxylic dianhydride and m-phenylene diamine.

Various additives can be used to enhance the mechanical and thermal resistance of PEI. The most common additives for PEI are glass fibres, beads or flakes used as reinforcement up to concentrations of 40% resulting in improved tensile, flexural, impact strength and a slight increase in HDT [95-97]. Another way to improve or modify PEI properties is to combine them with other polymers, i.e. blend formation. PEI can form a one-phase (miscible) blend with an impressive amount of other polymers, such as PEEK [98, 99], polyethylene terephthalate (PET) [100], polybutylene terephthalate (PBT) [101] and polyethylene naphthalate (PEN) [102]. All these blends possess a single glass transition temperature. In addition, lowering the glass transition promotes blends melt flow, which enhances processability. Immiscible PEI blends with nylons, polycarbonates and silicone polymers are used to improve the impact strength of PEI, heat resistance, stability in solvents, tribological properties and general processability [103, 104].

PEI products are used as metal, ceramic, wood or other polymers replacements in a wide range of applications. In the automobile industry metallised and light-weight PEI is used as a metal replacement for light reflectors [105], as dielectric and ignition resistance coating material for high voltage wires [106], and in aircraft applications as heat resistant and low smoke interior material [107], but also in various medical applications [108, 109]. In addition, thermoplastic PEI resin can be recycled via re-melting process and re-moulded or extruded.

PEI foams are used as high performance core material for the sandwich panels, with a wide range of applications. Sandwich materials are combining the light-weight of the core foam with outstanding mechanical properties of sheeting materials, i.e. typically carbon fibre reinforced

polymer composites [110]. Such sandwich panels are mainly used in aerospace*, automotive [111], marine industry [112] and other heavy-duty applications [113]. The main method to produce PEI foams is the gas blowing method [52]. One of the well-described approaches is solid-state foaming [114], where the polymer is saturating with invert gas (usually CO₂) under high pressure at room temperature. Here, the gas saturates the polymer phase until the equilibrium concentration has been reached. Afterwards, sudden pressure drops or temperature increase promotes gas expansion inside the polymer matrix. By solid-state foaming, only nanocellular foams can be produced and with increasing polymer wall/part thickness the saturation time also increases. Another similar approach is the solid-state foaming of PEI using supercritical CO₂ at elevated temperatures [63, 115]. In this case, the authors reached a significant reduction of the time to reach gas saturation and deeper gas penetration into the polymer matrix. This method is well-applicable to produce porous PEI beads [116, 117], which are used in polymer bead welding processes. PEI-based polymer blends also provide a possibility to produce foams via gas blowing methods and were successfully reported for PEI/PEEK [18, 118], PEI/polyamideimide [119] and PEI/polysulfone blends [120].

2.4. Polyetheretherketone: Synthesis, Properties, and Applications

Polyetheretherketone or PEEK is a semi-crystalline linear thermoplastic polymer with aromatic rings in the backbone, which are connected by ether- and ketone- groups. This chemical feature is typical for the whole PEAK family, of which PEEK is the most famous member. Due to the inert chemical nature of the polymer backbone, PEEK has extreme temperature stability, high mechanical durability and outstanding chemical resistance. PEEK is a rigid material with a density range from 1260 to 1320 kg/m³, T_g around 143°C, T_m of 343°C, HDT around 152°C, with a continuous usage temperature around 250°C and LOI of 35%. The tensile modulus of the unfilled PEEK is in the range from 3.5 to 4.0 GPa and with tensile strength in the range of 70 to 100 MPa [121]. PEEK has good compatibility with inert fillers, such as carbon and glass fibres which make it a popular matrix choice for high performance thermoplastic composites, or various (functionalised nano-)particles, such as carbon nanotubes, silica dioxide or hydroxyapatite [122-124].

* "LIGHTWEIGHT INTERIOR PANELS WITH ULTEM™ RESIN", link in: https://www.sabic.com/assets/en/Images/Tubus%20Bauer%20Aircraft%20Honeycomb-Core%20Panels%20-%20EN_tcm1010-5346.pdf accessed 13.12.2021, © 2016 Saudi Basic Industries Corporation (SABIC).

The degree of crystallinity of PEEK determines its properties, such as stiffness, chemical and thermal stability. The amorphous phase of PEEK consists of randomly oriented polymer chains, which are less durable than the highly-organised crystalline phase. Industrial or medical grade PEEK has typically degrees of crystallinity in the range from 20 to 40% [125]. Besides crystalline and amorphous phases, PEEK does contain a rigid amorphous phase, which is the intermediate between disordered amorphous and ordered crystalline states. The rigid amorphous phase demonstrates higher mechanical properties than pure amorphous PEEK and tends to crystallise during annealing [126, 127].

PEEK does not dissolve in most common solvents at temperatures below T_g . However, fully amorphous PEEK can be affected by common solvents, such as tetrahydrofuran, acetone, toluene and chloroform, by prolonged exposure and at elevated temperatures. The amorphous phase can swell and soften in N-methyl-2-pyrrolidone, chloroform, and tetrachlorethane [128, 129]. At the same time, the crystalline fraction of PEEK remains stable. PEEK can be only dissolved in high boiling solvents (e.g. diphenyl ketone, diphenyl sulfone, chlorophenols) at temperatures above T_g . In addition, concentrated sulfuric, methylsulfuric and nitric acids can attack PEEK aromatic rings which result in dissolution [130, 131].

PEEK was invented in 1978 and found first commercial applications already in 1981. More recently, after the patent rights expired, PEEK usage in various application fields started growing. However, PEEK synthesis still is a significant challenge for the industry because of its insolubility in common solvents at temperatures below T_g . For successful PEEK synthesis high-temperature aprotic solvents, such as diphenyl sulfone or diphenyl ketone, are required because synthesis takes place at process temperature above 300°C. Moreover, the PEEK synthesis is not a continuous process. All these factors make PEEK a rather expensive polymer [132].

There are two main PEEK synthesis routes – the electrophilic route involves linking ketone and ether groups while in the nucleophilic route aromatic ketones react with ether bonds. PEEK production via electrophilic route has very limited commercial applications because of the strong acid and extreme conditions (**Fig. 15a**). In addition, the resulting product of the electrophilic route requires an additional end-capping agent to prevent crosslinking between chains [133, 134]. The nucleophilic route provides a more straightforward synthesis and involves the reaction of aromatic dihalides with aromatic diphenolates. Solvent selection plays a crucial role – the solvents have to be thermally stable and phenoxide resistant. Diphenyl sulfone is commonly used (**Fig. 15b**) [135].

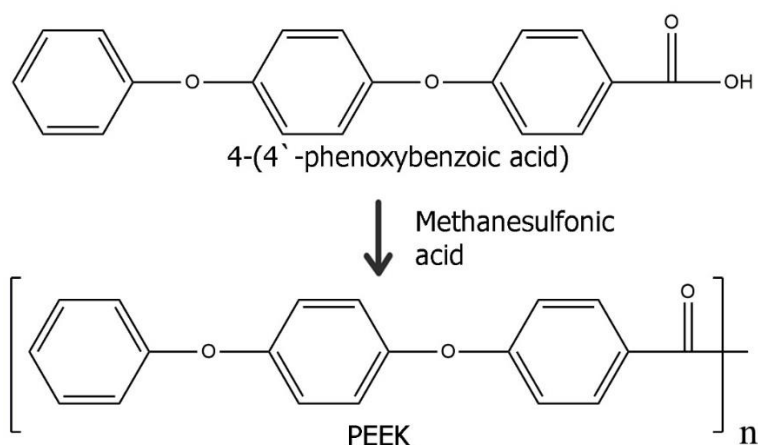


Fig. 15a: The electrophilic PEEK synthesis route (final step, without end-capping reaction).

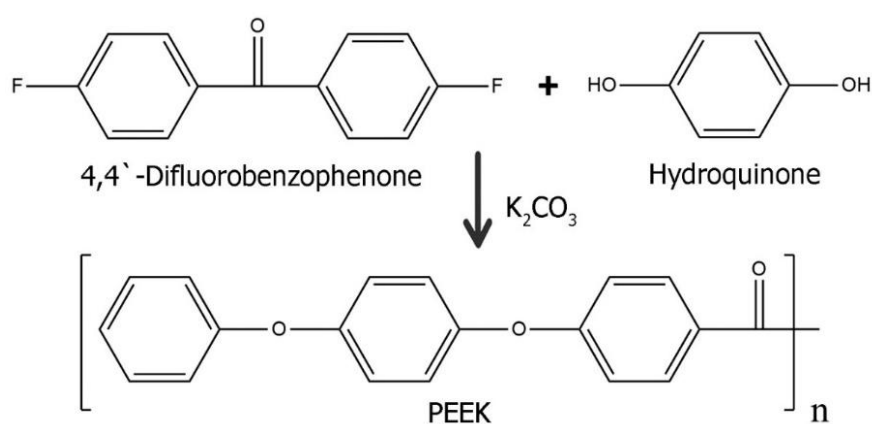


Fig. 15b: The nucleophilic PEEK synthesis route (final step).

Most common thermoplastic processing methods, such as extrusion, injection moulding, melt spinning, laser sintering and machining, are well suited to process PEEK but require process temperatures of around 400°C [136].

The combination of the superior properties of PEEK and high PEEK cost (80-100 US \$/kg) limits the applications of PEEK. It is mainly used in the aerospace industry to replace metals, as thermal insulators and materials for interior because of low smoke generation and high flame retardancy but also for medical applications, for instance as spinal and dental short-term or permanent implants because of its bioinert nature and chemical stability, suitable mechanical properties and good compatibility with reinforcement agents [137-139]. There are numerous other high-value applications, such as electro insulation, thin films and membranes, high duty sealing materials and fitting for precise instruments[†].

[†] "Popular Application of Polyetheretherketone (PEEK)", Link in: <https://omnexus.specialchem.com/selection-guide/polyetheretherketone-peek-thermoplastic/key-applications>, accessed on: 13.12.2021, Copyright © SpecialChem 2021

Introducing porosity into PEEK is a very demanding task, especially when considering the main applications of PEEK. The key advantage of porous materials used in biomedical applications is better implant integration, which is achieved by an increase of the surface/contact area. In the aerospace industry, the introduction of porosity allows to reduce part weight without losing mechanical stability, thermal and chemical resistance.

There are several methods to produce porous PEEK, which are available at industry- or lab-scale. Supercritical carbon dioxide foaming combined with extrusion or injection moulding was used to produce porous PEEK. In the initial step of this process, PEEK is saturated with supercritical CO₂ under high pressure and temperature above T_g . In the next step, the system is depressurized forming CO₂ bubbles which expand creating a microcellular structure [140]. The disadvantages of this method are that only a closed-cell structure can be produced with pore-size limitations, resulting in poor gas permeability through thick polymer walls.

Another method to fabricate porous PEEK is particulate leaching. Dry PEEK powder is mixed with an inert filler material (porogen) and then this mixture is compression moulded above the melting temperature of PEEK, cooled down and the porogen is leached using a suitable solvent (water in case of NaCl). Various substances such as NaCl particles [141], titanium wires [142], hydroxyapatite particles [143] or mixtures of NaCl with hydroxyapatite [144] could be used as porogens (**Fig. 16**). However, particulate leaching has significant disadvantages such as the lack of process versatility, poor pore interconnectivity and issues to remove all encapsulated porogens from the polymer matrix.

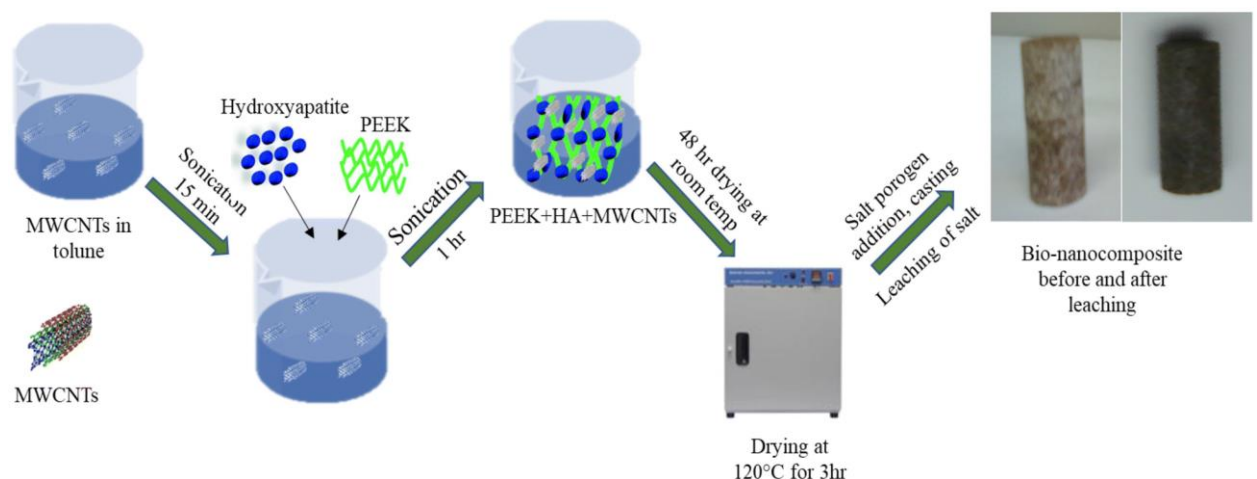


Fig. 16: Schematic of porogen leaching process for the production of porous PEEK [145]. (Link in: <https://link.springer.com/article/10.1007/s40204-019-00123-1>, accessed on 07.12.2021, open access under the terms of the Creative Commons Attribution 4.0 International License).

Particulate leaching was also reported to introduce surface porosity into PEEK. PEEK with an interconnected, thin (less than 1 mm) porous surface layer is widely used to guarantee implant osseointegration [146-148]. Such PEEK biomaterials were commercialised by several companies, including NuVasive and MedShape, for spinal, orthopaedic and bone implants (**Fig. 17**).

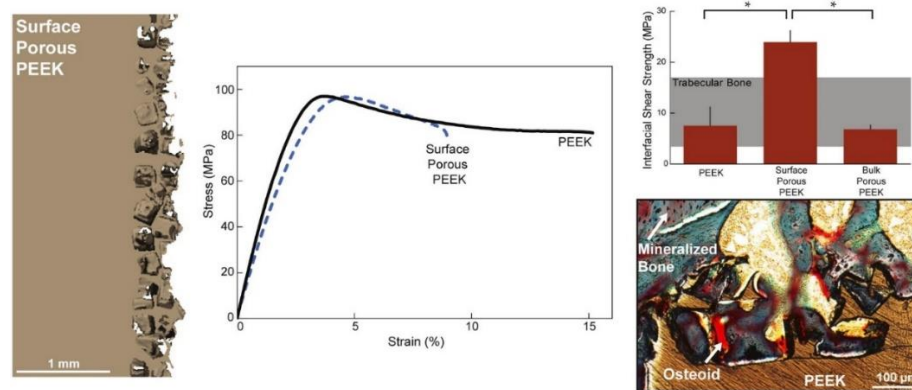


Fig. 17: Picture of the morphology of “surface-porous” PEEK [148]. (Link in: <https://www.sciencedirect.com/science/article/abs/pii/S1742706114005248>, accessed on: 13.12.2021, with permission from Elsevier).

Another approach to porous PEEK is phase separation methods (**Fig. 18**). PEEK is dissolved in suitable solvents and then cast to produce porous PEEK membranes [149, 150]. PEEK can be dissolved homogeneously in specific solvents, such as 4-chlorophenol, at temperatures around the glass transition and porous PEEK was produced by thermo-reversible gelation followed by solvent replacement by ethanol [75]. Another research group produced porous PEEK from PEEK in dichloroacetic acid or 4-chlorophenol solutions by PEEK gelation at various temperatures and times [73, 74, 151].

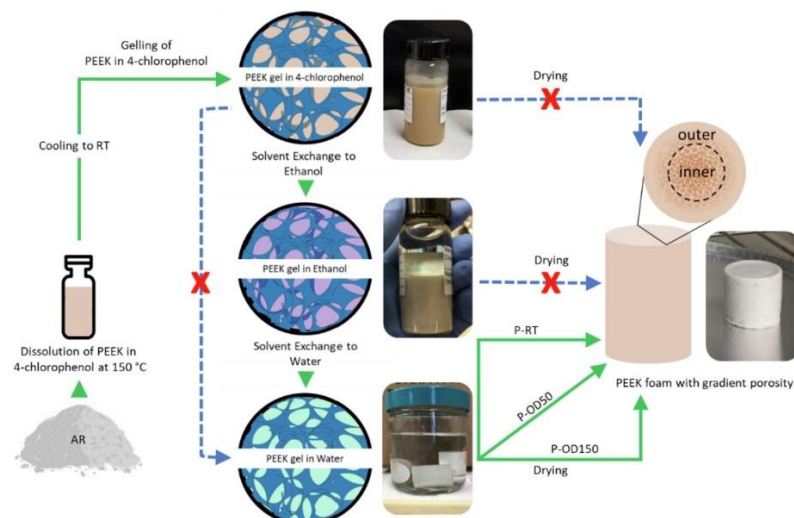


Fig. 18: Schematic of fabrication of porous PEEK using the solvent exchange process [75]. (Link in: <https://www.sciencedirect.com/science/article/abs/pii/S0032386119301971>, accessed on: 13.12.2021, with permission from Elsevier).

2.5. Polyetherketoneketone: Synthesis, Properties, and Applications

Another notable member of the PAEK polymers family is polyetherketoneketone; a linear semi-crystalline thermoplastic polymer with two keto- and one ether- groups attached to benzene rings (**Fig. 19**). PEKK has high thermal stability, superior chemical and outstanding mechanical performance. Most PEKK properties and applications are similar to PEEK. PEKK has tensile modulus of 5.1 GPa, tensile strength of 100-115 MPa, and a continuous usage temperature in the range of 250 – 260°C, HDT around 175°C. The LOI of PEKK is higher than that of PEEK (40%). PEKK has also good biocompatibility and high wear durability and is resistant to most common organic solvents. Semi-crystalline PEKK resist dissolution or swelling in most of the common solvents, however, several chemicals do interact with PEKK: i) halogens, which can halogenate the aromatic ring in polymer backbone, ii) strong concentrated acids (e.g. sulfuric or nitric) can react with carbonyl groups or the aromatic rings, and iii) high boiling aprotic solvents, at temperatures above T_g , do dissolve semi-crystalline PEKK [152].

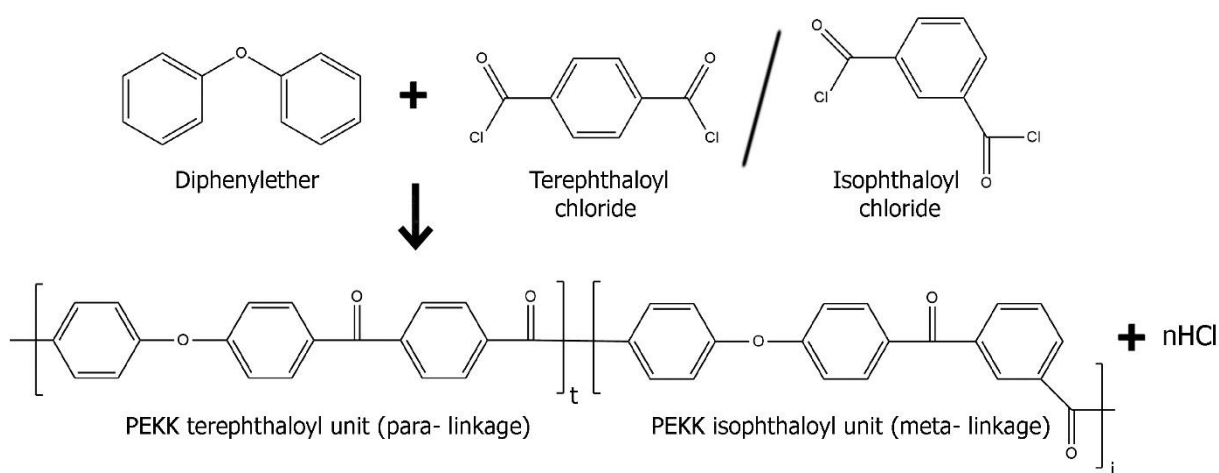


Fig. 19: Schematic of the electrophilic route of PEKK synthesis.

PEKK synthesis was first disclosed by Bonner in 1962 [153]. PEKK was synthesised in inert organic solvent from aryl ethers and polynuclear aromatic hydrocarbons in the presence of a Friedel-Crafts catalyst, in anhydrous conditions and at evaluated temperatures. PEKK can be produced by nucleophilic or electrophilic routes, where the electrophilic route is commercially preferable to nucleophilic because of the complexity of the monomers. PEKK synthesis involves Friedel-Crafts acylation of diphenylether and a mixture of phthaloyl chlorides in presence of aluminium chloride as catalyst (**Fig. 19**). It is possible to control the degree of crystallinity of synthesised PEKK as well as their thermo-mechanical properties by tuning the terephthaloyl (T) and isophthaloyl (I) (T/I) ratio in the phthaloyl chlorides mixture [154]. PEKK with a higher T/I ratio

has higher T_g , T_m , mechanical properties and degree of crystallinity than PEKK with a lower T/I ratio (**Table 1**) [155].

Table 1. Glass (T_g) and melting temperature (T_m), Young's modulus (E) and tensile strength (σ), and degree of crystallinity (χ) of PEKK (Arkema KEPTSAN®)[‡] as a function of the T/I ratio.

Ratio T/I	T_g , [°C]	T_m , [°C]	E , [GPa]	σ , [MPa]	χ , [%]
80/20	165	358	3.8	105-125	33 ± 1
70/30	162	332	3.8	70-110	27 ± 2
60/40	160	305	2.9	88	3 ± 2

The presence of two rigid ketone groups and the linear structure of PEKK connected in *para*-position (terephthaloyl units) results in a significantly higher PEKK chain rigidity, which leads to an increased degree of crystallinity and thermomechanical properties. However, introducing isophthaloyl units into the PEKK backbone results in *meta*-linkages, which disrupt the ordering of polymer chains and reduce T_m but only a minor T_g drop [155, 156]. Moreover, PEKK possesses crystalline phase polymorphism, where PEKK containing only *para*- units crystallised from the melt, has a crystalline structure similar to PEEK, which is called Form 1. The second crystalline structure (Form 2) can be obtained via solvent or cold crystallisation from the amorphous PEKK phase, which has lower thermomechanical properties than Form 1 [157].

Neat PEKK but also PEKK composites found applications in aerospace (as interior components, panels and fitting), in transport and automotive (metal-parts replacement, gaskets and sealing rings), oil and gas (sensor housings, pump components, connectors) industries. PEKK is also used for electronic device components and food processing equipment. PEKK has more notable biomedical applications; PEKK is used as short- or long-term body implant, surgery and dental instruments, tubing, catheters and as inert coating [158-160].

Due to the higher rigidity and processing temperature, the production of porous PEKK is even more difficult than porous PEEK, which is also a non-trivial industrial task. Porous PEKK is of interest for the same reasons as for PEEK – decreasing the price and material consumption; producing light, durable and thermochemically stable materials for aerospace application; or porous or surface-porous materials for biomedical applications (with enhanced

[‡] “Kepstan® PEKK Resins for Extremely Demanding Applications” Link in: https://www.extremematerials-arkema.com/en/product-families/kepstan-pek-polymer-range/?_ga=2.181005797.338711531.1639587492-1172189789.1638961445 accessed on 18.01.2022.

osseointegration). One of the possible approaches to produce porous PEKK is the use of the combination of compression moulding and particle leaching methods (**Fig. 20**). PEKK powder and leachable porogen (for example NaCl or hydroxyapatite beads) are mixed and then moulded under elevated pressure and temperature close to PEKK T_m , porogen leaching follows using water or acids that do not affect PEKK [161, 162]. In addition, the osseointegration with porous PEKK can be improved by subsequent surface treatment or the introduction of hydroxyapatite whiskers into the porous PEKK matrix [144, 163, 164]. Another foaming approach reported was based on the sulfonation/desulfonation of PEKK; during desulfonation a hydration induced foaming process takes place and resulting in flexible porous PEKK [165]. Gas blowing in combination with compression moulding is another possible method to produce a porous PEKK/PBZT (polyphenylenebenzobisthiazole) blend [166].

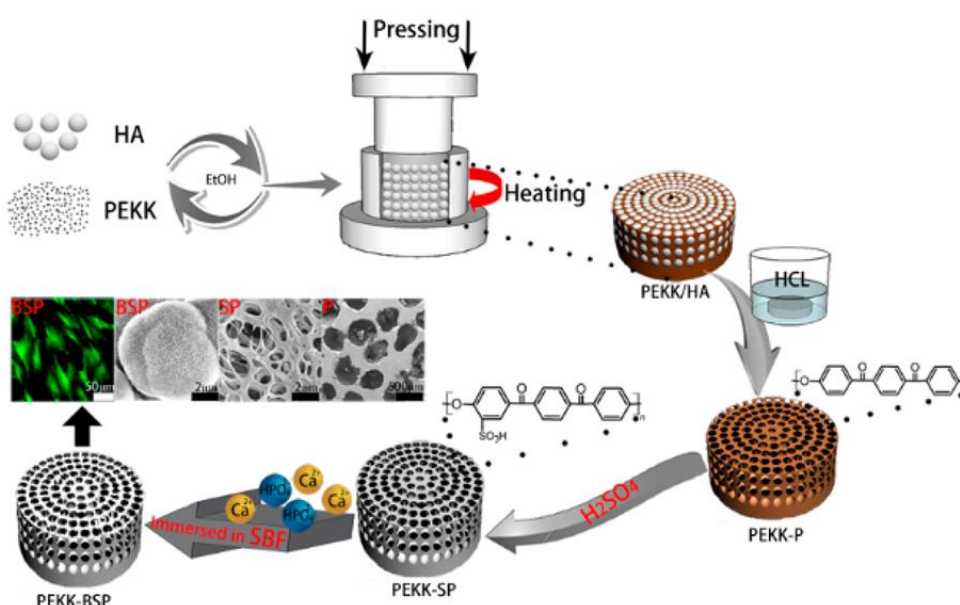


Fig. 20: Schematic of the production of porous PEKK (with subsequent surface treatment) preparation via compression moulding and porogen leaching [161]. (Link in: <https://pubs.acs.org/doi/10.1021/acsbiomaterials.6b00103>, accessed on: 08.12.2021, open access under the terms and conditions of the Creative Commons Attribution (CC BY) license).

2.6. Thermally Induced Phase Separation

Thermally induced phase separation (TIPS) as a method to produce porous membranes was introduced in 1981 by Castro [167]. In the 1980-90s the method has been used and further developed because of its process simplicity, universality, ability to control the pore morphology of porous polymers and the possibility to apply it to various polymers and polymer blends. TIPS has been mainly used to produce filtration membranes, tissue engineering scaffolds, hollow fibre membranes and separators for electrochemical cells (**Fig. 21**) [168].

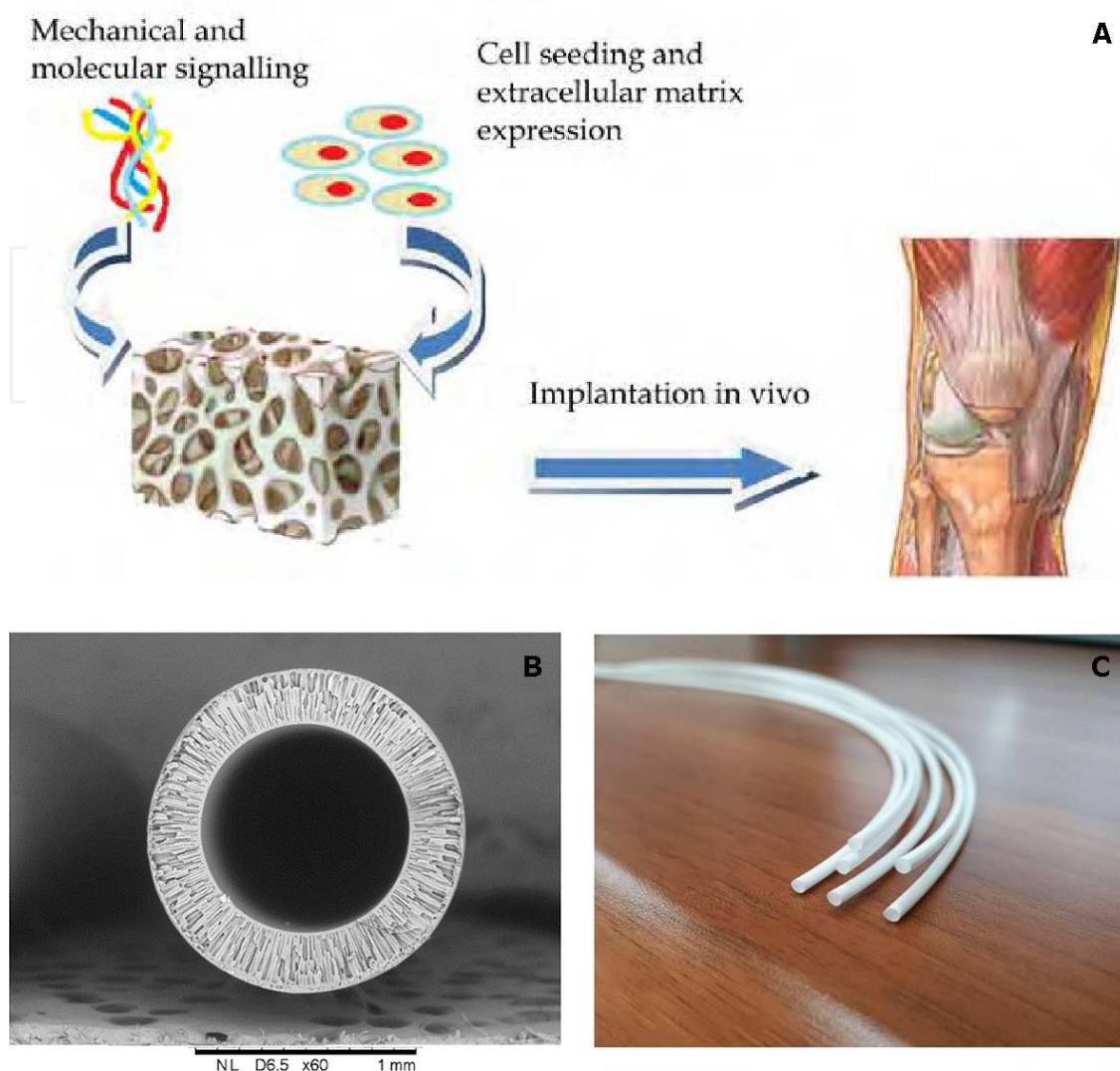


Fig. 21: Examples of applications of porous polymer products made using the TIPS process: schematic representation (A) of artificial scaffolds for tissue engineering [70] (Link in: <https://www.intechopen.com/chapters/23660>, accessed on 16.12.2021, open access under the terms and conditions of the Creative Commons Attribution (CC BY) license); cross-sectional (B) and general view (C) of hollow fibre membranes for gas-liquid separation [169] (Link in: <https://www.mdpi.com/2079-6439/6/4/76/htm>, accessed on: 16.12.2021, open access under the terms and conditions of the Creative Commons Attribution (CC BY) license).

In contrast to other phase inversion methods, such as non-solvent or vapour induced phase separation, where the main driving force for polymer phase separation is the solution composition, in TIPS the driving force for phase separation is temperature. All polymer phase separation methods are based on the phenomenon that polymer solubility is a function of solution composition (addition of a non-solvent) or condition (temperature). The typical TIPS implementation includes the following steps [55]:

1. Dissolve a polymer in a suitable low molecular weight inert solvent or solvents mixture until a homogeneous polymer solution is achieved. The dissolution occurs at room or elevated temperature but below the boiling point of the solvent(s).
2. The homogeneous polymer solution (dope) is cast into the desired shape and cooled at a controlled cooling rate to induce liquid-liquid (L-L) or solid-liquid (S-L) phase separation. In this step, the dope is phase separates into a polymer-rich and polymer-poor phases.
3. The solvent entrapped in the polymer-rich or solidified phase (in case the solvent crystallised), is removed by solvent extraction or lyophilisation to obtain a porous polymer material.

In comparison to other phase inversion methods, TIPS provides the following benefits: i) it can be applied to a wide range of polymers, including semi-crystalline polymers, ii) possibility to tune and control the porosity, pore size and pore morphology of the resulting porous polymer, iii) the application is limited only by choice of solvent or solvents mixtures for the selected polymer, iv) capability to produce flat (2D: membranes), bulk (3D: scaffolds) and porous polymer fibres (1D) with controllable pore structure and porosity. The main limitation of the TIPS method is the polymer solubility in a chosen solvent as the polymer has to dissolve without being degraded or modified (by chemical reactions) at concentrations high enough to enable the production of robust and durable porous materials [170].

A typical temperature-polymer concentration phase diagram of a polymer-solvent system for liquid-liquid (L-L) and solid-liquid (S-L) demixing is presented in **Fig. 22**. The binodal curve represents the thermodynamic equilibrium border; in the region above the polymer solution is homogeneous and stable, while below the spinodal curve the solution becomes unstable. In this region the phases are immiscible and phase separation occurs. The area between binodal and spinodal curves is called the meta-stable region, where phase separation is thermodynamically preferable but kinetic factors are obstructing the process. The point where spinodal and binodal curves intersect is called the critical point [171].

In TIPS L-L phase separation takes place as a consequence of the thermodynamic instability of a polymer solution, which is induced by lowering the temperature. If a homogeneous polymer solution with a temperature and concentration close to the critical point is cooled down, the solution passes directly into the unstable region without crossing the metastable region (**Fig. 22**: point A → B). Such a phase separation process is called spinodal decomposition and the resulting porous polymer has a regular, uniform pore size and highly interconnected structure [172].

However, when a homogeneous polymer solution passes through the metastable region during cooling, demixing occurs by nucleation and growth. During phase separation induced by cooling, in the case when the polymer fraction is much below the critical point, the polymer-rich phase will form bead-shaped or a mechanically fragile porous network (**Fig. 22**: point $D \rightarrow P$). When the polymer fraction is higher than the critical point, the polymer-poor phase forms separated droplets and the resulting porous polymer exhibits an interconnected structure with a non-homogeneous pore morphology (**Fig. 22**: point $E \rightarrow R$). Droplets, formed due to the demixing process, are growing driven by the concentration gradient aiming to minimise the interfacial energy [173]. The thermodynamics and kinetic of demixing is beyond the scope of my thesis but the interested reader is referred to [174].

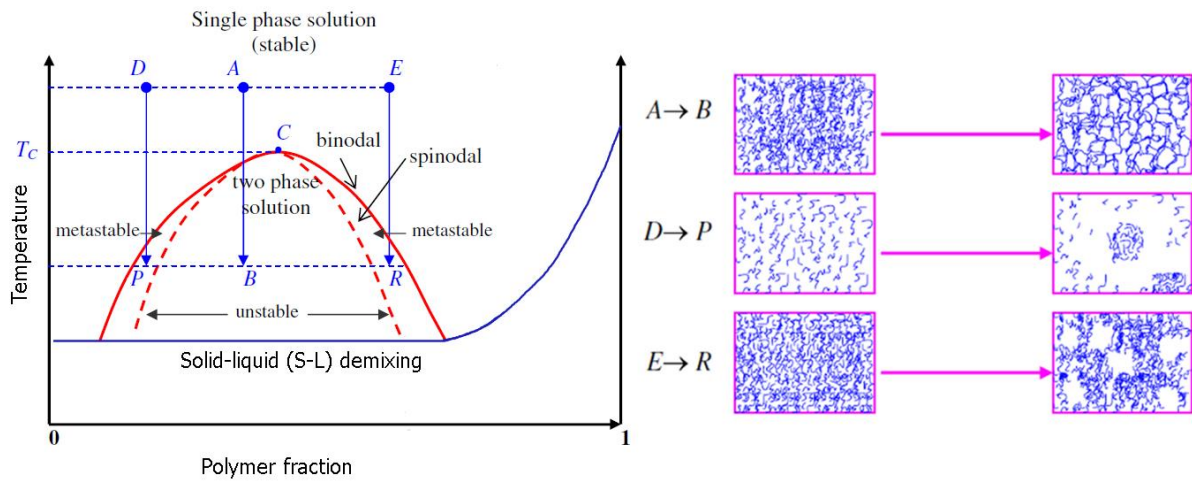


Fig. 22: Schematic phase diagram of a polymer-solvent system. The polymer fraction is plotted as a function of temperature (left image): C is the critical point. Schematic of phase demixing and the resulting pore morphology: $A \rightarrow B$ is the spinodal decomposition; $D \rightarrow P$ the nucleation and growth of the polymer-poor phase at a polymer fraction below the critical point; $E \rightarrow R$ nucleation and growth of the polymer-rich phase occurring at a polymer fraction above the critical point (right image). (Copied and modified from [171] with permission of Elsevier Books).

In S-L demixing, two cases are possible: i) polymer crystallisation from solution occurs due to the decreasing temperature or ii) solvent solidification or crystallisation occurs prior to polymer crystallisation. In the first case, when the temperature of the solution decreases below the polymer crystallisation temperature, polymer crystallisation becomes thermodynamically preferable. Polymer crystallisation can occur under isothermal or non-isothermal conditions. The resulting pore morphology depends on many factors, such as polymer concentration, kinetic aspects due to the crystal formation process (such as stirring), crystallisation time, etc. [175].

In case, S-L demixing is induced by solvent solidification/crystallisation the temperature gradient is crucial. Using the temperature gradient in the polymer solution it is possible to initiate directional (for example bottom-to-top) freezing, which allows to control of the resulting pore morphology. The resulting porous polymers possess a strongly-oriented ladder or micro-tubular morphology (Fig. 23). By adjusting the polymer concentration, it is possible to control the porosity, and by changing the temperature gradient the diameter of microtubes [176, 177].

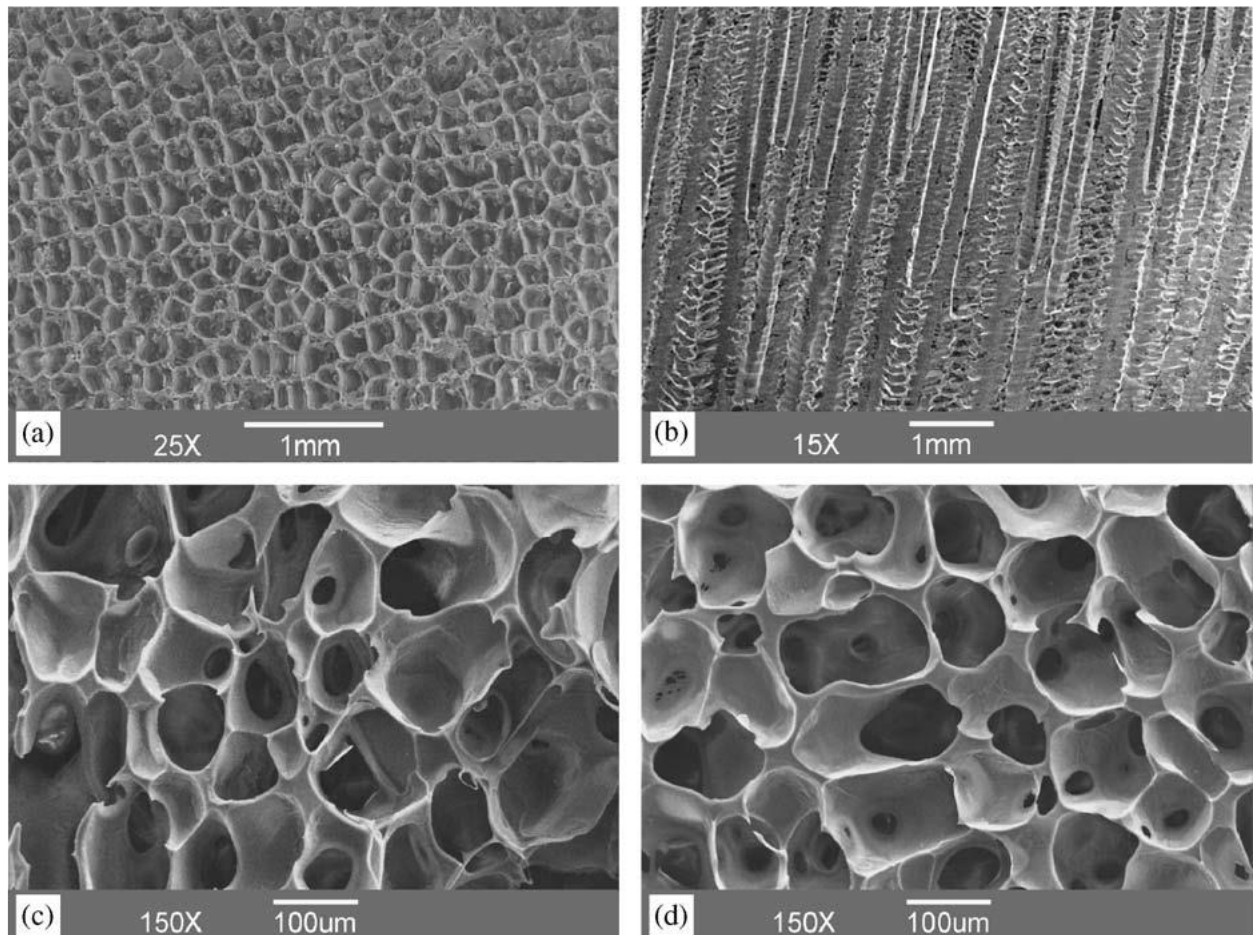


Fig. 23: Characteristic images of tissue engineering scaffolds made from poly(lactic-co-glycolic acid) (PLGA): (a) cross-section of microtubular structure of the PLGA scaffold and (b) vertical section, as well as a PLGA scaffold with an isotropic pore structure (c) cross-section and (d) vertical section [177]. (Link in: <https://www.sciencedirect.com/science/article/abs/pii/S0142961206004728>, accessed on 16.12.2021, with permission from Elsevier).

Chapter 3. Experimental

3.1. Materials and methods

PEEK (APC-2, Victrex) and PEKK powders (Cytec Engineered Materials, now Solvay group) with average particle sizes around 145 μm and 50 μm were kindly provided by Cytec. Cylindrical PEI (~ 2-3 mm height, ~ 1 mm diameter) pellets were purchased from Sigma Aldrich. All HPPs were dried in a vacuum oven at 80°C for at least 24 h prior to processing and/or characterisation. 4-Phenylphenol (97 % purity, $T_m \sim 166^\circ\text{C}$, $T_b \sim 321^\circ\text{C}$), 9-fluorenone (98% purity, $T_m \sim 86^\circ\text{C}$, $T_b \sim 342^\circ\text{C}$), diphenyl sulfone (97% purity, $T_m \sim 126^\circ\text{C}$, $T_b \sim 379^\circ\text{C}$) and diphenyl ketone (99% purity, $T_m \sim 48^\circ\text{C}$, $T_b \sim 305^\circ\text{C}$) were purchased from Sigma Aldrich and used as received.

3.2. Characterisation of (porous) high performance polymers

3.2.1. Density (absolute and foam) and porosity

Absolute or skeletal density (ρ_s) of the resulting (porous) HPPs was determined by gas (helium) displacement pycnometry (AccuPyc II 1340, Micromeritics Ltd, Norcross, USA). Using the pycnometer the absolute volume (V_s) of the material was determined by measuring the gas pressure inside the measuring chamber using the ideal gas law. Porous HPP samples with a total mass from 0.2 till 0.4 g were cut, broken or torn into pieces or fibres with at least one side not more than 10 mm from different spots of a sample. Samples were moved into the 3.5 cm^3 aluminium measurement chamber using tweezers. The final absolute density was calculated from sample mass (determined using Sartorius Cubis® MCA225P (Sartorius Weighting Technology GmbH, Goettingen, Germany) with an accuracy of 0.05 mg and measured sample volume.

Bulk or foam density (ρ_f) was determined using a density analyser (GeoPyc 1360, Micromeritics Ltd., Norcross, USA), which is measuring the envelope volume by solid medium displacement. Small, rigid spherical particles (DryFlo™, Micromeritics Ltd., Norcross, USA) with a narrow size distribution are used as a medium, which are compacted near the porous sample surface without invading into its pores.

At the first step of measurement, the sample cell is filled with dry medium and compressed using a plunger at constant force to compact the medium to determine the initial height of the compacted medium (h_0). Afterwards, pre-dried porous HPP sample with a size around 10 x 10 x 10 mm^3 was placed into the measuring cell and recompactd at the same compaction pressure.

The resulting height difference (h_t) and initial height (h_0) are used to calculate the displacement volume ($\Delta h = h_t - h_0$), which is then used to calculate the sample volume calculation:

$$V = \pi r^2 h \quad (\text{Eq. 1}).$$

At least three pieces were taken from the central part of each porous HPP sample for reproducibility.

The resulting porosity of porous HPP was calculated from the skeletal and foam densities for each sample using the following equation (Eq. 2):

$$P = \left(1 - \frac{\rho_f}{\rho_s}\right) \quad (\text{Eq. 2}).$$

3.2.2. Pore morphology

The pore morphology was investigated using scanning electron microscopy (SEM). In the case where magnification was up to 3000x, the benchtop SEM (JCM-6000, JEOL Ltd., Japan) was used. In the case where a magnification up to 15000x was required a high resolution SEM (CARL ZEISS SUPRA VP55, CARL ZEISS AG, Germany) was used. In both cases, an identical sample preparation procedure was used. From each porous HPP, a small piece with a length around 10 mm and 1-2 mm thickness was cut (using a sharp blade) or broken and then fixed onto a conductive cylindrical sample holder using conductive adhesive tape. To increase the conductivity between sample and adhesive tape, liquid silver paint (Achseon 1415 G 302, Agar Scientific, UK) was applied around the sample borders. Then the samples were sputtered with a thin gold layer in an argon atmosphere using a gold-coater (JFC-1200, JEOL Ltd, Japan). SEM images were taken from various places of the sample, with a wide range of magnifications and voltages from 5kV to 15 kV.

The specific surface area and pore size distribution of porous HPP samples were determined from nitrogen adsorption isotherms measured at 77 K using a surface area and porosity analyser (TriStar II 3020, Micrometrics Ltd., Norcross, USA) by applying Brunauer–Emmet–Teller (BET) and Barrett-Joyner-Halenda (BJH) methods. Initially, HPP samples were grinded or cut into 1-2 mm size pieces, weighted (the sample mass should be at least 0.2-0.3 g) and placed inside the measurement glass tube with a bulb-shape vial at the end. Then, the glass tube with the sample inside was placed for drying at 100°C with active nitrogen flow for 12 h into a (FlowPrep™ 060) sample preparation device. Afterwards, the sample tube with the sample was installed into the surface area analyser to measure N₂ adsorption isotherms in a relative pressure ($\frac{p}{p_0}$) range from 0.29 kPa to 97.12 kPa.

Due to the measurement, an adsorptive (nitrogen in my case) is applied to the sample at controlled conditions (temperature and pressure). After changing the adsorptive amount, the pressure in the sample vial is equilibrated and the amount of adsorbed/desorbed gas is recorded and plotted as adsorption/desorption isotherm (**Fig. 24**). The resulting isotherm was used to define the quantity of adsorbent required to form a monolayer. Afterwards, the surface area of porous HPP samples was determined using the BET equation (**Eq. 3**):

$$\frac{1}{x \left[\left(\frac{p_0}{p} \right) - 1 \right]} = \frac{1}{X_m C} + \frac{C-1}{X_m C} \left(\frac{p}{p_0} \right), \quad (\text{Eq. 3})$$

where X is the monolayer capacity, $\frac{p}{p_0}$ the relative pressure, X_m the volume of gas adsorbed by the sample surface and C a constant. The specific surface area, specific pore volume and pore size distribution can be determined using adsorption/desorption values obtained via surface area measurement using the modified Kelvin equation (**Eq. 4**):

$$r_p = r_k + t, \quad (\text{Eq. 4})$$

where r_p is the actual pore radius, r_k is the pore size calculated by Kelvin equation (**Eq. 5**) and t is the adsorbed layer thickness.

$$\ln \frac{p}{p_0} = \frac{-2\gamma V}{rRT} \cos \theta, \quad (\text{Eq. 5})$$

where $\frac{p}{p_0}$ is the relative pressure, γ the surface tension, r pore size radius, θ contact angle and V is the molar volume of the gas.

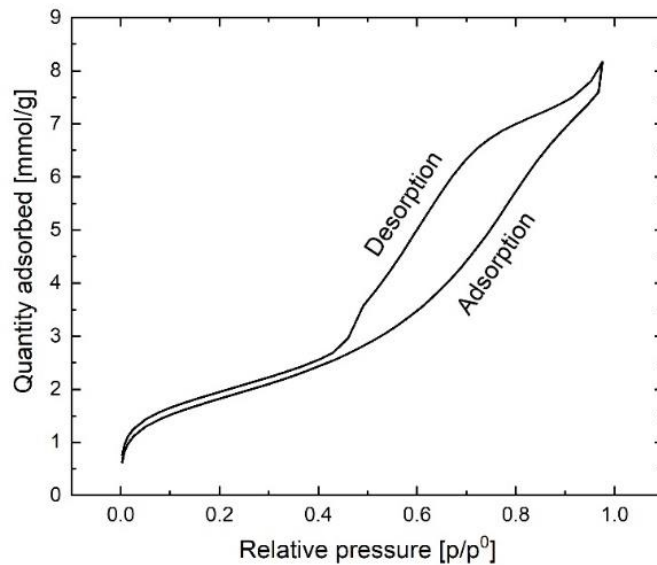


Fig. 24: Adsorption/desorption isotherm exemplarily shown for porous PEEK produced by HT-TIPS.

3.2.3. Mechanical (compression) properties

Mechanical properties of the porous HPP samples were measured according to ISO 844:2001 standard, which was adapted for my HPP samples. A dual-column universal testing machine (Instron 5969, Darmstadt, Germany) with a 50 kN load cell was used to measure stress-strain curves in compression. Original porous HPP samples were cut into several rectangular samples with dimensions of 10 x 10 x 10 mm³ using a band saw (PROXXON MBS 240/E). After cutting, the resulting cubes were mechanically polished (DREMEL 3000) to obtain flat and parallel sample surfaces. Fine-grained sand paper (P1500-2000) was used for surface finalisation. Samples with obvious cracks, surface heterogeneity, non-flat parallel surfaces or mechanically fragile samples were excluded from the measurements. At least 5 cubic samples for compression tests were used from each porous HPP sample. Each sample was tested at a compression speed of 1 mm/min and compressed to 75% of the initial height. The engineering stress-strain curve was recorded for each sample. The linear region of the curve was used to determine Young`s modulus and crush strength (Fig. 25).

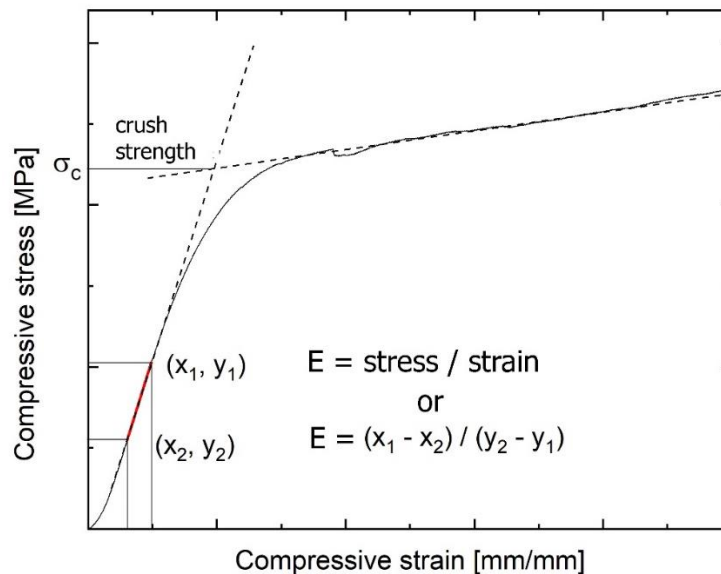


Fig. 25: Illustration of the determination of compression (crush) strength and Young`s modulus from a strain-stress curve.

3.2.4. Thermal properties and degree of crystallinity

The thermal properties and degree of crystallinity were examined by differential scanning calorimetry (DSC, Discovery series, TA Instruments) and Flash DSC (Mettler Toledo Flash DSC 2+, with UFS 1 MEMS sensors). Classic DSC measures the heat flux required to change the temperature of a sample compared to a reference (empty DSC pan). Flash DSC uses ultrafast

scanning rates (more than 100 K/s) which allow to obtain very accurate materials response without provoking material changes during the scanning procedure.

For classical DSC analysis 2-10 mg of pre-dried porous HPP sample was placed into an aluminium pan (TA Tzero Pan, TA Instruments, Switzerland) and closed with an aluminium lid (TA Tzero Lid, TA Instruments, Switzerland) with a small hole. Each sample was investigated by two heating and two cooling runs (heating-cooling-heating-cooling sequence) in a temperature range from 50 to 400°C at a scanning rate of 10 K/min. The degree of crystallinity was calculated from the peak melting enthalpy (ΔH_f^{peak}) of the first heating run (**Fig. 26**) by next equation (**Eq. 6**):

$$X_{DSC} = \frac{\Delta H_f^{peak}}{\Delta H^0}, \quad (\text{Eq. 6})$$

where ΔH^0 is the theoretical melting enthalpy of a fully-crystalline PEEK or PEKK (130 J/g) [178].

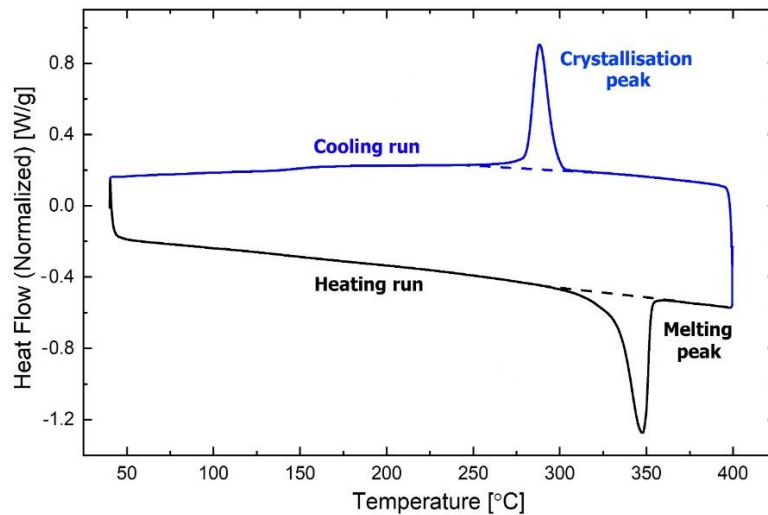


Fig. 26: Illustration of the evaluation of the degree of crystallinity from the melting peak(s) on DSC curve.

For Flash DSC the mass of the selected samples ranged from 5 to 700 ng with the scanning rate of 500 K/s. To create fully amorphous PEEK and PEKK by melting and subsequent quenching, a cooling rate of 5000 K/s was used. The mass of the analysed samples was calculated by the following equation (**Eq. 7**):

$$m_{FDSC} = \frac{\Delta\phi_\beta}{\beta \Delta c_p}, \quad (\text{Eq. 7})$$

where $\Delta\phi_\beta$ is the step of the heat flux at the T_g for a specific heating rate β , Δc_p the change in heat capacity for a fully amorphous sample at the T_g as defined from standard DSC and m_{FDSC} the mass of the FDSC sample.

Chapter 4. Results and discussion

4.1. High-Temperature Thermally Induced Phase Separation Process

4.1.1. Experimental Setup

A high temperature thermally induced phase separation (HT-TIPS) process for the production of monolithic porous high performance polymers was developed (**Publication 1**). A schematic of the process can be seen in **Fig. 27**. A double-walled, round bottom borosilicate glass vessel with an inner volume of 250 ml (GlassKeller, Basel AG, Switzerland) was used as a heating vessel for the HT-TIPS process (1). A two-necked glass cap with a flat ground-glass joint (DN 60) was used as vessel cover. A thermometer (Erbo TFX 410, Ingolstadt, Germany) with a 109 mm metal sensor and accuracy $\pm 0.1^\circ\text{C}$ was passed through one of the glass cap necks and placed into the sample to control its temperature (2). The assembled glass vessel was mounted in a vertical position and fixed on a stand. The vessel was connected by one-meter temperature-insulated hoses to a closed-bath (4), high temperature thermostat (Huber Unistat T305W HT, Germany) with PILOT ONE control unit (6). The thermostat was also connected to tap water for active water cooling, which allows for precise control of heating and cooling procedures (5). The thermostat has an inner thermosensor to control the temperature of the heat transfer fluid (DW-Therm HT, Huber, Germany). A glass-covered magnetic stirring bar with a length of 1 or 2 cm and basic heating plate (IKA RCT) were used for active mixing. A 50 mL borosilicate glass beaker placed inside the glass vessel was used as a mould during the HT-TIPS process (3). 250 ml round-bottom borosilicate vessel equipped with 100 ml Soxhlet extractor and glass coiled condenser were used for solvent extraction to remove the solidified solvent.



Fig. 27: HT-TIPS setup. On the left figure: glass vessel (1), thermometer (2), 50 mL glass beaker with polymer/solvent solution (3), high temperature hose connectors (4). On the right: pipes connected to tap water (5), Huber Unistat T305W HT thermostat with PILOT ONE control unit (6).

4.1.2. Preparation of porous high performance polymers

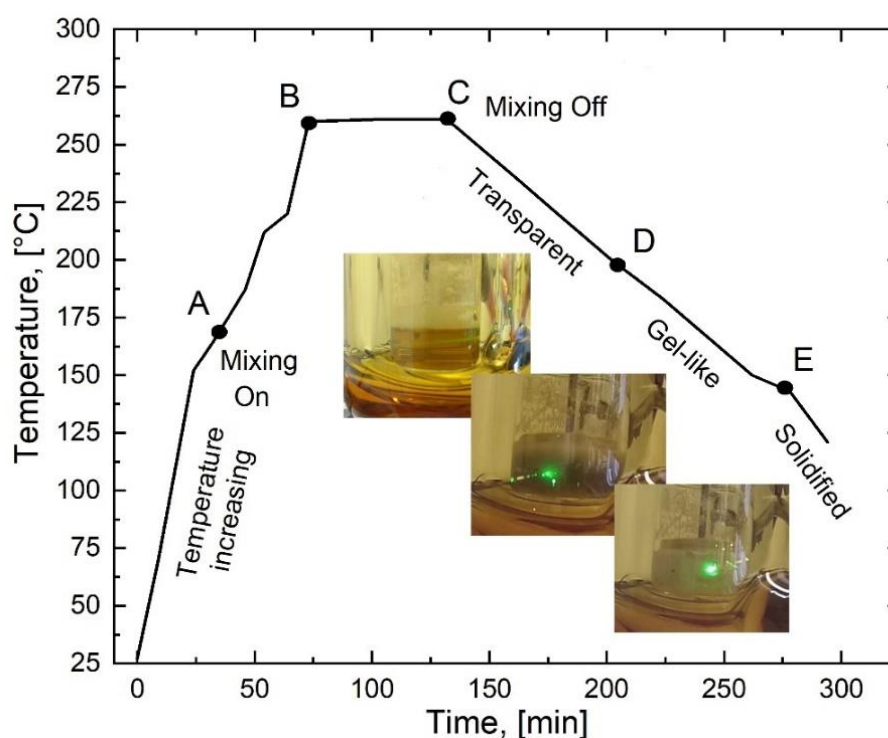


Fig. 28: Schematic representation of the fabrication of porous HPP samples using HT-TIPS process. The heating/cooling profile of 20 wt.% of PEEK in 4PPH with a cooling rate of 1°C/min was used as process example.

A certain amount of HPP powder or pellets (for PEI) and the chosen solvent were mechanically mixed inside a 50 ml borosilicate glass beaker (**Fig. 27, 3**), then a glass-coated magnetic stirrer was added into the polymer/solvent dry mixture. The beaker with the polymer/solvent mixture was placed into the glass vessel connected to the thermostat (**Fig. 27, 1**), sealed with a glass cup with a mounted thermometer (**Fig. 27, 2**). Then, the temperature inside the glass vessel was increased until the solvent melting point (**Fig. 28, point A**). When the whole amount of the solvent was liquid, stirring started on and the temperature was increased to the next point (**Fig. 28, point B**). At this temperature, stirring continued for a certain amount of time (**Fig. 28, point B→C**), which was empirically determined for all polymer/concentration/solvent combinations (**Table 2**), until a transparent solution was obtained, which was confirmed using a green laser pointer. Stirring was stopped (**Fig. 28, point C**), the magnetic stir bar was removed from the solution and the solution cooled at the chosen cooling rate. In a specific temperature range, the solution lost transparency due to polymer gelation/precipitation (**Fig. 28, point D**) and subsequent solvent solidification/crystallisation (**Fig. 28, point E**) or solvent solidification/crystallisation prior to polymer gelation/precipitation (**Fig. 28, point E, with passing through point D**). After solvent solidification, the vessel temperature continued to decrease at the same cooling rate for 15-20

min. Afterwards, the resulting sample was removed from the beaker and placed into a Soxhlet apparatus to extract the solidified solvent using ethanol for 24-48 h, which was followed by drying in a vacuum oven at 60°C for 12-24 h.

Table 2: Clear point solution temperatures for PEEK, PEKK and PEI as a function of polymer concentration and solvent nature.

Polymer	[Polymer] wt.%	Clear solution temperature, °C			
		4PPH	9FN	DPK	DPS
PEEK	10	260±4	n/a	n/a	n/a
	20	261±3	n/a	n/a	n/a
PEKK	10	244±5	252±3	270±1	265±3
	20	258±9	270±1	n/a	n/a
PEI	10	198±12	176±3	215±5	227±4
	20	200±11	202±10	214±7	230±1
	30	221±12	206±5	n/a	n/a

4.1.3. Solid-liquid demixing during the HT-TIPS process

Two types of demixing were observed during the cooling process, which were determined by two main factors – solvent melting point and polymer concentration in solution. As an example consider the following; PEKK with the same concentration (10 wt.%) dissolved in 4PPH or 9FN and cooled at the same rate of 1°C/min results in two different types of demixing (**Publication 3**):

- in 4PPH ($T_m \approx 168^\circ\text{C}$), the solvent reached its solidification temperature before the temperature at the PEKK solubility decreased enough for polymer gelation or precipitation and, therefore, solvent solidification occurs rapidly and follows the direction of temperature gradient in solution (usually from bottom to top). During solidification, the solvent creates directional pores having the orientation of solidification front. The freezing forces the dissolved polymer out resulting in a pore pattern defined by frozen solvent.
- in 9FN ($T_m \approx 84^\circ\text{C}$), PEKK gelation occurs at a temperature around 185°C, which is much higher than the solvent solidification temperature. The demixed, gelated PEKK has sufficient time to phase separate prior to solvent solidification resulting in a more homogeneous (isotropic) pore morphology.

Selecting a solvent with a higher melting point for the HT-TIPS process will result in solid-liquid demixing in which solvent crystallisation occurs prior to polymer gelation or precipitation and vice versa. However, increasing the polymer concentration shifted the polymer solidification/precipitation point to higher temperatures, which leads to solvent solidification after polymer gelation/precipitation. The polymer concentration effect is described in detail in **Publication 2** (for 5 and 20 wt.% solutions of PEEK in 4PPH) and **Publication 3** (for 10 and 20 wt.% of solutions of PEKK in 4PPH). Solvent solidification (especially when using the solvent 4PPH) did affect the resulting morphology of the produced porous polymers, which is described in **Publication 2** (for 5 and 10 wt.% solutions of PEEK in 4PPH).

4.2. Solvent selection for production of porous PEI, PEEK and PEKK

Four aprotic high boiling solvents (**Fig. 29**), namely diphenyl ketone (DPK), diphenyl sulfone (DPS), 4-phenylphenol (4PPH) and 9-fluorenone (9FN) were chosen as potential universal solvents for PEI, PEEK and PEKK. The solvents selection was based on Beck's [130] research, their commercial availability and the maximum acceptable temperature, which should not have exceeded 300°C because of thermostats maximum operating temperature. The solvents have a relatively similar chemical structure, which is also close to the structure of PEAKs, following the general solubility principle "like dissolve the like".

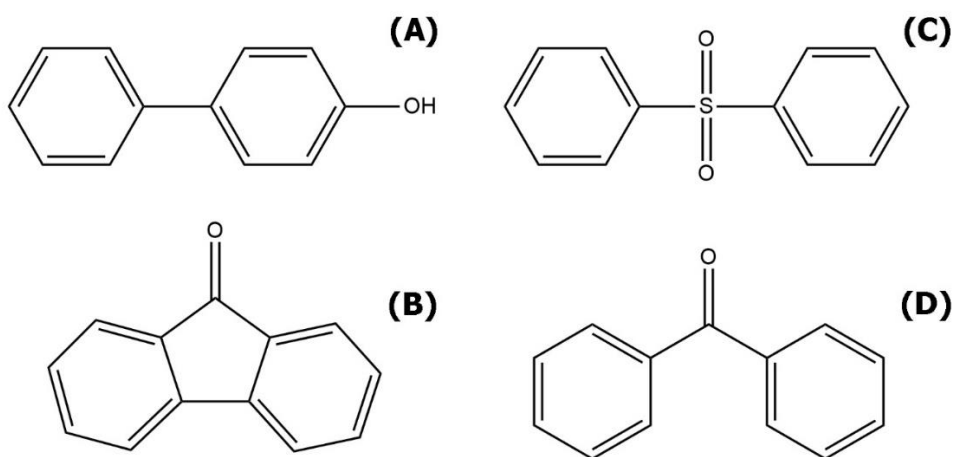


Fig. 29: Chemical structure of the selected solvents, where A is 4-phenylphenol, B is 9-fluorenone, C is diphenyl sulfone and D is diphenyl ketone.

However, not all selected solvents were shown to be suitable solvents for the HT-TIPS process. Several aspects for useful solvents for the HT-TIPS process were identified: i) the temperature limitation (300°C) of the thermostat and natural heat loss in the glass vessel, limited the maximum reachable temperature inside the vessel to 270°C; ii) even though the boiling points of all solvents were higher than 300°C, already at temperatures above 240-250°C with active mixing

(using a magnetic stirrer), the solvents started to evaporate from the polymer solution and recondensed on the glass cup and the vessel walls. As a consequence, the solvent concentration in the solution decreased, which resulted in a reduction of the polymer solubility. Long dissolution times also reduced the chance to obtain homogeneous polymer solutions if the selected solvent evaporated; iv) if only low polymer concentrations could be dissolved in a solvent, the resulting porous polymers lacked mechanical stability and thus could not be characterized. These observations resulted to established the following criteria for successful HT-TIPS processes for the chosen HPPs:

- The dissolution process should be as fast as possible
- The process temperature should be as low as possible and not exceed 270°C
- The optimal polymer concentration for the TIPS depends on the polymer-solvent pair.

4PPH, 9FN, DPK and DPS were tested as solvents for polyetherimide (PEI) in the HT-TIPS process. The (partially) successful production of porous PEI using HT-TIPS from 20 wt.% solutions of PEI in 4PPH was already described in **Publication 1**. In the following, I will describe the production of porous PEI using HT-TIPS from four different solutions with PEI concentrations of 10, 20 and 30 wt.% at a cooling rate of 1°C/min. The temperature at which PEI solutions became transparent is called “clear solution point” and the point at which the solutions lost transparency during cooling due to polymer solidification “cloud point” (see **Table 3**).

Table 3: Clear solution and cloud points for PEI in 4PPH, 9FN, DPK and DPS solutions.

	4PPH			9FN			DPK		DPS	
PEI, wt.%	10	20	30	10	20	30	10	20	10	20
Clear solution point, °C	198±12	200±11	221±12	176±3	202±10	206±5	215±5	214±7	227±4	230±1
Cloud point, °C	n/a	n/a	n/a	113±12	143±6	167±13	169±13	186±6	183±4	204±5

PEI could be dissolved up to concentrations of 30 wt.% in both 4PPH and 9FN requiring about the same temperatures; however, increasing PEI concentrations required higher temperatures to reach the clear solution point (**Table 3**). The important difference between 4PPH and 9FN was the presence of a cloud point in all 9FN solutions, which was increasing with increasing PEI concentration. In contrast, when using 4PPH as solvent for PEI it solidified during cooling prior to PEI gelation or precipitation. Such solid-liquid (4PPH from PEI) demixing leads to high anisotropy and a micro-tubular morphology of the resulting porous PEI (see **Fig. 30, A1-A3**). The existence

of a cloud point for PEI in 9FN solutions indicated PEI gelation prior to 9FN solidification (crystallisation) greatly influenced the pore morphology of porous PEI. After solvent extraction, the resulting porous PEI sample has a different appearance than that obtained from 4PPH. All samples possessed smooth and homogeneous fracture surfaces (**Fig. 30, B1-B3**). Samples obtained from 10 wt.% PEI concentration were extremely feeble and contained many cracks, whose number and size reduced with increasing PEI concentration. Porous PEI produced from 30 wt.% solutions seem solid and stable but during the cutting (using a razor blade) the samples fell apart in irregular shaped lumps, which made it impossible to characterise their mechanical properties.

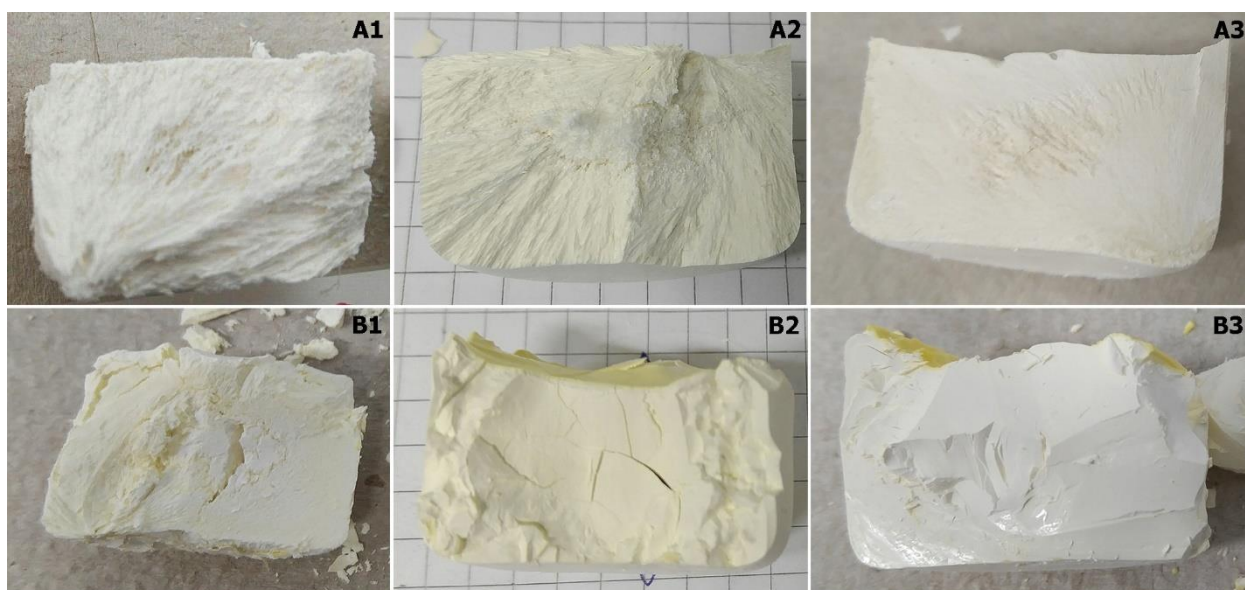


Fig. 30: Photos of fracture surfaces of cylindrical porous PEI samples obtained from 4PPH (row A) and from 9FN (row B) solutions with PEI concentrations of 10 (1), 20 (2) and 30 (3) wt.%.

DPK and DPS, when compared with 4PPH and 9FN, were both not suitable process solvents for the production of porous PEI using HT-TIPS, because they required higher dissolution temperatures and were unable to dissolve 30 wt.% PEI. Moreover, even 10 wt.% PEI solutions were not fully homogeneous. 20 wt.% PEI solutions were covered with a thin top layer of gelated PEI and still contained particles scattering light. DPK and DPS solutions underwent the same demixing process as PEI-in-9FN solutions. Their cloud points also increased with increasing PEI concentration. After solvent extraction, the resulting porous PEI samples also exhibited smooth fracture surface as those produced from 9FN but they were much more fragile. Porous PEI produced from 10 wt.% DPK solutions (**A1** in **Fig. 31**) had a homogeneous appearance but was extremely weak and crumbled into powder during handling. Porous PEI produced from 20 wt.% in DPK solutions was more robust compared to the samples produced from 10 wt.% solutions but

also fell apart into big pieces during cutting. Porous PEI obtained from 10 wt.% PEI in DPS solutions was extremely weak and already disintegrated during solvent extraction (**B1** in **Fig. 31**). In contrast to sample **B1**, porous PEI produced from 20 wt.% DPS solutions (**B2** in **Fig. 31**) exhibited the same behaviour as **A2** produced from DPK, which crumbled into pieces during cutting.

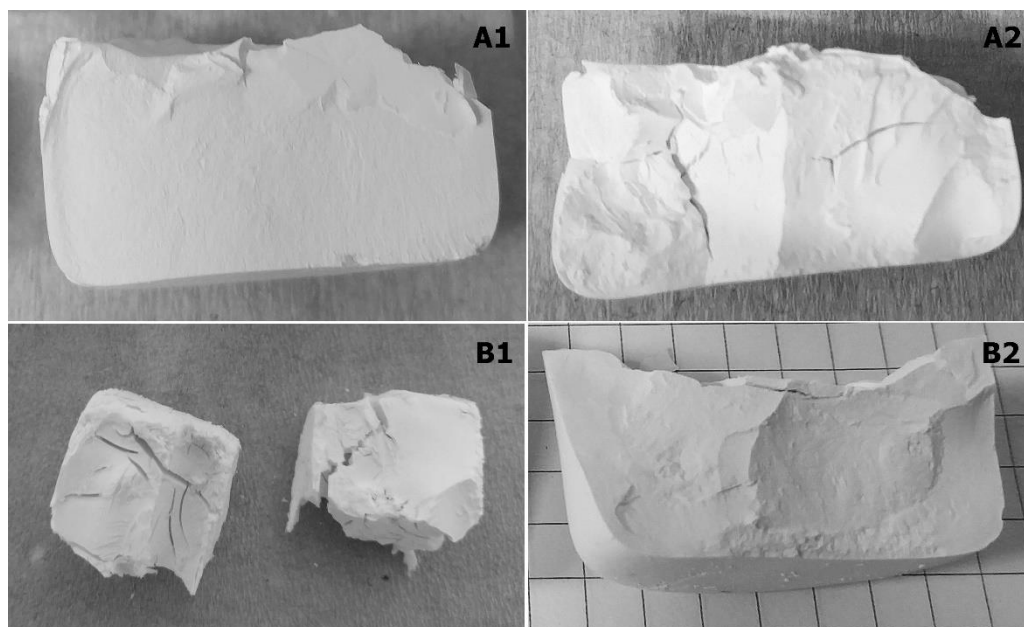


Fig. 31: Photos of fracture surfaces of porous PEI samples obtained from DPK (row A) and from DPS (row B) solutions with concentrations of 10 (1) and 20 (2) wt.%. Note it was impossible to dissolve more PEI in those solvents.

Although DPK and DPS are well-known PEEK solvents, they did not work well in the developed HT-TIPS process to produce porous PEEK and PEKK. In the case of PEEK in DPS or DPK solutions, it was impossible to produce homogeneous solutions at the maximum possible process temperature (270°C). Moreover, even at PEEK concentrations of 10 wt.% the viscosity of the resulting solution made it difficult to effectively mix the solution using a magnetic stirrer. Increasing the processing time caused additional solvent evaporation from the solution preventing the formation of a homogeneous solution. If the PEEK solution did not reach the transparent state, the resulting porous polymer sample was found to exhibit extremely poor mechanical stability or even fell apart during solvent extraction (**Fig. 32**). In the developed HT-TIPS process, DPK and DPS for found to result in porous PEEK materials with poor mechanical robustness and an inhomogeneous pore structure.

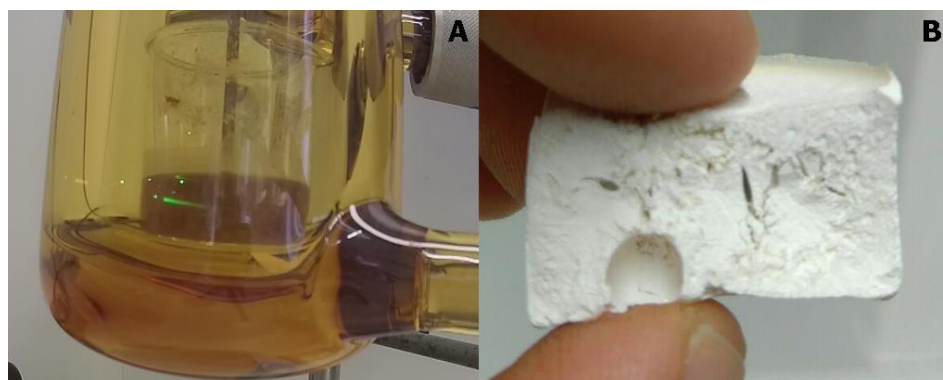


Fig. 32: Photographs showing the process issues during HT-TIPS of PEEK in DPS: A) Green laser pointer does not pass through a 10 wt.% PEEK in DPS solution indicating an inhomogeneous polymer solution and solvent recondensation on the beaker walls above the solution level and B) resulting porous PEEK sample obtained from 10 wt.% PEEK in DPS solution was fragile and exhibited a non-homogeneous pore structure.

PEKK in DPK at a concentration of 10 wt.% and HT-TIPS process temperature of 270°C also resulted in a cloudy solution, which indicated poor polymer solubility. After cooling down at the rate of 1°C/min and subsequent solvent extraction using ethanol, the resulting porous PEKK samples obtained exhibited significant shrinkage (around 30%), which rendered them dense and tough (**Fig. 33**). However, when attempting to cut samples for mechanical tests, the samples also fell apart. At concentrations above 10 wt.%, PEKK did not dissolve but formed a very viscous toffee-like substance, which could not be mixed. The resulting porous PEKK samples showed homogeneously dispersed irregular-shaped pores, which may be the result of the significant shrinkage occurring during solvent extraction.

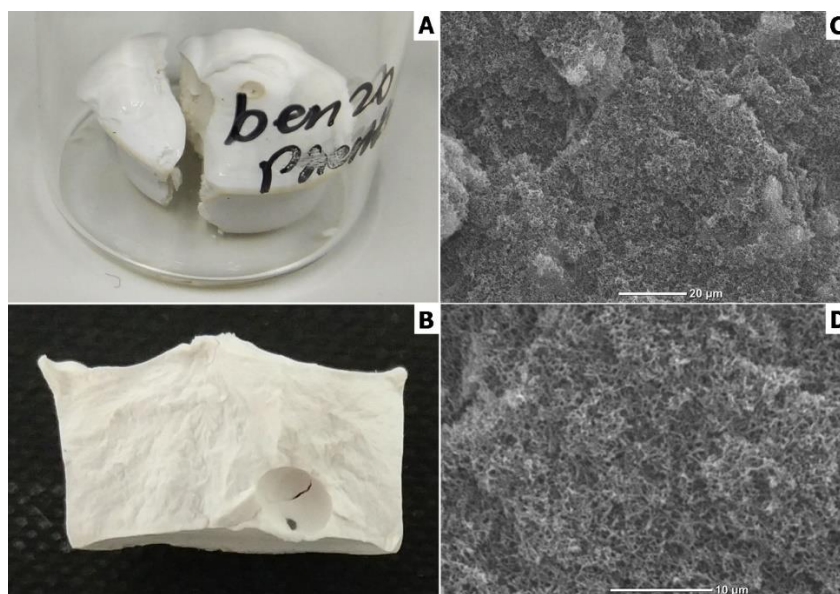


Fig. 33: The resulting porous PEKK shrunk inside a cylindrical mould (A) and fracture surface (B) of the same sample, which was obtained from 10 wt.% PEKK in DPK solution. SEM images of the porous PEKK at magnifications of 1000x (C) and 3000x (D).

PEKK could be dissolved in DPS at a concentration of 10 wt.% at a vessel temperature around 265°C. However, increasing PEKK concentration up to 20 wt.% resulted in poor PEKK solubility at the maximal possible vessel temperature (270°C). Visually, a 20 wt.% solution possessed a high viscosity and still contained insoluble floating particles. After cooling down at a rate of 1°C/min and subsequent solvent extraction using ethanol, both samples did not shrink but demonstrated two different morphologies. Porous PEKK obtained from 10 wt.% solution was extremely brittle and contained huge macroscale voids (unintentional pores) and cracks (**Fig. 34, A1**). These samples were very fragile, which can be explained by the very high porosity as a result of the low PEKK concentration leading to poor polymer connectivity. On the other hand, samples obtained from 20 wt.% solutions were harder and did not contain obvious voids (**Fig. 34, B1**). However, during the mechanical cutting and processing to produce samples for compression testing (1 x 1 x 1 cm³), these porous PEKK samples fell apart into hard, irregular-shaped fragments. Such an effect can be explained by incomplete polymer solubility at the given dissolution temperature. SEM images (**Fig. 34, A2, B2**) also confirm the non-homogenous nature of porous PEKK produced from 20 wt.% solutions, especially those obtained at 500x magnification. Porous PEKK produced from 10 wt.% solutions had a quite homogeneous pore structure, while those produced from 20 wt.% solutions contained agglomerates and resulting in a rough fracture surface. Very likely, increasing the process temperature would allow to produce homogeneous PEKK in DPS solutions at concentration of 20 wt.% but this was impossible using the current HT-TIPS setup.

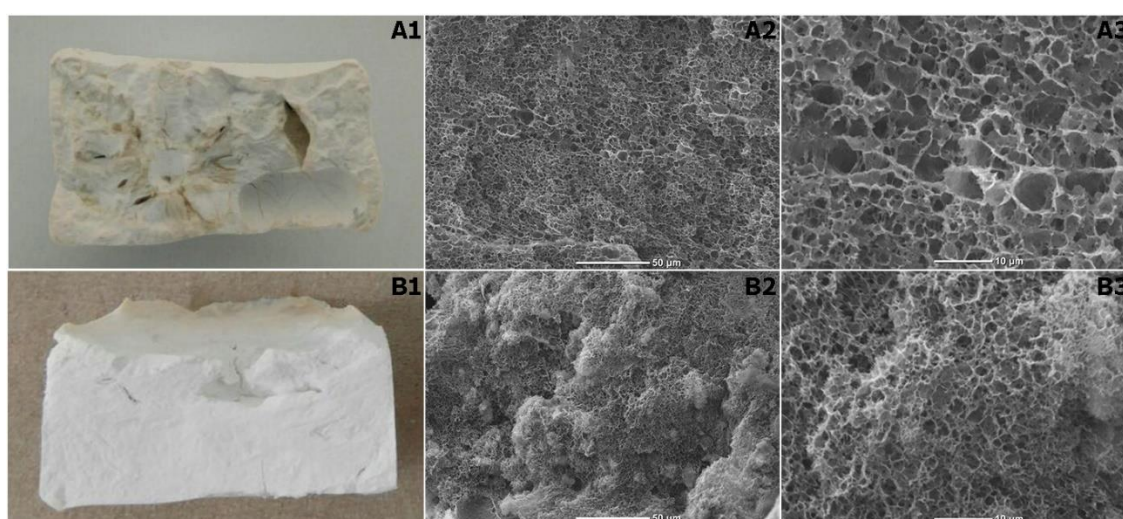


Fig. 34: Photos and SEM images of porous PEKK samples obtained from PEKK in DPS solutions with concentrations of 10 (row A) and 20 (row B) wt.%; SEM images obtained at magnifications of 500x (A2, B2) and 2000x (A3, B3).

For the above-mentioned reasons, DPK and DPS were excluded from the work as possible solvents for PEEK and PEKK in the current HT-TIPS implementation, because of the inability to achieve the required polymer concentrations at the current temperature limitation (max. 270°C).

4.3. Influence of polymer concentration on properties of porous PEEK and PEKK

4.3.1. Properties of porous PEEK

4PPH and 9FN were used as solvents for the production of porous PEEK and PEKK using the HT-TIPS process. 4PPH was shown to be a versatile solvent for both PAEK polymers allowing for the production of porous HPP samples with controllable porosity, good mechanical properties and the ability to customise the resulting properties of the porous HPP by varying the polymer concentration and cooling rate. PEEK and PEKK dissolved in 4PPH underwent two types of S-L demixing, where solvent solidification occurs prior to polymer gelation and vice versa. The resulting properties of porous PEEK are presented in **Table 4**. It was shown that porosity and foam densities of porous PEEK obtained from PEEK-in-4PPH solutions, can be controlled by changing polymer concentration.

Table 4: Skeletal ρ_s and foam ρ_f density, porosity P , surface area A_s , elastic modulus E and crush strength σ of porous PEEK samples produced from 4PPH solutions.

	[PEEK] / wt %	5	10	15	20
β / °C/min	Property				
0.5	ρ_f [g/cm ³]	0.11 ± 0.02	0.2 ± 0.04	0.27 ± 0.07	0.36 ± 0.06
	P [%]	92 ± 1	86 ± 2	81 ± 5	74 ± 4
	A_s [m ² /g]	159 ± 7	160 ± 10	170 ± 30	140 ± 10
	E [MPa]	n/a	13 ± 4	40 ± 10	130 ± 20
	σ [MPa]	n/a	0.8 ± 0.1	1.8 ± 0.6	6.6 ± 0.8
1	ρ_f [g/cm ³]	0.16 ± 0.06	0.17 ± 0.02	0.29 ± 0.08	0.36 ± 0.04
	P [%]	89 ± 4	88 ± 1	79 ± 6	73 ± 4
	A_s [m ² /g]	151 ± 2	150 ± 10	150 ± 20	140 ± 20
	E [MPa]	n/a	n/a	40 ± 10	100 ± 20
	σ [MPa]	n/a	n/a	1.9 ± 0.1	7 ± 1
2	ρ_f [g/cm ³]	0.12 ± 0.06	0.15 ± 0.02	0.24 ± 0.02	0.32 ± 0.06
	P [%]	91 ± 4	89 ± 3	83 ± 2	75 ± 7
	A_s [m ² /g]	140 ± 4	154 ± 2	149 ± 3	145 ± 4
	E [MPa]	n/a	n/a	17 ± 6	n/a
	σ [MPa]	n/a	n/a	1.9 ± 0.1	n/a
10	ρ_f [g/cm ³]	0.14 ± 0.04	0.13 ± 0.03	0.21 ± 0.08	0.29 ± 0.06
	P [%]	90 ± 3	91 ± 2	85 ± 5	79 ± 4
	A_s [m ² /g]	130 ± 20	137 ± 1	149 ± 4	141 ± 5
	E [MPa]	n/a	n/a	n/a	n/a
	σ [MPa]	n/a	n/a	n/a	n/a

Increasing the PEEK concentration in the solution results in decreasing porosities and accordingly larger foam densities. The mechanical properties of the resulting porous PEEK increased with increasing foam density. Young's moduli and crush strengths measured in compression were highest for porous PEEK obtained from 20 wt.% solutions (**Fig. 35**).

The mechanical properties of porous PEEK samples prepared from 5 wt.% of PEEK in 4PPH solutions could not be characterised because of their high anisotropy (see **Fig. 37**), which made it not possible to cut samples for compression tests. Homogeneous and robust porous PEEK samples could only be produced from 10 wt.% PEEK in 4PPH solutions at a cooling rate of 0.5°C/min., These samples having a porosity of $86 \pm 2\%$ and foam density of $0.2 \pm 0.04 \text{ g/cm}^3$ had Young's modulus of $13 \pm 4 \text{ MPa}$ and crush strength of $0.8 \pm 0.1 \text{ MPa}$. Porous PEEK obtained from 15 wt.% of PEEK in 4PPH solutions at cooling rates of 0.5 and 1°C/min had approx. the same Young's modulus and crush strength. However, the samples obtained at a cooling rate of 2°C/min possessed lower Young's moduli than samples obtained using the same PEEK concentration but lower cooling rates, which was caused by the non-homogeneous morphology of these samples (see **Fig. 37**). Porous PEEK samples prepared from 20 wt.% PEEK in 4PPH solutions possessed the highest mechanical properties of all porous PEEK samples. With a foam density of 0.36 g/cm^3 , samples obtained at 0.5 and 1°C/min cooling rates showed Young's moduli of $130 \pm 20 \text{ MPa}$ and $100 \pm 20 \text{ MPa}$, respectively, which exceed those reported for porous PEEKs with approx. same foam densities [74] (see **Fig. 35**).

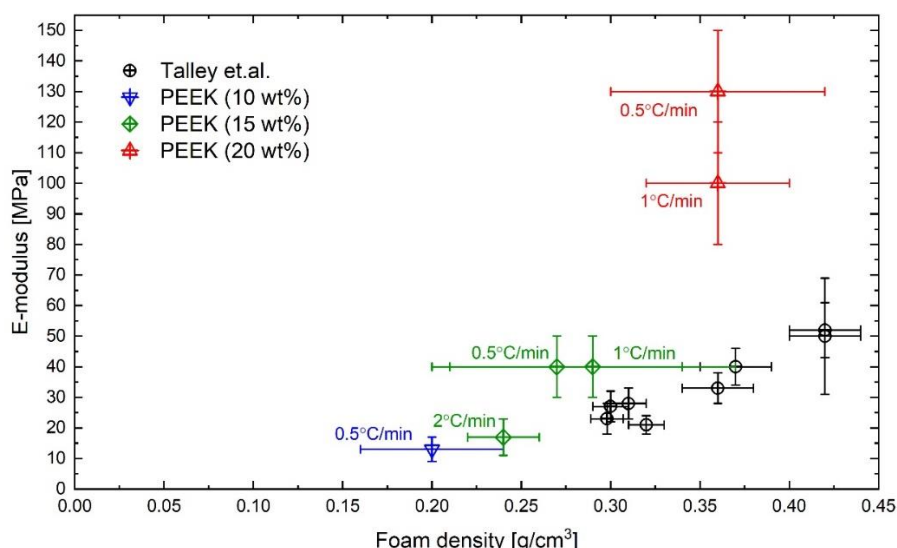


Fig. 35: Elastic moduli of our porous PEEK obtained from 4PPH solutions, using various cooling rates and polymer concentrations compared with literature data [74]. (Link in: <https://onlinelibrary.wiley.com/doi/full/10.1002/app.51423>, accessed on: 07.01.2022, open access under the terms and conditions of the Creative Commons Attribution (CC BY) license)

The specific surface area of the produced porous PEEK remained constant, irrespectively of the polymer concentrations and cooling rates used. The presence of a hysteresis loop in adsorption/desorption isotherm (**Fig. 24**) and relatively high surface area (from 132 to 173 m²/g) indicated the presence of a large amount of meso- and macroscale pores, which formed during the extraction of solidified 4PPH from PEEK.

Any potential applications of the porous PEEK produced using the HT-TIPS process rely on the purity of the materials. In order to check whether any solvent remained entrapped in the purified samples, the ferric chloride test was used to check for the presence of free phenol groups presence. The tests showed that no solvent remained within the porous polymers (see Supplementary Information **Fig. S4 Publication 2**). The properties of the produced porous PEEK from PEEK-in-4PPH solutions are described in detail in **Publication 2**.

4.3.2. Properties of porous PEKK

9FN was also used as a solvent for PEEK and PEKK but acceptable solubility for successful HT-TIPS implementation was only found for PEKK. In a contrast to PEEK dissolved in 4PPH, PEKK in 9FN exhibited only one type of demixing; polymer gelation always occurred prior to solvent solidification/crystallisation. As in the 4PPH case, the polymer concentration greatly influenced the properties of the resulting porous PEKK, while the cooling rate did not significantly affect them. Another important difference between porous PEKK produced from 10 wt.% in 9FN and 4PPH solutions was the drastic shrinkage of samples obtained from 9FN solutions, which made it impossible to measure mechanical properties for these samples (**Fig. 38**). When comparing porous PEKK produced from 20 wt.% 4PPH or 9FN solutions, samples obtained from 9FN had a smooth fracture surface and a more homogeneous pore morphology, higher surface area and better mechanical properties (**Table 5** and **Fig. 36**).

The resulting properties of porous PEKK obtained from 4PPH and 9FN solutions are presented in **Table 5**. As for porous PEEK, increasing the PEKK concentration in PEKK-in-4PPH solutions results in porous PEKKs with higher foam densities and lower porosities. For porous PEKK obtained from PEKK-in-9FN solutions containing 10 wt.% of PEKK, the foam densities (and porosities) were in some cases higher or identical compared to samples obtained from 20 wt.% PEKK-in-9FN solutions because of the observed shrinkage of the samples after solid solvent extraction, which caused pore collapse. The specific surface area of the samples obtained from the same solvent but prepared from different concentrations was not significantly different. Only porous PEKK obtained from 4PPH solutions at fast cooling rate possessed lower specific surface areas (**Table**

5) This can be explained by pores collapse occurring during rapid cooling. Porous PEKK obtained from 9FN solutions had significantly higher surface areas than obtained from 4PPH solutions, which was caused by the presence of a large number of spherical pores with uniform slit-like pores on the pore walls (**Fig. 38**). The properties of produced porous PEKKs from PEKK-in-4PPH and PEKK-in-9FN solutions are described in detail in **Publication 3**.

The mechanical properties of the resulting porous PEKK samples were measured only for samples obtained from 20 wt.% solutions. The significant difference in mechanical properties between porous PEKK obtained from 4PPH and 9FN solutions can be explained by their pore morphology (see **Fig. 38**). The samples obtained from 4PPH solutions were anisotropic (contained elongated pores), while porous PEKK obtained from 9FN solutions possessed an isotropic pore structure containing homogeneously dispersed spherical pores, which rendered these samples more mechanically robust. In comparison with literature, porous PEKK samples obtained from 9FN solutions had the same Young's moduli but higher crush strength but possessed higher porosities (**Fig. 36**) making them lighter and stronger than porous PEKK produced by particle leaching [163]. The reason for this is the more homogeneous pore morphology and the higher degree of crystallinity for the porous PEKK produced by solution (9FN) processing as compared with porous PEKK materials obtained by melt processing followed by particle leaching.

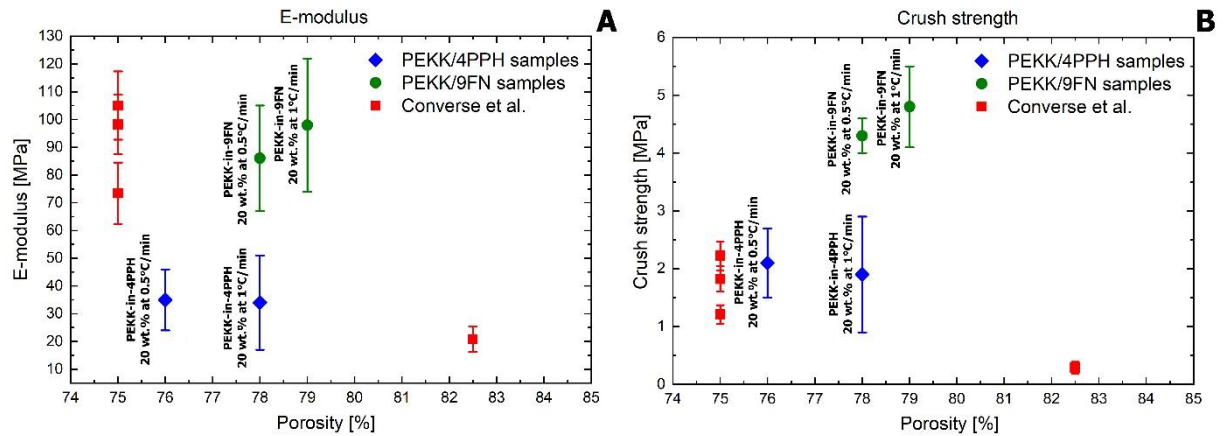


Fig. 36: Elastic modulus (A) and crush strength (B) of porous PEKK produced from 20 wt.% PEKK in 4PPH and 9FN using cooling rates $\beta = 0.5$ and 1 °C/min as a function of porosity and compared with literature data [163].

Table 5: Skeletal ρ_s and foam ρ_f density, porosity P , surface area A_s , elastic modulus E and crush strength σ of porous PEKK samples produced from 4PPH and 9FN solutions.

	Solvent	4PPH		9FN	
β / °C/min	Property / [PEKK] / wt %	10	20	10	20
0.5	ρ_f [g/cm ³]	0.19 ± 0.03	0.33 ± 0.07	0.41 ± 0.02	0.31 ± 0.03
	P [%]	86 ± 2	76 ± 5	71 ± 2	78 ± 3
	A_s [m ² /g]	87 ± 13	86 ± 15	181 ± 10	178 ± 12
	E [MPa]	n/a	35 ± 11	n/a	86 ± 19
	σ [MPa]	n/a	2.1 ± 0.6	n/a	4.3 ± 0.3
1	ρ_f [g/cm ³]	0.18 ± 0.04	0.30 ± 0.05	0.29 ± 0.06	0.30 ± 0.05
	P [%]	87 ± 3	78 ± 4	81 ± 7	79 ± 4
	A_s [m ² /g]	75 ± 17	75 ± 14	183 ± 11	178 ± 16
	E [MPa]	n/a	34 ± 17	n/a	98 ± 24
	σ [MPa]	n/a	1.9 ± 1	n/a	4.8 ± 0.7
2	ρ_f [g/cm ³]	0.15 ± 0.02	0.24 ± 0.05	0.34 ± 0.1	0.27 ± 0.03
	P [%]	89 ± 1	83 ± 3	76 ± 10	81 ± 2
	A_s [m ² /g]	39 ± 2	69 ± 11	194 ± 8	163 ± 7
	E [MPa]	n/a	n/a	n/a	n/a
	σ [MPa]	n/a	n/a	n/a	n/a
10	ρ_f [g/cm ³]	0.19 ± 0.02	0.22 ± 0.06	0.38 ± 0.05	0.31 ± 0.02
	P [%]	87 ± 2	84 ± 5	73 ± 4	78 ± 2
	A_s [m ² /g]	35 ± 3	29 ± 3	184 ± 3	166 ± 6
	E [MPa]	n/a	n/a	n/a	n/a
	σ [MPa]	n/a	n/a	n/a	n/a

4.4. Influence of cooling rate on morphology of porous PEEK and PEKK

Another crucial factor affecting the properties of porous high performance polymers produced using the HT-TIPS process is the cooling rate. In my work, I used four cooling rates: 0.5°C/min, 1°C/min, 2°C/min and 10°C/min. These four cooling rates were used for PEEK in 4PPH and PEKK in 4PPH or 9FN. Low cooling rates (0.5 and 1°C/min) did not affect the macro- and microscale pore structure of porous PEEK obtained from 5 wt.%, 10 wt.%, 15 wt.% and 20 wt.% polymer solutions. However, changing the cooling rate to 2°C/min resulted in crack formation due to residual thermal stresses within the solidified polymer solution. With a cooling rate of 10°C/min, the effect of residual thermal stresses was even more apparent resulting only in samples containing many cracks (**Fig. 37**). Moreover, when using PEEK solutions with concentrations of 5, 10 and 15 wt.% and high cooling rates (10°C/min) caused solvent solidification always occurs prior to or close to PEEK gelation/precipitation resulting in anisotropic and fibre-like macroscale morphology for these porous PEEK samples. Only when using 20 wt.% PEEK solutions the resulting porous polymers possessed a homogenous pore structure and morphology. Detailed descriptions with macro- and microscale pore structure can be found in **Publication 2**.

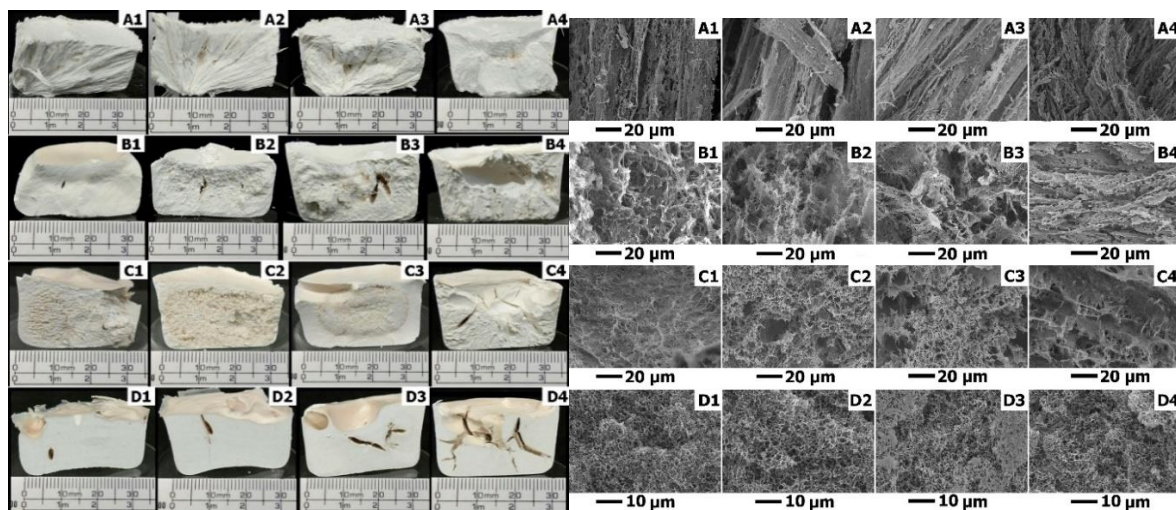


Fig. 37: Photographs (left) and SEM images (right) of porous PEEK samples produced from 4PPH solutions, produced by HT-TIPS from 5 wt.% (row A), 10 wt.% (row B), 15 wt.% (row C) and 20 wt.% (row D) at cooling rates β of 1) 0.5 °C/min, 2) 1 °C/min, 3) 2 °C/min and 4) 10 °C/min.

Porous PEKK samples obtained from 10 wt.% solutions in 4PPH had an anisotropic fibre-like morphology, which was only observed for porous PEEK produced from 5 wt.% solutions. Also, even porous PEKK produced from 20 wt.% solutions, in comparison with the analogue PEEK samples, possessed a higher degree of anisotropy, which could be explained by the lower solubility of PEKK in 4PPH as compared to PEEK or by the smaller temperature gap between polymer gelation and solvent crystallisation points. At high cooling rates (10 °C/min) all PEKK samples contained many cracks (**Fig. 38**). Comparing porous PEKK to PEEK produced from 20 wt.% solutions, they all possessed a fibre-like structure whereas the porous PEEK had a homogeneous pore structure when produced using a cooling rate of 10 °C/min. Also for PEKK foams produced from PEKK-in-9FN solutions, cooling rates did not affect the pore morphology (**Fig. 38**).

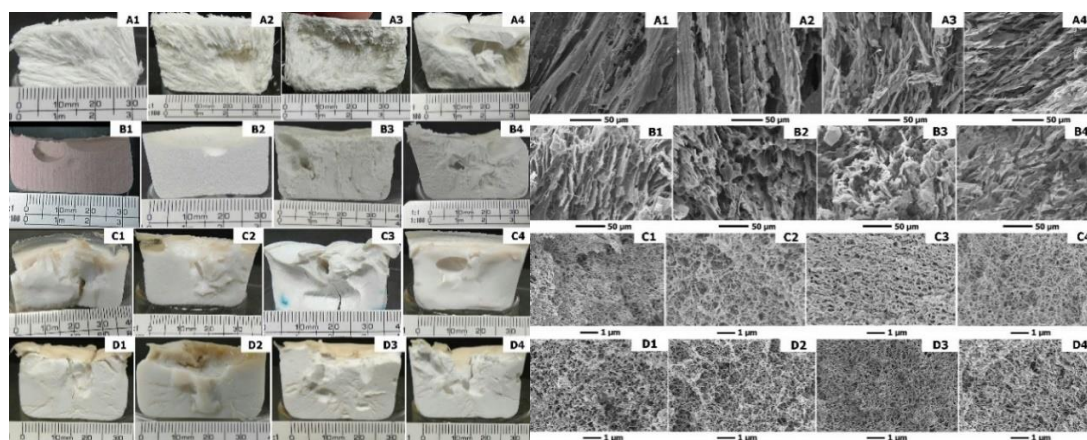


Fig. 38: Photographs (left) and SEM images (right) of porous PEKK samples produced from 4PPH (row A and B) and from 9FN (row C and D) solutions, produced by HT-TIPS from 10 wt.% (row A and C) and 20 wt.% (row B and D) at cooling rates β of 1) 0.5 °C/min, 2) 1 °C/min, 3) 2 °C/min and 4) 10 °C/min.

4.5. Influence of cooling rate on degree of crystallinity of porous PEEK and PEKK

The degree of crystallinity of the resulting porous PEEK and PEKK samples was investigated by DSC. The first heating run was used to determine the crystallinity of as-produced porous polymers (**Table 6**). The degree of crystallinity of melt-processed commercially available PEEK or PEKK ranges typically from 20 to 40% [125, 179]. However, porous PEEK and PEKK samples obtained from polymer solutions using the HT-TIPS process possessed a higher degree of crystallinities; they were in the range from 48 to 57% for PEEK and from 40 to 49% for PEKK (**Table 6**). However, during re-crystallisation from the melt (during cooling in the DSC) PEEK and PEKK had again typical degrees of crystallinity.

Table 6: Degree of crystallinity χ of porous PEEK and PEKK produced from 4PPH and 9FN solutions containing various amounts of polymer using cooling rates of 0.5 – 10 °C/min calculated from the heat of melting (first heating run) and crystallisation (first cooling run) as measured using standard DSC. χ determined from the first heating run represents the polymer crystallinity for materials crystallised from solution while χ obtained from the cooling run represents that of melt crystallised polymers.

		χ determined by DSC, [%]							
Cooling rate, [°C/min]		0.5		1		2		10	
Polymer/solvent system	[Polymer] [%]	heating	cooling	heating	cooling	heating	cooling	heating	cooling
PEEK/4PPH	5	54 ± 2	40 ± 1	54 ± 2	40 ± 1	50 ± 2	38 ± 1	49 ± 1	38 ± 2
	10	54 ± 2	38 ± 1	55 ± 1	40 ± 1	53 ± 3	41 ± 1	48 ± 3	38 ± 3
	15	55 ± 1	36 ± 1	55 ± 1	41 ± 1	55 ± 1	41 ± 1	51 ± 2	41 ± 2
	20	56 ± 2	41 ± 1	57 ± 1	42 ± 1	55 ± 1	40 ± 1	52 ± 4	39 ± 1
PEKK/4PPH	10	40 ± 3	36 ± 1	42 ± 1	35 ± 2	43 ± 3	34 ± 3	40 ± 2	34 ± 1
	20	44 ± 1	35 ± 1	44 ± 2	36 ± 1	44 ± 5	33 ± 1	40 ± 1	35 ± 2
PEKK/9FN	10	49 ± 4	27 ± 1	48 ± 2	27 ± 1	48 ± 1	27 ± 1	45 ± 4	26 ± 1
	20	45 ± 1	27 ± 1	47 ± 4	27 ± 1	44 ± 2	26 ± 1	45 ± 3	27 ± 1

Such a high degree of crystallinity could be explained by the following:

- Fully dissolved (PEEK or PEKK) chains have higher mobility in solution than in the melt, which allows for a more preferable transition from the amorphous to crystalline state [180]. This statement is supported by the following evidence: the degree of crystallinity tends to decrease with increasing cooling rate for porous polymers produced from solutions with the same polymer concentration. With increasing cooling rate, the dissolved polymer has less time to transition from the amorphous to crystalline state. In

other words, a slower cooling rate results in a higher degree of crystallinity than higher cooling rates.

- During DSC analysis cold-crystallisation during which the amorphous phase crystallises at temperatures above T_g could occur. However, Flash-DSC suppresses this effect [181]. Flash-DSC confirmed the high degree of crystallinity of porous PEEK (**Publication 2, Table 4**) and PEKK samples (**Publication 3, Table 4**).

Chapter 5. Overall Conclusions

5.1. Conclusion

The aim of my PhD thesis was to develop a universal method for the production of monolithic high performance polymer foams with controllable properties of the resulting porous materials. The method developed was based on thermally induced phase separation, which I adapted for high performance polymers. The developed method was called HT-TIPS and was successfully tested for semi-crystalline (PEEK and PEKK) and amorphous (PEI) high performance polymers. Foam density, porosity, surface area, pore morphology, degree of crystallinity and mechanical properties of the resulting porous high performance materials could be controlled by adjusting the process parameters, polymer concentration and solvent selection.

The first objective of my thesis was to identify the most suitable solvent or solvents for the chosen polymers. Among the tested solvents, only two of them, 4-phenylphenol and 9-fluorenone, allowed for the production of porous PEEK, PEKK and PEI that could be fully characterised. In the case of 4-phenylphenol, solvent solidification occurred before polymer gelation which resulted in an anisotropic micro-tubular pore morphology. However, when polymer gelation occurred prior to solvent solidification the resulting pore morphology was more homogeneous and isotropic.

The developed HT-TIPS process was tested with respect to polymer concentration, cooling rates and polymer dissolution time and temperature. The polymer concentration had the greatest impact on the properties of resulting porous polymers, except for the degree of crystallinity and specific surface area. The polymer concentration defined the type of demixing during cooling in the HT-TIPS process, the foam density and porosity, morphology and thus the mechanical compression properties. The cooling rate had a minor effect on the resulting properties, except for the highest cooling rate (10°C/min), which resulted in the accumulation of thermal residual stresses causing the formation of cracks after solvent extraction. The dissolution time and

temperature affected the polymer dissolution. Optimal dissolution times in a temperature range, where the temperature was enough to dissolve the chosen polymer without unwanted additional solvent evaporation from polymer-in solvent solution, were identified.

Foam density/porosity correlated with the mechanical properties; decreasing the porosity (or increasing the foam density) resulted in improved mechanical properties of the porous samples. Compression properties (Young's moduli) of the samples obtained from 20 wt.% PEEK in 4PPH solutions were much higher than those reported for PEEK aerogels with approx. the same foam densities, which can be related to their pore morphology and higher degree of crystallinity. On the other hand, PEKK samples obtained from 20 wt.% in 9FN solutions had comparable properties as porous PEKK reported in literature results having approx. the same foam densities/porosities produced by melt processing of PEKK followed by particle leaching. Pore morphology and degree of crystallinity also contributed to the mechanical properties of the porous PEEK and PEKK produced using my HT-TIPS process, which outperformed porous PEEK and PEKK reported in the literature. However, the influence of the pore morphology on mechanical properties can only be compared between porous PEKK produced from PEKK-in-4PPH and PEKK-in-9FN solutions; samples with a more homogeneous pore structure obtained from PEKK-in-9FN solutions had higher Young's moduli and compression strengths than samples obtained from PEKK-in-4PPH solutions with irregular-shaped pores.

I showed that the developed HT-TIPS is universal and suitable for various high performance polymers, with only one main limitation – a suitable solvent for a desired high performance polymer needs to be identified. Simple apparatus implementation, freedom in shape selection, solvent recovery after extraction and potential for scaling up the process renders the HT-TIPS process suitable to produce porous high performance polymers with controllable properties.

5.2. Outlook for future work

The work presented in this thesis lays the foundations for future research focusing on the production of porous high performance polymers. It was shown that solvent choice has a huge impact on the HT-TIPS process and the properties of the resulting porous polymers. Thus, future studies should focus on the identification of solvents that allow to obtain porous polymers with required morphology and as a consequence, mechanical properties.

An important question requiring clarification is the identification of the phase separation process, which influences the resulting morphology. Moreover, the precise identification of the clear

solution point and the cloud point is also essential. As shown in my thesis, polymer solubility is the key factor for successful HT-TIPS implementation, especially as the solvent nature influences the resulting mechanical properties of the produced porous polymers. I only managed to determine the clear solution points empirically, by repeating a significant amount of experiments with various combinations of solvent and polymer concentrations, using visual identification of the clear solution point. Precise identification of the clear point can allow for successful implementation of the HT-TIPS. The cloud point, the next important characteristic of the TIPS process, and depends on the polymer concentration, cooling rate and solvent nature. The precise identification of the cloud point can clarify the relation between HT-TIPS process parameters, type of demixing and resulting pore morphology. All these characteristics have a crucial influence on the properties of the resulting high performance porous polymers. One of the possible methods to determine the clear solution and cloud points is the light scattering method [182, 183], which allows to identify the moment when a polymer reaches acceptable solubility and the moment, where polymer phase separation starts. This knowledge can help to understand the relationship between the main process parameters and the resulting properties of the porous high performance polymers.

Miscible polymer blends or reinforcement using (nano)particles would allow for the production of porous high performance polymer blends/composites. The high degree of crystallinity obtained by HT-TIPS solution processing can also become a promising subject for further research because the increased degree of crystallinity does significantly contribute to the mechanical properties and chemical stability of porous high performance polymers. Moreover, additional annealing at temperatures above T_g for resulting porous semi-crystalline high-performance polymers can further improve the degree of crystallinity, which would further enhance the already impressive mechanical properties of porous semi-crystalline HPP. This would make such lightweight materials even more desirable for aerospace applications.

Furthermore, more research is needed to scale up the HT-TIPS process, which could be achieved for instance using extrusion. Extrusion was successfully utilised to produce high performance polymer porous membranes, thin films [184-186] or, in a combination with gas blowing [22], to produce porous polymers. The presented thesis showed, that by the selection of a suitable high boiling point solvent (solid at room temperature) it is possible to produce bulk, monolithic porous HPPs in the desired shape (cylindrical in my case). Extrusion with HT-TIPS process resulting in porous fibres could be combined with additive manufacturing (AM) to produce high performance

porous polymer structures, which currently is a highly demanding task. Polymer/solvent powder mixture could be loaded in extruder AM printing head, printed and after solidification the solvent can be removed by dissolution resulting in a shaped porous high performance polymer with the desired 2.5D or 3D structure.

References:

1. Mittal, V., *High Performance Polymers: An Overview*, in *High Performance Polymers and Engineering Plastics*. 2011. p. 1-20.
2. Parker, D., J. Bussink, H.T. van de Grampel, G.W. Wheatley, E.-U. Dorf, E. Ostlinning, K. Reinking, F. Schubert, and O. Jünger, *Polymers, High-Temperature*, in *Ullmann's Encyclopedia of Industrial Chemistry*. 2012.
3. Kurtz, S.M. and J.N. Devine, *PEEK biomaterials in trauma, orthopedic, and spinal implants*. *Biomaterials*, 2007. **28**(32): p. 4845-69.
4. Mattiasson, B., A. Kumar, and I. Galaev, *Macroporous polymers: Production properties and biotechnological/biomedical applications*. 2009. 1-501.
5. Mills, N., *Polymer Foams Handbook: Engineering and Biomechanics Applications and Design Guide*. 2007: Elsevier Science.
6. Silverstein, M.S., N.R. Cameron, and M.A. Hillmyer, *Porous Polymers*. 2011: Wiley.
7. Jarman-Smith, M., M. Brady, S.M. Kurtz, N.M. Cordaro, and W.R. Walsh, *Chapter 12 - Porosity in Polyaryletheretherketone*, in *PEEK Biomaterials Handbook*, S.M. Kurtz, Editor. 2012, William Andrew Publishing: Oxford. p. 181-199.
8. Coste, G., C. Negrell, and S. Caillol, *From gas release to foam synthesis, the second breath of blowing agents*. *European Polymer Journal*, 2020. **140**: p. 110029.
9. Štěpek, J. and H. Daoust, *Chemical and Physical Blowing Agents*, in *Additives for Plastics*. 1983, Springer New York: New York, NY. p. 112-123.
10. Rakovsky, A., I. Gotman, E. Rabkin, and E.Y. Gutmanas, *β -TCP–polylactide composite scaffolds with high strength and enhanced permeability prepared by a modified salt leaching method*. *Journal of the Mechanical Behavior of Biomedical Materials*, 2014. **32**: p. 89-98.
11. Hossain, K.M.Z., R.M. Felfel, P.S. Ogbilikana, D. Thakker, D.M. Grant, C.A. Scotchford, and I. Ahmed, *Single Solvent-Based Film Casting Method for the Production of Porous Polymer Films*. *Macromolecular Materials and Engineering*, 2018. **303**(4): p. 1700628.
12. Bueno, A., C. Luebbert, S. Enders, G. Sadowski, and I. Smirnova, *Production of polylactic acid aerogels via phase separation and supercritical CO₂ drying: thermodynamic analysis of the gelation and drying process*. *Journal of Materials Science*, 2021. **56**(34): p. 18926-18945.
13. Ghosal, K., A. Chandra, P. G. S. S. Roy, C. Agatemor, S. Thomas, and I. Provaznik, *Electrospinning over Solvent Casting: Tuning of Mechanical Properties of Membranes*. *Sci Rep*, 2018. **8**(1): p. 5058.
14. Silverstein, M.S., *PolyHIPEs: Recent advances in emulsion-templated porous polymers*. *Progress in Polymer Science*, 2014. **39**(1): p. 199-234.
15. Ligon, S.C., R. Liska, J. Stampfl, M. Gurr, and R. Mülhaupt, *Polymers for 3D Printing and Customized Additive Manufacturing*. *Chemical Reviews*, 2017. **117**(15): p. 10212-10290.
16. Vaezi, M. and S. Yang, *Extrusion-based additive manufacturing of PEEK for biomedical applications*. *Virtual and Physical Prototyping*, 2015. **10**(3): p. 123-135.
17. Zhang, Y., R. Li, W. Wu, Y.a. Qing, X. Tang, W. Ye, Z. Zhang, and Y. Qin, *Adhesion and Proliferation of Osteoblast-Like Cells on Porous Polyetherimide Scaffolds*. *BioMed Research International*, 2018. **2018**: p. 1491028.
18. Cafiero, L., S. Iannace, and L. Sorrentino, *Microcellular foams from high performance miscible blends based on PEEK and PEI*. *European Polymer Journal*, 2016. **78**: p. 116-128.

19. Govinna, N.D., T. Keller, C. Schick, and P. Cebe, *Melt-electrospinning of poly(ether ether ketone) fibers to avoid sulfonation*. Polymer, 2019. **171**: p. 50-57.
20. Mehta, R.H., D.A. Madsen, and D.S. Kalika, *Microporous membranes based on poly(ether ether ketone) via thermally-induced phase separation*. Journal of Membrane Science, 1995. **107**(1): p. 93-106.
21. Jia, H., J.-Z. Zhao, F.-Y. Jin, W.-F. Pu, Y.-M. Li, K.-X. Li, and J.-M. Li, *New Insights into the Gelation Behavior of Polyethyleneimine Cross-Linking Partially Hydrolyzed Polyacrylamide Gels*. Industrial & Engineering Chemistry Research, 2012. **51**(38): p. 12155-12166.
22. Verdejo, R., P. Werner, J. Sandler, V. Altstädt, and M.S.P. Shaffer, *Morphology and properties of injection-moulded carbon-nanofibre poly(etheretherketone) foams*. Journal of Materials Science, 2009. **44**(6): p. 1427-1434.
23. Zhang, J. and M.F. Ashby, *Mechanical selection of foams and honeycombs used for packaging and energy absorption*. Journal of Materials Science, 1994. **29**(1): p. 157-163.
24. Sorrentino, L., M. Aurilia, and S. Iannace, *Polymeric foams from high-performance thermoplastics*. Advances in Polymer Technology, 2011. **30**(3): p. 234-243.
25. Li, J., G. Zhang, J. Li, L. Zhou, Z. Jing, and Z. Ma, *Preparation and properties of polyimide/chopped carbon fiber composite foams*. Polymers for Advanced Technologies, 2017. **28**(1): p. 28-34.
26. Paciorek-Sadowska, J., M. Borowicz, B. Czapryński, and M. Isbrandt, *Effect of Evening Primrose Oil-Based Polyol on the Properties of Rigid Polyurethane–Polyisocyanurate Foams for Thermal Insulation*. Polymers, 2018. **10**(12): p. 1334.
27. Seibert, H.F., *Applications for PMI foams in aerospace sandwich structures*. Reinforced Plastics, 2006. **50**(1): p. 44-48.
28. Schilling, K. and M. Zessner, *Foam in the aquatic environment*. Water Research, 2011. **45**(15): p. 4355-4366.
29. Verdejo, R., R. Stämpfli, M. Alvarez-Lainez, S. Mourad, M.A. Rodriguez-Perez, P.A. Brühwiler, and M. Shaffer, *Enhanced acoustic damping in flexible polyurethane foams filled with carbon nanotubes*. Composites Science and Technology, 2009. **69**(10): p. 1564-1569.
30. Gerges, I., M. Tamplenizza, F. Martello, C. Recordati, C. Martelli, L. Ottobri, M. Tamplenizza, S.A. Guelcher, A. Tocchio, and C. Lenardi, *Exploring the potential of polyurethane-based soft foam as cell-free scaffold for soft tissue regeneration*. Acta Biomaterialia, 2018. **73**: p. 141-153.
31. Tiuc, A.-E., H. Vermeşan, T. Gabor, and O. Vasile, *Improved Sound Absorption Properties of Polyurethane Foam Mixed with Textile Waste*. Energy Procedia, 2016. **85**: p. 559-565.
32. Weiser, E.S., T.F. Johnson, T.L. St Clair, Y. Echigo, H. Kaneshiro, and B.W. Grimsley, *Polyimide Foams for Aerospace Vehicles*. High Performance Polymers, 2000. **12**(1): p. 1-12.
33. Liu, P.S. and G.F. Chen, *Chapter One - General Introduction to Porous Materials*, in *Porous Materials*, P.S. Liu and G.F. Chen, Editors. 2014, Butterworth-Heinemann: Boston. p. 1-20.
34. Hu, X., E.M. Wouterson, and M. Liu, *Polymer Foam Technology*, in *Handbook of Manufacturing Engineering and Technology*, A.Y.C. Nee, Editor. 2015, Springer London: London. p. 125-168.
35. Gibson, L.J. and M.F. Ashby, *Cellular Solids: Structure and Properties*. 2 ed. Cambridge Solid State Science Series. 1997, Cambridge: Cambridge University Press.
36. Reglero Ruiz, J.A., M. Vincent, J.-F. Agassant, T. Sadik, C. Pillon, and C. Carrot, *Polymer foaming with chemical blowing agents: Experiment and modeling*. Polymer Engineering & Science, 2015. **55**(9): p. 2018-2029.
37. Mensitieri, G., *Chapter 3 - Gas foaming with physical blowing agents*, in *Supercritical Fluid Science and Technology*, E. Di Maio, S. Iannace, and G. Mensitieri, Editors. 2021, Elsevier. p. 33-54.
38. Wypych, G., *Mechanisms of Action of Blowing Agents*, in *Handbook of Foaming and Blowing Agents*, G. Wypych, Editor. 2017, ChemTec Publishing. p. 29-43.
39. Tersac, G., *Chemistry and technology of polyols for polyurethanes*. Milhail Ionescu. Rapra Technology, Shrewsbury, UK. Polymer International, 2007. **56**(6): p. 820-820.
40. Rohleder, M. and F. Jakob, *2 - Foam Injection Molding*, in *Specialized Injection Molding Techniques*, H.-P. Heim, Editor. 2016, William Andrew Publishing. p. 53-106.
41. Quinn, S., *Chemical blowing agents: providing production, economic and physical improvements to a wide range of polymers*. Plastics, Additives and Compounding, 2001. **3**(5): p. 16-21.

42. Lee, J.W.S. and C.B. Park, *Use of Nitrogen as a Blowing Agent for the Production of Fine-Celled High-Density Polyethylene Foams*. Macromolecular Materials and Engineering, 2006. **291**(10): p. 1233-1244.
43. Grignard, B., J.M. Thomassin, S. Gennen, L. Poussard, L. Bonnaud, J.M. Raquez, P. Dubois, M.P. Tran, C.B. Park, C. Jerome, and C. Detrembleur, *CO₂-blown microcellular non-isocyanate polyurethane (NIPU) foams: from bio- and CO₂-sourced monomers to potentially thermal insulating materials*. Green Chemistry, 2016. **18**(7): p. 2206-2215.
44. Orsi, S., E. Di Maio, S. Iannace, and P.A. Netti, *Hollow micro- and nano-particles by gas foaming*. Nano Research, 2014. **7**(7): p. 1018-1026.
45. Shutov, F.A. *Syntactic polymer foams*. 1986. Berlin, Heidelberg: Springer Berlin Heidelberg.
46. Velders, G.J., S.O. Andersen, J.S. Daniel, D.W. Fahey, and M. McFarland, *The importance of the Montreal Protocol in protecting climate*. Proc Natl Acad Sci U S A, 2007. **104**(12): p. 4814-9.
47. Ramanathan, V. and Y. Feng, *Air pollution, greenhouse gases and climate change: Global and regional perspectives*. Atmospheric Environment, 2009. **43**(1): p. 37-50.
48. Marlin, L., A.J. Durante, and E.G. Schwarz, *Mechanically Frothed Urethane: A New Process for Controlled Gauge, High Density Foam*. Journal of Cellular Plastics, 1975. **11**(6): p. 317-322.
49. Jalalian, M., Q. Jiang, A. Coulon, M. Storb, R. Woodward, and A. Bismarck, *Mechanically whipped phenolic froths as versatile templates for manufacturing phenolic and carbon foams*. Materials & Design, 2019. **168**: p. 107658.
50. Wong, J.C.H., E. Tervoort, S. Busato, U.T. Gonzenbach, A.R. Studart, P. Ermanni, and L.J. Gauckler, *Designing macroporous polymers from particle-stabilized foams*. Journal of Materials Chemistry, 2010. **20**(27): p. 5628.
51. Lee, K.-Y., L.L.C. Wong, J.J. Blaker, J.M. Hodgkinson, and A. Bismarck, *Bio-based macroporous polymer nanocomposites made by mechanical frothing of acrylated epoxidised soybean oil*. Green Chemistry, 2011. **13**(11): p. 3117-3123.
52. Jin, F.-L., M. Zhao, M. Park, and S.-J. Park, *Recent Trends of Foaming in Polymer Processing: A Review*. Polymers, 2019. **11**(6): p. 953.
53. Altan, M., *Thermoplastic Foams: Processing, Manufacturing, and Characterization*, in *Recent Research in Polymerization*. 2018.
54. Liu, P.S. and G.F. Chen, *Chapter Seven - Producing Polymer Foams*, in *Porous Materials*, P.S. Liu and G.F. Chen, Editors. 2014, Butterworth-Heinemann: Boston. p. 345-382.
55. van de Witte, P., P.J. Dijkstra, J.W.A. van den Berg, and J. Feijen, *Phase separation processes in polymer solutions in relation to membrane formation*. Journal of Membrane Science, 1996. **117**(1-2): p. 1-31.
56. Onder, O.C., E. Yilgor, and I. Yilgor, *Preparation of monolithic polycaprolactone foams with controlled morphology*. Polymer, 2018. **136**: p. 166-178.
57. Tasselli, F., *Non-solvent Induced Phase Separation Process (NIPS) for Membrane Preparation*, in *Encyclopedia of Membranes*, E. Drioli and L. Giorno, Editors. 2015, Springer Berlin Heidelberg: Berlin, Heidelberg. p. 1-3.
58. Khare, V.P., A.R. Greenberg, and W.B. Krantz, *Vapor-induced phase separation—effect of the humid air exposure step on membrane morphology: Part I. Insights from mathematical modeling*. Journal of Membrane Science, 2005. **258**(1): p. 140-156.
59. Matsuyama, H., M. Teramoto, and T. Uesaka, *Membrane formation and structure development by dry-cast process*. Journal of Membrane Science, 1997. **135**(2): p. 271-288.
60. Even, W.R. and D.P. Gregory, *Emulsion-Derived Foams: Preparation, Properties, and Application*. MRS Bulletin, 1994. **19**(4): p. 29-33.
61. Jiang, Q., A. Menner, and A. Bismarck, *Emulsion-templated macroporous polymer/polymer composites with switchable stiffness*. Pure and Applied Chemistry, 2014. **86**(2): p. 203-213.
62. Aldemir Dikici, B. and F. Claeysens, *Basic Principles of Emulsion Templating and Its Use as an Emerging Manufacturing Method of Tissue Engineering Scaffolds*. Frontiers in Bioengineering and Biotechnology, 2020. **8**(875).
63. Abbasi, H., M. Antunes, and J.I. Velasco, *Polyetherimide Foams Filled with Low Content of Graphene Nanoplatelets Prepared by scCO₂ Dissolution*. Polymers, 2019. **11**(2): p. 328.

64. Li, Z., Y. Jia, and S. Bai, *Polysulfone foam with high expansion ratio prepared by supercritical carbon dioxide assisted molding foaming method*. RSC Advances, 2018. **8**(6): p. 2880-2886.
65. Hu, D.-d., Y. Gu, T. Liu, and L. Zhao, *Microcellular foaming of polysulfones in supercritical CO₂ and the effect of co-blowing agent*. The Journal of Supercritical Fluids, 2018. **140**: p. 21-31.
66. Abbasi, H., M. Antunes, and J. Velasco, *Graphene nanoplatelets-reinforced polyetherimide foams prepared by water vapor-induced phase separation*. eXPRESS Polymer Letters, 2015. **9**: p. 412-423.
67. Werner, P., R. Verdejo, F. Wöllecke, V. Altstädt, J.K.W. Sandler, and M.S.P. Shaffer, *Carbon Nanofibers Allow Foaming of Semicrystalline Poly(ether ether ketone)*. Advanced Materials, 2005. **17**(23): p. 2864-2869.
68. Worgull, M., *Hot Embossing*, in *Micro-Manufacturing Engineering and Technology*, Y. Qin, Editor. 2010, William Andrew Publishing: Boston. p. 68-89.
69. Akartuna, I., E. Tervoort, J.C.H. Wong, A.R. Studart, and L.J. Gauckler, *Macroporous polymers from particle-stabilized emulsions*. Polymer, 2009. **50**(15): p. 3645-3651.
70. A, C., I. Olivas-Armendariz, J. S, and P. E, *Scaffolds for Tissue Engineering Via Thermally Induced Phase Separation*, in *Advances in Regenerative Medicine*. 2011.
71. Rusakov, D., A. Menner, and A. Bismarck, *High-Performance Polymer Foams by Thermally Induced Phase Separation*. Macromol Rapid Commun, 2020. **41**(11): p. e2000110.
72. Rusakov, D., A. Menner, F. Spieckermann, H. Wilhelm, and A. Bismarck, *Morphology and properties of foamed high crystallinity PEEK prepared by high temperature thermally induced phase separation*. Journal of Applied Polymer Science. **139**(1): p. 51423.
73. Talley, S.J., S.L. Vivod, B.A. Nguyen, M.A.B. Meador, A. Radulescu, and R.B. Moore, *Hierarchical Morphology of Poly(ether ether ketone) Aerogels*. ACS Appl Mater Interfaces, 2019. **11**(34): p. 31508-31519.
74. Talley, S.J., C.L. AndersonSchoepe, C.J. Berger, K.A. Leary, S.A. Snyder, and R.B. Moore, *Mechanically robust and superhydrophobic aerogels of poly(ether ether ketone)*. Polymer, 2017. **126**: p. 437-445.
75. Venkatraman, P., C. Rader, N. Bohmann, and E.J. Foster, *Structure-property-processing relationship of ethanol solvent exchanged PEEK*. Polymer, 2019. **169**: p. 154-159.
76. Kemmish, D.J., *Practical Guide to High Performance Engineering Plastics*. 2011: Smithers Rapra Technology.
77. *Time and Temperature Behavior of Polymers*, in *Polymer Engineering Science and Viscoelasticity*. 2008, Springer US: Boston, MA. p. 221-274.
78. Brostow, W., *Reliability and prediction of long-term performance of polymer-based materials*. Pure and Applied Chemistry, 2009. **81**(3): p. 417-432.
79. de Leon, A.C.C., Í.G.M. da Silva, K.D. Pangilinan, Q. Chen, E.B. Caldon, and R.C. Advincula, *High performance polymers for oil and gas applications*. Reactive and Functional Polymers, 2021. **162**: p. 104878.
80. Sezer Hicyilmaz, A. and A. Celik Bedeloglu, *Applications of polyimide coatings: a review*. SN Applied Sciences, 2021. **3**(3): p. 363.
81. Liaw, D.-J., K.-L. Wang, Y.-C. Huang, K.-R. Lee, J.-Y. Lai, and C.-S. Ha, *Advanced polyimide materials: Syntheses, physical properties and applications*. Progress in Polymer Science, 2012. **37**(7): p. 907-974.
82. Seymour, R.B. and C.E. Carraher, *Thermal Properties of Polymers*, in *Structure—Property Relationships in Polymers*. 1984, Springer: Boston, MA. p. 83-93.
83. Chartoff, R.P., J.D. Menczel, and S.H. Dillman, *Dynamic Mechanical Analysis (DMA)*, in *Thermal Analysis of Polymers*. 2009. p. 387-495.
84. Ehrenstein, G.W. and S. Pongratz, *Part 1: Principles of Aging*, in *Resistance and Stability of Polymers*, G.W. Ehrenstein and S. Pongratz, Editors. 2013, Hanser. p. 1-138.
85. Brinson, H.F. and L.C. Brinson, *Time and Temperature Behavior of Polymers*, in *Polymer Engineering Science and Viscoelasticity*. 2015, Springer US: Boston, MA. p. 231-285.
86. Williams, F.J. and P.E. Donahue, *Reactions of phenoxides with nitro- and halo-substituted phthalimides*. The Journal of Organic Chemistry, 1977. **42**(21): p. 3414-3419.

87. Melton, G.H., E.N. Peters, and R.K. Arisman, 2 - *Engineering Thermoplastics*, in *Applied Plastics Engineering Handbook*, M. Kutz, Editor. 2011, William Andrew Publishing: Oxford. p. 7-21.
88. Feng, X. and J. Liu, *Thermoplastic Polyimide (TPI)*, in *High Performance Polymers and Their Nanocomposites*. 2018. p. 149-219.
89. Georgiev, A., D. Dimov, E. Spassova, J. Assa, P. Dineff, and G. Danev, *Chemical and Physical Properties of Polyimides: Biomedical and Engineering Applications*, in *High Performance Polymers - Polyimides Based - From Chemistry to Applications*. 2012.
90. Belana, J., J.C. Cañadas, J.A. Diego, M. Mudarra, R. Díaz-Calleja, S. Friederichs, C. Jaimes, and M.J. Sanchis, *Comparative study of mechanical and electrical relaxations in poly(etherimide). Part 1*. *Polymer International*, 1998. **46**(1): p. 11-19.
91. Díaz Calleja, R., S. Friederichs, C. Jaimes, M.J. Sanchis, J. Belana, J.C. Cañadas, J.A. Diego, and M. Mudarra, *Comparative study of mechanical and electrical relaxations in poly(etherimide). Part 2*. *Polymer International*, 1998. **46**(1): p. 20-28.
92. White, S.A., S.R. Weissman, and R.P. Kambour, *Resistance of a polyetherimide to environmental stress crazing and cracking*. *Journal of Applied Polymer Science*, 1982. **27**(7): p. 2675-2682.
93. Machatschek, R., M. Heuchel, and A. Lendlein, *Hydrolytic stability of polyetherimide investigated in ultrathin films*. *Journal of Materials Research*, 2021. **36**(14): p. 2987-2994.
94. Ghosh, M.K., & Mittal, K.L., *Polyimides*. 2018: CRC Press.
95. Johnson, R.O. and E.O. Teutsch, *Thermoplastic aromatic polyimide composites*. *Polymer Composites*, 1983. **4**(3): p. 162-166.
96. Hsissou, R., R. Seghiri, Z. Benzekri, M. Hilali, M. Rafik, and A. Elharfi, *Polymer composite materials: A comprehensive review*. *Composite Structures*, 2021. **262**: p. 113640.
97. Yilmaz, T. and T. Sinmazcelik, *Effects of hydrothermal aging on glass-fiber/polyetherimide (PEI) composites*. *Journal of Materials Science*, 2010. **45**(2): p. 399-404.
98. Kumar, S., R.K. Mishra, and T. Nandi, *Experimental and theoretical investigations of the high performance blends of PEEK/PEI*. *Journal of Polymer Engineering*, 2018. **38**(4): p. 351-361.
99. Frigione, M., C. Naddeo, and D. Acierno, *Crystallization behavior and mechanical properties of poly(aryl ether ether ketone)/poly(ether imide) blends*. *Polymer Engineering & Science*, 1996. **36**(16): p. 2119-2128.
100. Jo, W.H., M.R. Lee, B.G. Min, and M.S. Lee, *Miscibility of poly(ether imide)/poly(ethylene terephthalate) blends*. *Polymer Bulletin*, 1994. **33**(1): p. 113-118.
101. Chen, H.-L., H. Jenn Chiu, C.-C. Chen, R.-C. Wang, D.-M. Fang, and M.-J. Tsai, *Phase behaviour of amorphous and semicrystalline blends of poly(butylene terephthalate) and poly(ether imide)*. *Polymer*, 1997. **38**(11): p. 2747-2752.
102. Zhou, X. and M. Cakmak, *Influence of composition and annealing on the structure development in biaxially stretched PEN/PEI/PEEK ternary blends*. *Polymer*, 2006. **47**(18): p. 6362-6378.
103. Lee, J.H., S.-G. Lee, K.-Y. Choi, and J. Liu, *Crystallization and Melting Behavior of Nylon 66/Poly(ether imide) Blends*. *Polymer Journal*, 1998. **30**(7): p. 531-537.
104. Chun, Y.S., H.S. Lee, W.N. Kim, and T.S. Oh, *Thermal properties and morphology of blends of poly(ether imide) and polycarbonate*. *Polymer Engineering & Science*, 1996. **36**(22): p. 2694-2702.
105. Bloomfield, R., D.L. Crossman, and A. Raeissi. *Using Polyetherimide Thermoplastic for Forward Lighting Complex Reflectors*. 1999.
106. Biondi, G., *Poly(esterimide) Wire Enamels: Coatings with the Right Combination of Thermal and Mechanical Properties for Many Applications*. *Macromolecular Materials and Engineering*, 2008. **293**(5): p. 361-372.
107. Traßi, C., D. Holleyn, and K. Bernhard, *PEI particle foams for applications in aircraft interiors*, 20200207939, 2020
108. Zou, Y., D. Li, M. Shen, and X. Shi, *Polyethylenimine-Based Nanogels for Biomedical Applications*. *Macromolecular Bioscience*, 2019. **19**(11): p. 1900272.
109. Seifert, B., G. Mihanetzis, T. Groth, W. Albrecht, K. Richau, Y.F. Missirlis, D. Paul, and G. von Sengbusch, *Polyetherimide: a new membrane-forming polymer for biomedical applications*. *Artificial organs*, 2002. **26** 2: p. 189-99.
110. Tarlochan, F., *Sandwich Structures for Energy Absorption Applications: A Review*. *Materials*, 2021. **14**(16): p. 4731.

111. Belingardi, G., M.P. Cavatorta, and R. Duella, *Material characterization of a composite-foam sandwich for the front structure of a high speed train*. Composite Structures, 2003. **61**(1): p. 13-25.
112. Weber, J., *The Role of Curvature and Structural Compliance on Water Impact Loading of Composite Structures*. 2017, ResearchSpace@ Auckland.
113. Grünewald, J., P.P. Parlevliet, A. Matschinski, and V. Altstädt, *Mechanical performance of CF/PEEK-PEI foam core sandwich structures*. Journal of Sandwich Structures & Materials, 2019. **21**(8): p. 2680-2699.
114. Miller, D., P. Chatchaisucha, and V. Kumar, *Microcellular and nanocellular solid-state polyetherimide (PEI) foams using sub-critical carbon dioxide I. Processing and structure*. Polymer, 2009. **50**(23): p. 5576-5584.
115. Zhou, C., N. Vaccaro, S.S. Sundarram, and W. Li, *Fabrication and characterization of polyetherimide nanofoams using supercritical CO₂*. Journal of Cellular Plastics, 2012. **48**(3): p. 239-255.
116. Jiang, J., W. Feng, D. Zhao, and W. Zhai, *Poly(ether imide)/Epoxy Foam Composites with a Microcellular Structure and Ultralow Density: Bead Foam Fabrication, Compression Molding, Mechanical Properties, Thermal Stability, and Flame-Retardant Properties*. ACS Omega, 2020. **5**(40): p. 25784-25797.
117. Feng, D., L. Li, and Q. Wang, *Fabrication of three-dimensional polyetherimide bead foams via supercritical CO₂/ethanol co-foaming technology*. RSC Advances, 2019. **9**(7): p. 4072-4081.
118. Nemoto, T., J. Takagi, and M. Ohshima, *Nanocellular foams—cell structure difference between immiscible and miscible PEEK/PEI polymer blends*. Polymer Engineering & Science, 2010. **50**(12): p. 2408-2416.
119. Abbasi, H., M. Antunes, and J.I. Velasco, *Influence of polyamide-imide concentration on the cellular structure and thermo-mechanical properties of polyetherimide/polyamide-imide blend foams*. European Polymer Journal, 2015. **69**: p. 273-283.
120. Krause, B., K. Diekmann, N.F.A. van der Vegt, and M. Wessling, *Open Nanoporous Morphologies from Polymeric Blends by Carbon Dioxide Foaming*. Macromolecules, 2002. **35**(5): p. 1738-1745.
121. Olabisi, O. and K. Adewale, *Handbook of Thermoplastics*. 2016: CRC Press.
122. Ma, R. and D. Guo, *Evaluating the bioactivity of a hydroxyapatite-incorporated polyetheretherketone biocomposite*. Journal of Orthopaedic Surgery and Research, 2019. **14**(1): p. 32.
123. Deng, F., T. Ogasawara, and N. Takeda, *Tensile properties at different temperature and observation of micro deformation of carbon nanotubes-poly(ether ether ketone) composites*. Composites Science and Technology, 2007. **67**(14): p. 2959-2964.
124. Zhang, G., L. Chang, and A.K. Schlarb, *The roles of nano-SiO₂ particles on the tribological behavior of short carbon fiber reinforced PEEK*. Composites Science and Technology, 2009. **69**(7): p. 1029-1035.
125. Jin, L., J. Ball, T. Bremner, and H.-J. Sue, *Crystallization behavior and morphological characterization of poly(ether ether ketone)*. Polymer, 2014. **55**(20): p. 5255-5265.
126. Huo, P. and P. Cebe, *Temperature-dependent relaxation of the crystal-amorphous interphase in poly(ether ether ketone)*. Macromolecules, 1992. **25**(2): p. 902-909.
127. Audoit, J., L. Rivière, J. Dandurand, A. Lonjon, E. Dantras, and C. Lacabanne, *Thermal, mechanical and dielectric behaviour of poly(aryl ether ketone) with low melting temperature*. Journal of Thermal Analysis and Calorimetry, 2018. **135**(4): p. 2147-2157.
128. Iqbal, T., B.J. Briscoe, and P.F. Luckham, *Surface Plasticization of Poly(ether ether ketone)*. European Polymer Journal, 2011. **47**(12): p. 2244-2258.
129. Ahmad, A., T. Iqbal, S. Yasin, R. Hanif, S. Riaz, and P. Luckham, *Stability of Amorphous PEEK in Organic Solvents*. Journal- Chemical Society of Pakistan, 2018. **40**: p. 810.
130. Beck, H.N., *Solubility characteristics of poly(etheretherketone) and poly(phenylene sulfide)*. Journal of Applied Polymer Science, 1992. **45**(8): p. 1361-1366.
131. da Silva Bursal, J., L.G. Peeva, S. Kumbharkar, and A. Livingston, *Organic solvent resistant poly(ether-ether-ketone) nanofiltration membranes*. Journal of Membrane Science, 2015. **479**: p. 105-116.

132. Fink, J.K., *Chapter 6 - Poly(aryl ether ketone)s*, in *High Performance Polymers (Second Edition)*, J.K. Fink, Editor. 2014, William Andrew Publishing. p. 153-175.
133. Colquhoun, H.M. and D.F. Lewis, *Synthesis of aromatic polyetherketones in trifluoromethanesulphonic acid*. *Polymer*, 1988. **29**(10): p. 1902-1908.
134. Kemmish, D.J. and B. Wilson, *Aromatic polyetherketones.*, 2003: CRC Press.
135. Attwood, T.E., P.C. Dawson, J.L. Freeman, L.R.J. Hoy, J.B. Rose, and P.A. Staniland, *Synthesis and properties of polyaryletherketones*. *Polymer*, 1981. **22**(8): p. 1096-1103.
136. Cakmak, M. and M. Simhambhatla, *Dynamics of uni and biaxial deformation and its effects on the thickness uniformity and surface roughness of poly (ether ether ketone) films*. *Polymer Engineering & Science*, 1995. **35**(19): p. 1562-1568.
137. Denault, J. and M. Dumouchel, *Consolidation Process of PEEK/Carbon Composite for Aerospace Applications*. *Advanced Performance Materials*, 1998. **5**(1): p. 83-96.
138. Panayotov, I.V., V. Orti, F. Cuisinier, and J. Yachouh, *Polyetheretherketone (PEEK) for medical applications*. *J Mater Sci Mater Med*, 2016. **27**(7): p. 118.
139. Haleem, A. and M. Javaid, *Polyether ether ketone (PEEK) and its 3D printed implants applications in medical field: An overview*. *Clinical Epidemiology and Global Health*, 2019. **7**(4): p. 571-577.
140. Wang, D., H. Gao, W. Jiang, and Z. Jiang, *Microcellular processing and relaxation of poly(ether ether ketone)*. *Journal of Polymer Science Part B: Polymer Physics*, 2007. **45**(20): p. 2890-2898.
141. Siddiq, A.R. and A.R. Kennedy, *Porous poly-ether ether ketone (PEEK) manufactured by a novel powder route using near-spherical salt bead porogens: characterisation and mechanical properties*. *Mater Sci Eng C Mater Biol Appl*, 2015. **47**: p. 180-8.
142. Li, Q., Y. Zhang, D. Wang, H. Wang, and G. He, *Porous polyether ether ketone: A candidate for hard tissue implant materials*. *Materials & Design*, 2017. **116**: p. 171-175.
143. Roeder, R., S.M. Smith, T.L. Conrad, N.J. Yanchak, C.H. Merrill, and G. Converse, *Porous and bioactive PEEK implants for interbody spinal fusion*. *Adv Mater Process*, 2009. **167**: p. 46-48.
144. Conrad, T.L. and R.K. Roeder, *Effects of porogen morphology on the architecture, permeability, and mechanical properties of hydroxyapatite whisker reinforced polyetheretherketone scaffolds*. *Journal of the Mechanical Behavior of Biomedical Materials*, 2020. **106**: p. 103730.
145. Uddin, M.N., P.S. Dhanasekaran, and R. Asmatulu, *Mechanical properties of highly porous PEEK bionanocomposites incorporated with carbon and hydroxyapatite nanoparticles for scaffold applications*. *Progress in Biomaterials*, 2019. **8**(3): p. 211-221.
146. Torstrick, F.B., N.T. Evans, H.Y. Stevens, K. Gall, and R.E. Guldberg, *Do Surface Porosity and Pore Size Influence Mechanical Properties and Cellular Response to PEEK?* *Clin Orthop Relat Res*, 2016. **474**(11): p. 2373-2383.
147. Torstrick, F.B., A.S.P. Lin, D. Potter, D.L. Safranski, T.A. Sulchek, K. Gall, and R.E. Guldberg, *Porous PEEK improves the bone-implant interface compared to plasma-sprayed titanium coating on PEEK*. *Biomaterials*, 2018. **185**: p. 106-116.
148. Evans, N.T., F.B. Torstrick, C.S. Lee, K.M. Dupont, D.L. Safranski, W.A. Chang, A.E. Macedo, A.S. Lin, J.M. Boothby, D.C. Whittingslow, R.A. Carson, R.E. Guldberg, and K. Gall, *High-strength, surface-porous polyether-ether-ketone for load-bearing orthopedic implants*. *Acta Biomater*, 2015. **13**: p. 159-67.
149. Sonnenschein, M.F., *Porosity-dependent Young's modulus of membranes from polyetherether ketone*. *Journal of Polymer Science Part B: Polymer Physics*, 2003. **41**(11): p. 1168-1174.
150. Ding, H., Q. Zhang, Y. Tian, Y. Shi, and B. Liu, *Preparation of porous structure in the system of PEEK/PPS/diphenyl ketone via thermally induced phase separation*. *Journal of Applied Polymer Science*, 2007. **104**(3): p. 1523-1530.
151. Talley, S.J., X. Yuan, and R.B. Moore, *Thermoreversible Gelation of Poly(ether ether ketone)*. *ACS Macro Letters*, 2017. **6**(3): p. 262-266.
152. Kemmish, D., *Update on the technology and applications of polyaryletherketones*. 2010, Shawbury, Shrewsbury, Shropshire, UK: ISmithers.
153. Bonner, W.H., *Aromatic polyketones and preparation thereof.*, US3065205A, 1962.
154. Gay, F.P. and C.M. Brunette, *Ordered polyetherketones.*, EP0192260A1, 1989.

155. Cortès, L.Q., N. Caussé, E. Dantras, A. Lonjon, and C. Lacabanne, *Morphology and dynamical mechanical properties of poly ether ketone ketone (PEKK) with meta phenyl links*. J. Appl. Polym. Sci., 2016. **133**: p. 43396.
156. Krishnaswamy, R.K. and D.S. Kalika, *Glass transition characteristics of poly(arylether ketone ketone) and its copolymers*. Polymer, 1996. **37**: p. 1915.
157. Gardner, K.H., B.S. Hsiao, and K.L. Faron, *Polymorphism in poly(aryl ether ketone)s*. Polymer, 1994. **35**: p. 2290.
158. Grange, N., P. Tadini, K. Chetehouna, N. Gascoin, G. Bouchez, S. Senave, and I. Reynaud, *Experimental determination of fire degradation kinetic for an aeronautical polymer composite material*. International Journal of Structural Integrity, 2017. **9**: p. 76-92.
159. Gupta, R., S. Shinde, A. Yella, C. Subramaniam, and S.K. Saha, *Thermomechanical characterisations of PTFE, PEEK, PEKK as encapsulation materials for medium temperature solar applications*. Energy, 2020. **194**: p. 116921.
160. Alqurashi, H., Z. Khurshid, A.U.Y. Syed, S. Rashid Habib, D. Rokaya, and M.S. Zafar, *Polyetherketoneketone (PEKK): An emerging biomaterial for oral implants and dental prostheses*. Journal of Advanced Research, 2021. **28**: p. 87-95.
161. Yuan, B., Y. Chen, H. Lin, Y. Song, X. Yang, H. Tang, E. Xie, T. Hsu, X. Yang, X. Zhu, K. Zhang, and X. Zhang, *Processing and Properties of Bioactive Surface-Porous PEKK*. ACS Biomaterials Science & Engineering, 2016. **2**(6): p. 977-986.
162. Yuan, B., Q. Cheng, R. Zhao, X. Zhu, X. Yang, X. Yang, K. Zhang, Y. Song, and X. Zhang, *Comparison of osteointegration property between PEKK and PEEK: Effects of surface structure and chemistry*. Biomaterials, 2018. **170**: p. 116-126.
163. Converse, G.L., T.L. Conrad, and R.K. Roeder, *Mechanical properties of hydroxyapatite whisker reinforced polyetherketoneketone composite scaffolds*. J Mech Behav Biomed Mater, 2009. **2**(6): p. 627-35.
164. Converse, G.L., T.L. Conrad, C.H. Merrill, and R.K. Roeder, *Hydroxyapatite whisker-reinforced polyetherketoneketone bone ingrowth scaffolds*. Acta Biomater, 2010. **6**(3): p. 856-63.
165. Li, B., T. Liu, Z.C.W. Tang, and W.-H. Zhong, *Fabrication and characterization of flexible high performance thermoplastic foams derived from rigid polyetherketoneketone via a VOC-free foaming method*. Journal of Materials Science, 2013. **48**(9): p. 3517-3527.
166. Tan, S.C., Z. Bai, H. Sun, J.E. Mark, F.E. Arnold, and C.Y.C. Lee, *Processing of microcellular foams from polybenzobisthiazole/polyetherketoneketone molecular composites*. Journal of Materials Science, 2003. **38**(19): p. 4013-4019.
167. Castro, A.J., *Methods for making microporous products*, US4247498A, 1981.
168. Caneba, G.T. and D.S. Soong, *Polymer membrane formation through the thermal-inversion process. 2. Mathematical modeling of membrane structure formation*. Macromolecules, 2002. **18**(12): p. 2545-2555.
169. Bazhenov, S.D., A.V. Bilyukevich, and A.V. Volkov, *Gas-Liquid Hollow Fiber Membrane Contactors for Different Applications*. Fibers, 2018. **6**(4): p. 76.
170. Kim, J.F., J.H. Kim, Y.M. Lee, and E. Drioli, *Thermally induced phase separation and electrospinning methods for emerging membrane applications: A review*. AIChE Journal, 2016. **62**(2): p. 461-490.
171. Khayet, M. and T. Matsuura, *Chapter 5 - Thermally Induced Phase Separation for MD Membrane Formation*, in *Membrane Distillation*, M. Khayet and T. Matsuura, Editors. 2011, Elsevier: Amsterdam. p. 89-120.
172. Song, S.-W. and J.M. Torkelson, *Coarsening effects on the formation of microporous membranes produced via thermally induced phase separation of polystyrene-cyclohexanol solutions*. Journal of Membrane Science, 1995. **98**(3): p. 209-222.
173. Lloyd, D.R., S.S. Kim, and K.E. Kinzer, *Microporous membrane formation via thermally-induced phase separation. II. Liquid—liquid phase separation*. Journal of Membrane Science, 1991. **64**(1): p. 1-11.
174. Koningsveld, R., R. Koningsveld, W.H. Stockmayer, and E. Nies, *Polymer Phase Diagrams: A Textbook*. 2001: Oxford University Press.

175. Lloyd, D.R., K.E. Kinzer, and H.S. Tseng, *Microporous membrane formation via thermally induced phase separation. I. Solid-liquid phase separation*. Journal of Membrane Science, 1990. **52**(3): p. 239-261.
176. Goh, Y.Q. and C.P. Ooi, *Fabrication and characterization of porous poly(L-lactide) scaffolds using solid-liquid phase separation*. J Mater Sci Mater Med, 2008. **19**(6): p. 2445-52.
177. Yang, F., X. Qu, W. Cui, J. Bei, F. Yu, S. Lu, and S. Wang, *Manufacturing and morphology structure of polylactide-type microtubules orientation-structured scaffolds*. Biomaterials, 2006. **27**(28): p. 4923-33.
178. Blundell, D.J. and B.N. Osborn, *The morphology of poly(aryl-ether-ether-ketone)*. Polymer, 1983. **24**(8): p. 953-958.
179. Quiroga Cortés, L., N. Caussé, E. Dantras, A. Lonjon, and C. Lacabanne, *Morphology and dynamical mechanical properties of poly ether ketone ketone (PEKK) with meta phenyl links*. Journal of Applied Polymer Science, 2016. **133**(19): p. 43396.
180. Sanchez, I.C. and E.A. DiMarzio, *Dilute Solution Theory of Polymer Crystal Growth: Fractionation Effects*. J Res Natl Bur Stand A Phys Chem, 1972. **76A**(3): p. 213-223.
181. Quick, C.R., J.E.K. Schawe, P.J. Uggowitzer, and S. Pogatscher, *Measurement of specific heat capacity via fast scanning calorimetry—Accuracy and loss corrections*. Thermochimica Acta, 2019. **677**: p. 12-20.
182. Wacharawichanant, S., S. Thongyai, S. Tanodekaew, J.S. Higgins, and N. Clarke, *Spinodal decomposition as a probe to measure the effects on molecular motion in poly(styrene-co-acrylonitrile) and poly(methyl methacrylate) blends after mixing with a low molar mass liquid crystal or commercial lubricant*. Polymer, 2004. **45**(7): p. 2201-2209.
183. Young, A.M., R. Garcia, J.S. Higgins, A.M. Timbo, and D.G. Peiffer, *Dynamic light scattering and rheology of associating sulfonated polystyrene ionomers in non-polar solvents*. Polymer, 1998. **39**(8): p. 1525-1532.
184. Landy, B.C., S.B. Vangordon, P.S. McFetridge, V.I. Sikavitsas, and M. Jarman-Smith, *Mechanical and in vitro investigation of a porous PEEK foam for medical device implants*. J Appl Biomater Funct Mater, 2013. **11**(1): p. e35-44.
185. Li, S., T.J. Pyrzynski, N.B. Klinghoffer, T. Tamale, Y. Zhong, J.L. Aderhold, S. James Zhou, H.S. Meyer, Y. Ding, and B. Bikson, *Scale-up of PEEK hollow fiber membrane contactor for post-combustion CO₂ capture*. Journal of Membrane Science, 2017. **527**: p. 92-101.
186. Yang, Q., G. Zhang, Z. Ma, J. Li, and X. Fan, *Effects of processing parameters and thermal history on microcellular foaming behaviors of PEEK using supercritical CO₂*. Journal of Applied Polymer Science, 2015. **132**(39): p. 42576.

Publication 1

Rusakov, D., Menner, A., Bismarck, A., High-Performance Polymer Foams by Thermally Induced Phase Separation. *Macromolecular Rapid Communications* **41** (2020), 2000110. DOI: 10.1002/marc.202000110

© 2020 The Authors. Published by WILEY-VCH Verlag GmbH & Co. KGaA, Weinheim. This is an open access article under the terms of the [Creative Commons Attribution](#) License, which permits use, distribution and reproduction in any medium, provided the original work is properly cited.



High-Performance Polymer Foams by Thermally Induced Phase Separation

Dmitrii Rusakov, Angelika Menner, and Alexander Bismarck*

Macroporous, low-density polyetheretherketone, polyetherketoneketone, and polyetherimide foams are produced using a high-temperature, thermally induced phase separation method. A high-boiling-point solvent, which is suitable to dissolve at least 20 wt% of these high-performance polymers at temperatures above 250 °C, is identified. The foam morphology is controlled by the cooling procedure. The resulting polymer foams have porosities close to 80% with surface areas up to 140 m² g⁻¹ and elastic moduli up to 97 MPa.

High performance polymers are a group of polymers characterized by excellent mechanical properties (polyetheretherketone [PEEK] and polyetherketoneketone [PEKK] E-modulus 3–4 GPa, tensile strength ≈100–120 MPa and polyetherimide [PEI] E-modulus ≈3 GPa, tensile strength ≈150–160 MPa), outstanding chemical resistance and high continuous service temperatures but are more expensive than engineering polymers.^[1] High melting temperatures, low melt strength, and insolubility in most common solvents makes it difficult to introduce porosity into high performance polymers. PEEK and PEKK are linear, semicrystalline polymers from the polyaryletherketone (PAEK) family with high glass transition (143 and 153 °C, respectively) and melting (343 and 350 °C, respectively) temperatures. In contrast to PAEKs, PEI is a linear amorphous high-performance polymer with a glass transition temperature of 217 °C. These three high-performance materials are widely used as insulation materials^[2] in the aerospace industry,^[3] as biomaterials or biomedical materials, especially for implants,^[4,5] and as light-weight, high-duty construction materials.^[6,7]

D. Rusakov, Dr. A. Menner, Prof. A. Bismarck
Institute of Material Chemistry and Research
Polymer and Composite Engineering (PaCE) Group
Faculty of Chemistry
University of Vienna
Währinger Straße 42, Vienna 1090, Austria
E-mail: alexander.bismarck@univie.ac.at
Prof. A. Bismarck
Department of Chemical Engineering
Imperial College London
South Kensington Campus, London SW7 2AZ, UK

The ORCID identification number(s) for the author(s) of this article can be found under <https://doi.org/10.1002/marc.202000110>.

© 2020 The Authors. Published by WILEY-VCH Verlag GmbH & Co. KGaA, Weinheim. This is an open access article under the terms of the Creative Commons Attribution License, which permits use, distribution and reproduction in any medium, provided the original work is properly cited.

DOI: 10.1002/marc.202000110

Porous polymers, with their combination of low density, high surface area, and good insulation properties, have found many applications in the modern world for instance as insulation materials,^[8] in composites^[9] and as membranes.^[10] Only a few examples of porous PEEK membranes and fibers^[11,12] or foam monoliths^[29] prepared by a temperature induced liquid–liquid phase separation or phase inversion process were reported. Most other examples of porous high performance polymer foams were produced by chemical or physical (gas) blowing^[13,14] or particulate leaching.^[15,16] However, the bulk production of PEEK and PEKK foams, and to a lesser degree PEI foams^[17,18] is still a huge challenge. Gas blowing and particulate leaching methods have limitations restricting their suitability for high performance polymers, because of the small processing window for semicrystalline polymers^[19] and high temperature and pressure requirements.^[16,20,21] Another possible approach to access high performance polymer foams uses polymer particles to stabilize either high internal phase emulsions^[22] or foams,^[23] which are subsequently dried and sintered. However, a major disadvantage of this method is the massive shrinkage of emulsion template and green body during drying and sintering.

The method to produce high performance porous polymers used by us is based on the commonly used thermally induced phase separation (TIPS) technique, which makes use of polymer solubility gradients at various temperatures.^[24,25] A polymer is initially dissolved in a solvent at a specific temperature until a homogeneous solution is obtained and then, the temperature is decreased either rapidly or at a specific rate until solid–liquid or liquid–liquid demixing occurs. During demixing a polymer-rich and polymer-poor phase form and thus after removal of the solvent, typically by drying, a porous material is obtained from the polymer rich phase. The solvent can be reused for the next process.

Here we present a high temperature TIPS method to produce high porosity, macroporous high-performance polymer foams with controllable pore morphology. PEEK, PEKK, and PEI were used to demonstrate the versatility of this method. 4-Phenylphenol (4PPH) was used as a universal aprotic, high boiling solvent (melting point +166 °C, boiling point +321 °C) for all three polymers. One major advantage of this solvent is that it can easily be recycled and, therefore, the environmental impact can be reduced. Under laboratory conditions we managed to recover and reuse between 80% and 90% of 4PPH. Foam density, surface area, pore morphology and the mechanical properties in compression of the resulting foams will be investigated.

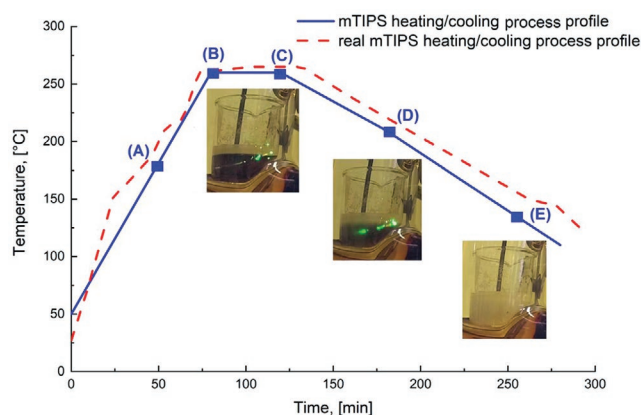


Figure 1. Schematic illustration of the TIPS process. The blue line shows the desired heating/cooling profile and red dashed line is an actual heating/cooling profile. The inserts are photographs of PEEK in 4PPH solutions taken during the process between points (A) and (B), at (D) and (E). A) 4PPH melting and initiation of the mixing process. B) Onset of temperature plateau with continued mixing. C) All polymer was dissolved and clear polymer solution observed, mixing was stopped, magnetic stirrer removed and cooling procedure began. D) Onset of gelation (only for PEEK and PEKK solutions), where the polymer phase separated into a gel. E) 4PPH crystallization point "freezing" the solution.

The TIPS procedure used for the preparation of porous high-performance polymers consisted of the following steps (**Figure 1**); initially, polymer powder (5 g) was mechanically mixed with 4PPH powder (20 g) in a 50 mL glass beaker. The beaker containing the mixture was then placed into a 250 mL glass round-bottom double-walled heating vessel connected to a thermostat (Huber Unistat T305w HT, Germany). An internal thermocouple (Erbo TX-401) was inserted into the powder mixture to control the temperature of the polymer/solvent mixture. The thermostat temperature was increased to $\approx 170^\circ\text{C}$ when all 4PPH melted fully and mixing using a glass-coated magnetic stirrer bar started (**Figure 1A**). The solution temperature was increased until a transparent polymer solution was observed, afterward the temperature T_i (**Table 1**) was held constant for 30 min (**Figure 1B**) while mixing continued to ensure complete dissolution (**Figure 1C**). The magnetic stirrer was then removed, and the vessel temperature decreased at 1°C min^{-1} until 120°C . Although the high-performance polymer in 4PPH solution crystallized at around 150°C , cooling continued until 120°C to ensure a homogeneous temperature profile of polymer/solvent mixture. Then, the temperature was decreased at a faster cooling rate ($50^\circ\text{C min}^{-1}$) until room temperature. Afterward, samples were purified using Soxhlet extraction for 48 h in ethanol before being dried to constant weight in an oven at 60°C for 24 h.

During cooling, two effects could be observed, namely solid-liquid demixing accompanied by gelation of the solution at T_{gel} (**Figure 1D**, **Table 1**) and solvent crystallization at T_{sol} (**Figure 1E**, **Table 1**). Gelation was not observed in PEI solutions but transparent PEI in 4PPH solutions solidified during the cooling process when reaching the solvent crystallization temperature T_{sol} (**Figure 1**, from point C directly to point E), which greatly affected the morphology of the produced porous **PEI** (we use bold and italic letters to indicate our foam samples). Conversely, during cooling PEEK and PEKK solutions became increasingly more turbid (we used a laser beam to check transparency, see **Figure 1** inserts), a sign of the onset of solid-liquid demixing resulting in gelation of the solution (**Figure 1D**), which was followed by solvent crystallization immobilizing the gel-like polymer network (**Figure 1E**).

After purification and drying, visible differences between samples without and with gelation stage during the cooling process were apparent (**Figure 2**). The macroscale **PEI** foam (**Figure 2 A1**) had a fiber structure, which formed when the solvent started to crystallize separating the dissolved polymer in to a fiber-like pattern. However, the weak interactions between the fibrous layers result in porous **PEI**, which was feeble and could be easily torn apart parallel to the fiber plane. On the microscale (**Figure 2 A2,A3**) porous **PEI** has a high degree of anisotropy characterized by the oriented fiber-like structure with gaps between the fibers (width $\approx 4.2 \pm 0.8 \mu\text{m}$), which is typical for porous polymers obtained by solid-liquid TIPS processes in which solvent crystallization occurs.^[26–28] In this case, the solvent crystals grow along the temperature gradient and produce the pore morphology, which is called microtubular structure.^[26–28] The cause of the temperature gradient across the sample is a tiny temperature gradient between top and bottom of the open heating vessel.

Macroscopic **PEKK** and **PEEK** foams (**Figure 2 B1,C1**) are more homogeneous to the naked eye the **PEI** foam (**Figure 2 A1**). During gelation, when solid-liquid demixing occurred, 4PPH was still liquid, but the solubility of PEEK and PEKK in the solvent decreased forming a gel structure in the solution during cooling. During 4PPH crystallization the liquid turns solid, which resulted in the immobilization of the gel structure. On the microscale, porous **PEEK** (**Figure 2 C2,C3**) possessed an isotropic structure with uniform spherical pores with an average diameter of $0.9 \pm 0.3 \mu\text{m}$, while the microstructure of porous **PEKK** (**Figure 2 B2-B3**) is somewhat in between porous **PEI** and **PEEK**. Porous **PEKK** has well-defined but elongated pores (length $\approx 21 \pm 7 \mu\text{m}$, width $\approx 8 \pm 2 \mu\text{m}$) embedded within a fiber-like structure. In this case the fibers are linked resulting in significant anisotropy of the pore structure. This observation suggests that the pore structure (**Figure 2**) is not only determined by the gelation process but

Table 1. Transparent solution temperature T_i , gelation temperature T_{gel} , solution crystallisation temperature T_{sol} as observed during TIPS processing, and measured physical and mechanical properties: foam density ρ_f , porosity P , elastic modulus E , crush strength σ and surface area A_s .

Polymer	T_i [$^\circ\text{C}$]	T_{gel} [$^\circ\text{C}$]	T_{sol} [$^\circ\text{C}$]	ρ_f [g cm^{-3}]	P [%]	E [MPa]	σ [MPa]	A_s [$\text{m}^2 \text{g}^{-1}$]
PEI	245 ± 10	—	150 ± 4	0.37 ± 0.03	73 ± 3	n/a	n/a	4 ± 2
PEKK	258 ± 8	177 ± 8	149 ± 8	0.31 ± 0.03	77 ± 2	26 ± 8	1.4 ± 0.5	79 ± 9
PEEK	261 ± 1	200 ± 10	143 ± 2	0.36 ± 0.04	74 ± 3	97 ± 20	7 ± 1	140 ± 15

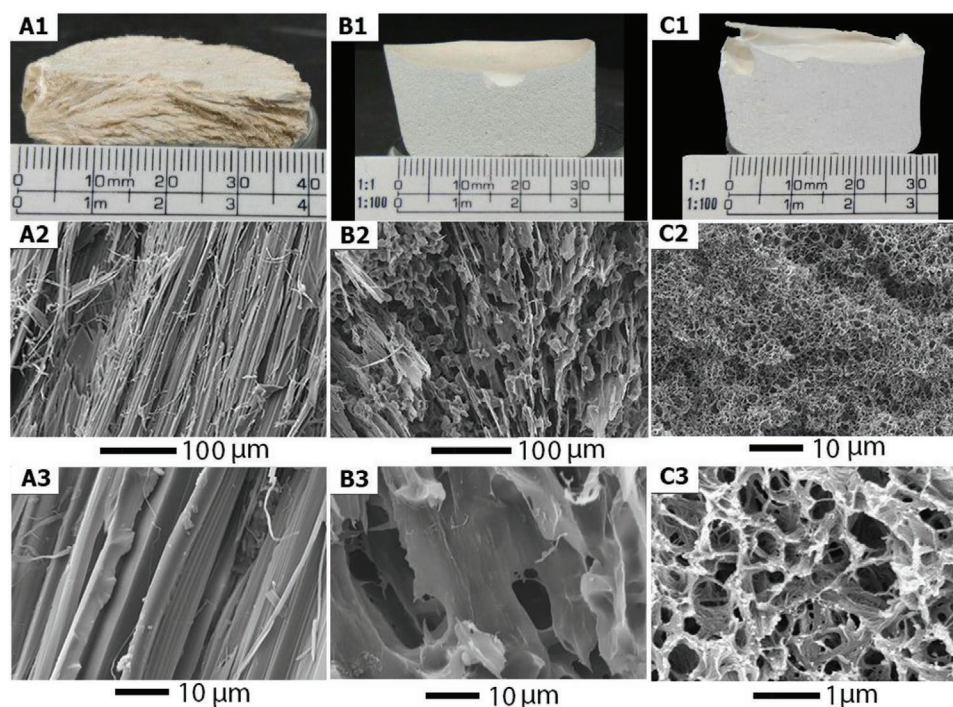


Figure 2. Photographs of cylindrical A) *PEI*, B) *PEKK*, C) and *PEEK* foams cut laterally. Below: SEM images of the corresponding foams at two magnifications.

also the time period between gelation and solvent crystallization (Figure 1, between point D and E),^[29] which is longest for *PEEK* (≈ 50 min) followed by *PEKK* (≈ 25 – 30 min) and absent for *PEI* solutions.

Porosity and foam density of the produced polymer foams are listed in Table 1. *PEI* foams with various porosities and foam densities are already commercially available, however, research into novel porous *PEI* production methods is still of significant interest.^[30–32] The TIPS method utilized by us yielded porous *PEI* with a microtubular structure and porosity of $73 \pm 3\%$ and a foam density of $0.37 \pm 0.03 \text{ g cm}^{-3}$. Unfortunately, the obtained porous *PEI* was too feeble to be cut into compression test samples.

So far porous *PEKK* has only been produced by particulate leaching.^[15,33,34] Reported porosities for porous *PEKK* obtained by porogen leaching were around 75 – 90% ,^[33,34] which are close to that achieved by us ($77 \pm 2\%$). Converse et al.^[33] reported compression properties of porous *PEKK* produced by porogen leaching, the E-moduli reported are of the same order of magnitude as those measured by us while the compression strength is identical within error (for a comparison see Figure S4, Supporting Information).

Most porous *PEEK* monoliths were produced using gas blowing,^[14,19,35] particulate leaching^[16,20,36,37] or solvent exchange/gel preparation.^[29,38–40] Using our TIPS process we were able to produce porous *PEEK* with a porosity of $74 \pm 3\%$ and a foam density of $0.36 \pm 0.04 \text{ g cm}^{-3}$ without the need for blowing agents, high pressure and temperatures exceeding the melting point of *PEEK*. Besides, our porous *PEEK* possessed excellent mechanical properties (E-modulus = $97 \pm 20 \text{ MPa}$) when compared to the scarce literature data (Figure 3A,B).

Using the particulate leaching method the porosity of *PEEK* foams can be controlled; foams with lower porosities have higher moduli^[36] and vice versa^[16] (Figure 3A). Our data point fits this trend. Two research groups reported a (thermoreversible) gelation process to produce porous *PEEK* also in high boiling point solvents. Venkatraman et al.^[38] produced porous *PEEK* using a solvent exchange process using the solvent 4-chlorophenol, however, their porous *PEEK* shrunk significantly during the drying process resulting in a porous *PEEK* with a foam density of only 0.84 g cm^{-3} (Figure 3B). Therefore, it is not surprising that the E-modulus of those samples was around 180 MPa . Talley et al.^[29,39,40] reported porous *PEEK* with foam densities around 0.3 – 0.45 g cm^{-3} having E-moduli ranging from 20 to 60 MPa . The *PEEK* foams produced by us however had E-moduli of $\approx 100 \text{ MPa}$ despite having the same foam density. Furthermore, we did not use corrosive solvents (Figure 3B).

Despite using the same process to produce porous *PEEK*, *PEKK*, and *PEI* the surface area varied significantly. The adsorption isotherm (Figure S2, Supporting Information) of porous *PEI* was type III. This *PEI* foam possessed the lowest surface area (Table 1). Such low surface area is indicative of macroscale pores and the absence of micro and mesopores in the pore walls,^[41] which is reflected in the BJH analysis (Figure S3, Supporting Information). Porous *PEEK* exhibited a type IV adsorption isotherm (Figure S2, Supporting Information). The adsorption isotherm had a small hysteresis loop, due to the capillary condensation occurring in mesopores present in the polymer structure.^[42] Porous *PEEK* had the highest surface area of the produced porous polymers with $140 \pm 15 \text{ m}^2 \text{ g}^{-1}$. The BJH-pore distribution analysis

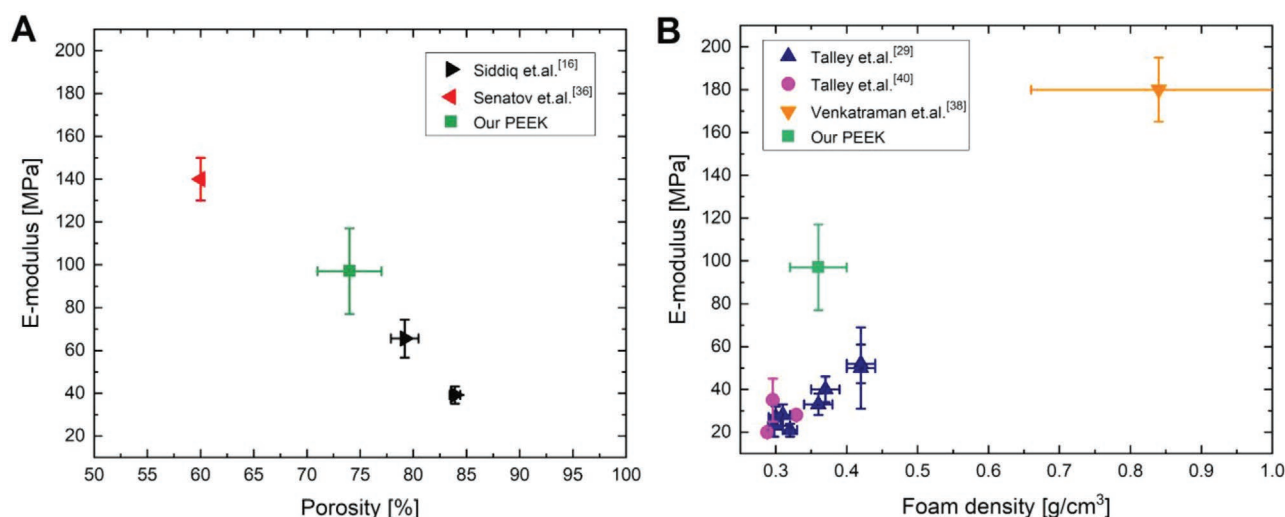


Figure 3. Elastic modulus of our porous **PEEK** foams (green square) compared to literature data as a function of A) porosity and B) foam density. Unfortunately, not all authors reported the foam densities and, therefore, it was impossible to collate all the data in a single graph.

(Figure S3, Supporting Information) showed the presence of mesopores with diameters ranging from 2 to 18 nm. The surface area of porous **PEEK** was $70 \pm 10 \text{ m}^2 \text{ g}^{-1}$. The adsorption isotherms of porous **PEEK** (type IV) also exhibited a hysteresis loop, typical of mesoporous materials with multilayer capillary condensation^[43,44] occurring in mesopores with a pore diameter of 2–18 nm (Figure S3, Supporting Information).

Here we presented a versatile TIPS method to produce high porosity high performance polymer foams using a high boiling point solvent ($T_b = +321 \text{ }^\circ\text{C}$), of which up to 90% could be recovered after ethanol extraction and reused. Our method does not require an extruder capable of processing high performance polymers or polymer solvent mixtures. In addition, the mechanical properties of the resulting **PEEK** foams are higher than many reported analogues with the same foam density/porosity. It is worth noting, that the interaction of one solvent with different polymers leads to varying foam morphologies and this indicates that the interaction of one particular polymer with different solvents will also lead to varying morphologies, which will be demonstrated in the future.

Supporting Information

Supporting Information is available from the Wiley Online Library or from the author.

Acknowledgements

The authors acknowledge the support of the Austrian Science Fund (FWF) through the project I1800.

Conflict of Interest

The authors declare no conflict of interest.

Keywords

high-performance polymers, polyetheretherketone, polymer foams, porous polymers

Received: March 3, 2020

Revised: March 26, 2020

Published online: May 4, 2020

- [1] P. M. Hergenrother, *High Perform. Polym.* **2003**, *15*, 3.
- [2] V. Mittal, *High Performance Polymers and Engineering Plastics*, Wiley, Hoboken, NJ **2011**.
- [3] N. Grange, P. Tadini, K. Chetehouna, N. Gascoin, G. Bouchez, S. Senave, I. Reynaud, *Int. J. of Struc. Integr.* **2018**, *9*, 76.
- [4] M. G. Wiesli, M. Ozcan, *Implant Dent.* **2015**, *24*, 448.
- [5] S. M. Kurtz, *PEEK Biomaterials Handbook*, Elsevier, Waltham, USA **2012**.
- [6] M. Madhukar Mahendra, P. Jitender, *Int. J. Eng. Res. Technol.* **2017**, *6*, 350.
- [7] S. Meenakshi, N. Srinivas, Y. S. Siddarth, C. V. S. Kamal, K. Sudheendra, S. Bhowmik, M. K. Pitchan, J. A. Epaarachchi, *Mater. Res. Express* **2019**, *6*, 095333.
- [8] J. Li, A. Zhang, S. Zhang, Q. Gao, W. Zhang, J. Li, *Composites, Part B* **2019**, *156*, 368.
- [9] W. Gong, H. Fu, C. Zhang, D. Ban, X. Yin, Y. He, L. He, X. Pei, *Polymers* **2018**, *10*, 1375.
- [10] B. Zhu, M. Duke, L. F. Dumeé, A. Merenda, E. des Ligneris, L. Kong, P. D. Hodgson, S. Gray, *Membranes* **2018**, *8*, 83.
- [11] M. F. Sonnenschein, *J. Appl. Polym. Sci.* **1999**, *72*, 175.
- [12] M. F. Sonnenschein, *J. Appl. Polym. Sci.* **1999**, *74*, 1146.
- [13] R. Verdejo, P. Werner, J. Sandler, V. Altstädt, M. S. P. Shaffer, *J. Mater. Sci.* **2009**, *44*, 1427.
- [14] L. Cafiero, S. Iannace, L. Sorrentino, *Eur. Polym. J.* **2016**, *78*, 116.
- [15] B. Yuan, Y. Chen, H. Lin, Y. Song, X. Yang, H. Tang, E. Xie, T. Hsu, X. Yang, X. Zhu, K. Zhang, X. Zhang, *ACS Biomater. Sci. Eng.* **2016**, *2*, 977.
- [16] A. R. Siddiq, A. R. Kennedy, *Mater. Sci. Eng., C* **2015**, *47*, 180.
- [17] L. Sorrentino, M. Aurilia, S. Iannace, *Adv. Polym. Technol.* **2011**, *30*, 234.

- [18] D. Miller, P. Chatchaisucha, V. Kumar, *Polymer* **2009**, 50, 5576.
- [19] P. Werner, R. Verdejo, F. Wöllecke, V. Altstädt, J. K. W. Sandler, M. S. P. Shaffer, *Adv. Mater.* **2005**, 17, 2864.
- [20] Q. Li, Y. Zhang, D. Wang, H. Wang, G. He, *Mater. Des.* **2017**, 116, 171.
- [21] T. Garg, O. Singh, S. Arora, R. Murthy, *Crit. Rev. Ther. Drug Carrier Syst.* **2012**, 29, 1.
- [22] I. Akartuna, E. Tervoort, J. C. H. Wong, A. R. Studart, L. J. Gauckler, *Polymer* **2009**, 50, 3645.
- [23] J. C. H. Wong, E. Tervoort, S. Busato, U. T. Gonzenbach, A. R. Studart, P. Ermanni, L. J. Gauckler, *J. Mater. Chem.* **2009**, 19, 5129.
- [24] J. F. Kim, J. H. Kim, Y. M. Lee, E. Drioli, *AIChE J.* **2016**, 62, 461.
- [25] P. van de Witte, P. J. Dijkstra, J. W. A. van den Berg, J. Feijen, *J. Membr. Sci.* **1996**, 117, 1.
- [26] F. Yang, X. Qu, W. Cui, J. Bei, F. Yu, S. Lu, S. Wang, *Biomaterials* **2006**, 27, 4923.
- [27] J. Guan, K. L. Fujimoto, M. S. Sacks, W. R. Wagner, *Biomaterials* **2005**, 26, 3961.
- [28] P. X. Ma, R. Zhang, *J. Biomed. Mater. Res.* **2001**, 56, 469.
- [29] S. J. Talley, C. L. Anderson Schoepe, C. J. Berger, K. A. Leary, S. A. Snyder, R. B. Moore, *Polymer* **2017**, 126, 437.
- [30] D. Feng, L. Li, Q. Wang, *RSC Adv.* **2019**, 9, 4072.
- [31] H. Sehaqui, M. E. Galvez, V. Becatinni, Y. C. Ng, A. Steinfeld, T. Zimmermann, P. Tingaut, *Environ. Sci. Technol.* **2015**, 49, 3167.
- [32] G. Bakeri, A. F. Ismail, M. R. DashtArzhandi, T. Matsuura, *J. Membr. Sci.* **2015**, 475, 57.
- [33] G. L. Converse, T. L. Conrad, R. K. Roeder, *J. Mech. Behav. Biomed. Mater.* **2009**, 2, 627.
- [34] G. L. Converse, T. L. Conrad, C. H. Merrill, R. K. Roeder, *Acta Biomater.* **2010**, 6, 856.
- [35] Q. Yang, G. Zhang, Z. Ma, J. Li, X. Fan, *J. Appl. Polym. Sci.* **2015**, 132, 42576.
- [36] F. S. Senatov, A. V. Chubrik, A. V. Maksimkin, E. A. Kolesnikov, A. I. Salimon, *Mater. Lett.* **2019**, 239, 63.
- [37] L. Cai, Y. Pan, S. Tang, Q. Li, T. Tang, K. Zheng, A. R. Boccaccini, S. Wei, J. Wei, J. Su, *J. Mater. Chem. B* **2017**, 5, 8337.
- [38] P. Venkatraman, C. Rader, N. Bohmann, E. J. Foster, *Polymer* **2019**, 169, 154.
- [39] S. J. Talley, X. Yuan, R. B. Moore, *ACS Macro Lett.* **2017**, 6, 262.
- [40] S. J. Talley, S. L. Vivod, B. A. Nguyen, M. A. B. Meador, A. Radulescu, R. B. Moore, *ACS Appl. Mater. Interfaces* **2019**, 11, 31508.
- [41] Z. Allothman, *Materials* **2012**, 5, 2874.
- [42] M. Thommes, K. Kaneko, A. V. Neimark, J. P. Olivier, F. Rodriguez-Reinoso, J. Rouquerol, K. S. W. Sing, *Pure Appl. Chem.* **2015**, 87, 1051.
- [43] A. Grosman, C. Ortega, *Langmuir* **2008**, 24, 3977.
- [44] M. Thommes, *Chem. Ing. Tech.* **2010**, 82, 1059.



Supporting Information

for *Macromol. Rapid Commun.*, DOI: 10.1002/marc.202000110

High-Performance Polymer Foams by Thermally Induced Phase Separation

Dmitrii Rusakov, Angelika Menner, and Alexander Bismarck*

Supplementary information

Experimental section.

Materials. PEEK APC-2 powder and PEKK powder were kindly supplied by Cytec (Solvay Group) supply. PEI pellets and 4-phenylphenol (97% purity) were purchased from Sigma-Aldrich. 96% purity ethanol were purchased from Brenntag NV (Belgium). All material was used as received.

Characterisation Methods. Foam density and porosity was measured as follows: the skeletal density (ρ_s) was measured using a helium gas-displacement pycnometer (AccuPyc II 1340, Micromeritics Ltd, Norcross, USA). Dried foamed samples with total mass around 0.4 g were cut out from various positions of foam samples (of which at least four replicates were prepared) and measured in 3.5 cm³ aluminium chamber. The foam density (ρ_f) was determined by powder pycnometry (GeoPyc 1360, Micromeritics Ltd, Norcross, USA). Three foam pieces of approx. 10 x 10 x 10 mm³ in size were cut from each foamed sample and taken for individual measurement. The porosity (P) calculated by followed equation.

$$P = \left(1 - \frac{\rho_f}{\rho_s}\right).$$

To determine the pore morphology a benchtop scanning electron microscope (JEOL JCM-6000, JEOL Ltd, Japan) was used. Foamed samples were physically broken and small piece from each sample was fixed to the sample holder using black carbon tape. Then, samples were gold coated in an argon atmosphere using a fine coater (JEOL JFC-1200). The sample surface area was measured using a surface area analyzer (TriStar II 3020, Micromeritics Ltd., Norcross, USA) via nitrogen adsorption at 77 K. BET (Brunauer–Emmet–Teller) and BJH (Barrett–Joyner–Halenda) methods were used to determine the surface and pore area distribution. Foamed samples were grinded or cut for small pieces with total mass from 0.2 to 0.4 g, placed into glass vial and dried at +100°C with active nitrogen purge overnight.

The compression properties of bulk polymer foams were measured using a dual column universal test frame (Instron 5969, Darmstadt, Germany) equipped with a 50 kN load cell. **PEEK** and **PEKK** samples were cut using a band saw (PROXXON MBS 240/E) into cubic samples with dimensions of 10 x 10 x 10 mm³. After cutting, the samples were carefully polished using fine sandpaper or a mechanical polishing machine to ensure that the surfaces were parallel. Samples with obvious cracks or large voids were discarded. 6 **PEEK** and 15 **PEKK** cubic samples were prepared for compression test. All samples were compressed to 75% of their original height at a testing speed of 1 mm/min. The elastic modulus (E) was determined from the slope of the initial linear region of the stress-strain curve. The crush strength (σ_c) was determined as shown in **Figure S1**.

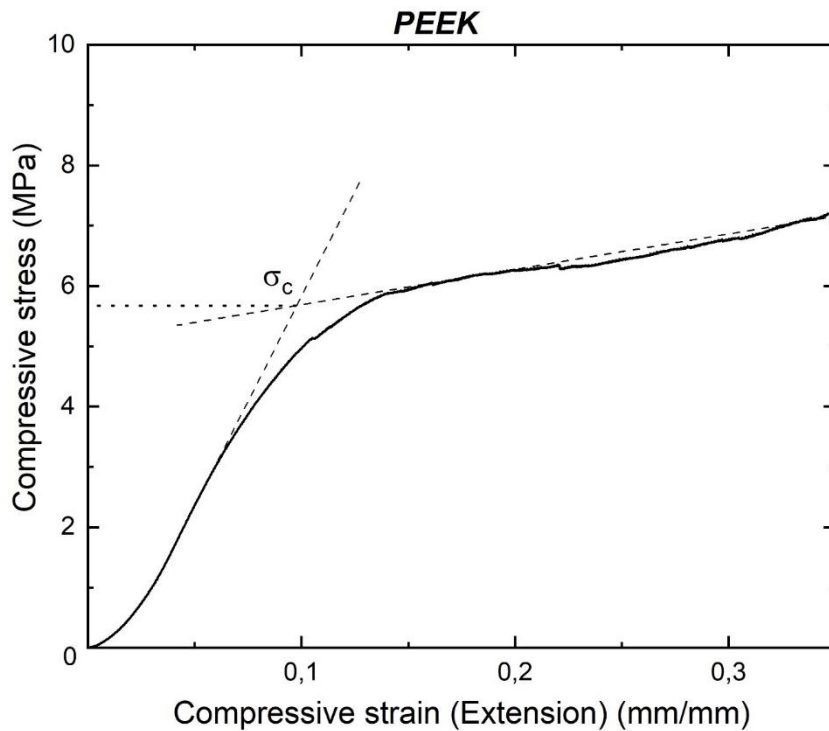


Figure S1. The crush strength (σ_c) determination on the compression stress-strain curve.

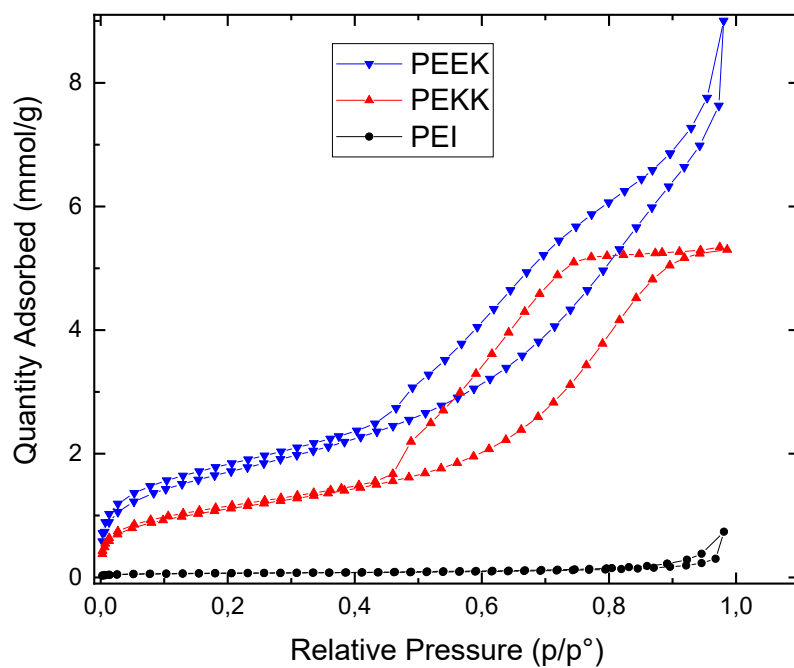


Figure S2. The adsorption BET isotherm for porous *PEI*, *PEKK* and *PEEK* samples.

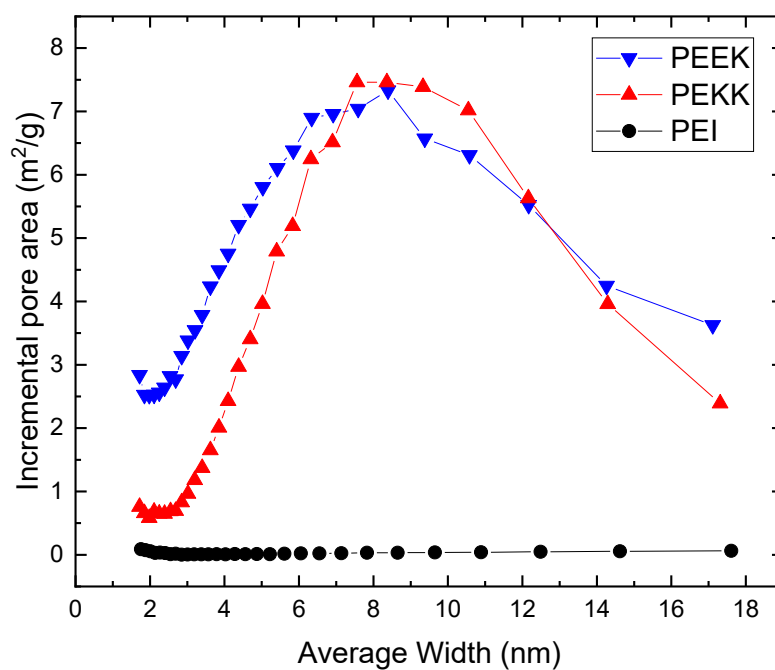


Figure S3. Incremental pore area distribution as function of average pore width for foamed *PEI*, *PEKK* and *PEEK*.

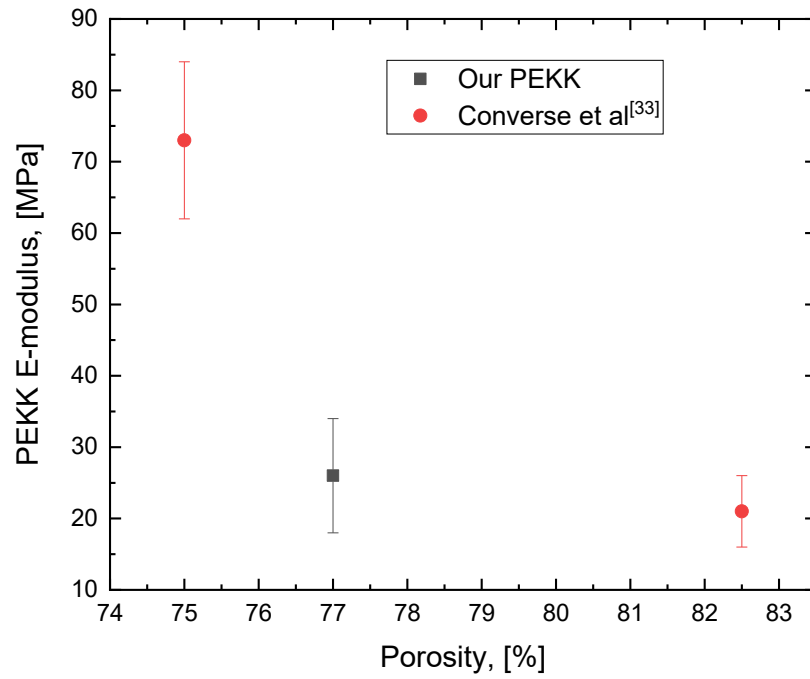


Figure S4. Elastic modulus of our porous **PEKK** compared to literature data (Converse et al. [33]) as a function of porosity.

Publication 2

Rusakov, D., Menner, A., Spieckermann, F., Wilhelm, H., Bismarck, A., *Morphology and properties of foamed high crystallinity PEEK prepared by high temperature thermally induced phase separation*. Journal of Applied Polymer Science **139** (2021), 51423. DOI: 10.1002/app.51423

© 2021 The Authors. Journal of Applied Polymer Science published by Wiley Periodicals LLC. This is an open access article under the terms of the [Creative Commons Attribution](#) License, which permits use, distribution and reproduction in any medium, provided the original work is properly cited.

ARTICLE

Morphology and properties of foamed high crystallinity PEEK prepared by high temperature thermally induced phase separation

Dmitrii Rusakov¹  | Angelika Menner¹  | Florian Spieckermann²  | Harald Wilhelm³  | Alexander Bismarck^{1,4} 

¹Institute of Material Chemistry and Research, Polymer and Composite Engineering (PaCE) Group, Faculty of Chemistry, University of Vienna, Vienna, Austria

²Materials Physics, Department Materials Science, University of Leoben, Leoben, Austria

³Laboratory of Polymer Engineering (LKT-TGM), Vienna, Austria

⁴Department of Chemical Engineering, Imperial College London, London, UK

Correspondence

Alexander Bismarck, Department of Chemical Engineering, Imperial College London, South Kensington Campus, London SW7 2AZ, UK.

Email: alexander.bismarck@univie.ac.at

Funding information

Austrian Science Fund, Grant/Award Number: I1800

Abstract

Polyetheretherketone (PEEK) is a high-performance semi-crystalline thermoplastic polymer with outstanding mechanical properties, high thermal stability, resistance to most common solvents, and good biocompatibility. A high temperature thermally induced phase separation technique was used to produce PEEK foams with controlled foam density from PEEK in 4-phenylphenol (4PPH) solutions. Physical and mechanical properties, foam and bulk density, surface area, and pore morphology of foamed PEEK were characterized and the role of PEEK concentration and cooling rate was investigated. Porous PEEK with densities ranging from 110 to 360 kg/m³ with elastic moduli and crush strength ranging from 13 to 125 MPa and 0.8 to 7 MPa, respectively, was produced.

KEYWORDS

Poly ether ether ketone (PEE)K, porous polymers, Temperature induced phase separation (TIPS)

1 | INTRODUCTION

Polymers are currently among the most commonly used materials globally because they are lightweight and durable, have good mechanical properties and low production costs. These features facilitate their use in a wide range of applications, such as consumer products, construction materials, insulation, films, membranes, and so on. One of the most promising classes of industrial high-performance polymers are polyaryletherketones, which possess high continuous service temperatures, that is, the maximum temperature at which the polymers can be used without significant change

in properties, outstanding mechanical properties and high chemical resistance.^{1,2} One such high-performance polymer is polyetheretherketone (PEEK) – a semi-crystalline linear polymer with a high elastic modulus ($E = 3\text{--}4$ GPa) and tensile strength ($\sigma \approx 100$ MPa) and a glass transition temperature (T_g) of 143°C and melting temperature T_m of 343°C. The aromatic rings and saturated bonds within PEEKs structure provide good biocompatibility, high oxidation stability and chemical resistance at temperatures below T_g .³ In fact, at temperatures below T_g PEEK can only be dissolved in concentrated sulfuric and methanesulphonic acid.⁴ While at temperatures exceeding the glass transition

This is an open access article under the terms of the Creative Commons Attribution License, which permits use, distribution and reproduction in any medium, provided the original work is properly cited.

© 2021 The Authors. *Journal of Applied Polymer Science* published by Wiley Periodicals LLC.

temperature, it is possible to dissolve PEEK in high boiling solvents, such as dichloroacetic acid, benzophenone, 4-phenylphenol, diphenyl sulfone, and chlorophenols.^{5–7}

PEEK adheres well to carbon fibers,⁸ carbon nanotubes⁹ and other fillers,¹⁰ which can be used to further improve the mechanical and thermal properties of PEEK. PEEK and reinforced PEEK are widely used in biomedical applications as artificial scaffolds¹¹ or as implants without requiring any additional coatings or modifications because of their bioinert nature.^{12,13} PEEK is also used for the fabrication of membranes¹⁴ or high-pressure fittings¹⁵ and construction materials for aerospace applications.¹⁶ More recently, PEEK found also use as material for additive manufacturing using fused deposition modeling.¹⁷

Porous polymers are a class of polymer materials, which combine low density with good mechanical properties and high surface areas.¹⁸ Porous polymers are consequently used as membranes,¹⁹ filtration materials,²⁰ separators in batteries⁴ and scaffolds in biomedical applications.²¹ Foam density, pore morphology and pore size distribution all significantly influence the material properties of porous polymers, however, control of these properties for semicrystalline polymers during manufacturing is still challenging. Unfortunately, the insolubility of PEEK in many common solvents and its small melt processing window and low melt strength²² make it difficult to produce porous PEEK, for instance by chemical or physical blowing.^{23,24} As PEEK is synthesized by step-growth polymerization in polar high boiling point aprotic solvents at relatively high-temperatures¹⁵ it is also difficult to produce PEEK foams directly during synthesis.

Despite these challenges, several methods to produce porous PEEK have been reported. One of the most common methods is the use of sacrificial porogens, such as sodium chloride²³ or titanium wires,²⁵ which are then removed by leaching, or by blowing (for instance using Clariant XH907 with azodicarbonamide as the main component).²⁴ In porogen leaching, PEEK powder and spherical salt beads or other porogens are mechanically mixed, compression molded and sintered at high pressure and temperature (around or above melting temperature). The porogen is then washed out using water (in case of NaCl) or other specific leaching agents resulting in PEEK foams. However, the complete removal of porogens and production of mesoscale porosity is typically not straight forward. Porous PEEK can also be produced by laser sintering.²⁶ PEEK foams were produced by physical blowing, that is, by absorbing supercritical CO₂ at high pressure in PEEK followed by expansion of the absorbed CO₂ at temperatures ranging from 240 to 340°C.²⁷ CO₂ was also used as a foaming agent to produce foamed PEEK/polyetherimide (PEI) blends²⁸; PEEK/PEI blends were saturated with CO₂ at temperatures (close or above T_g)

followed by expansion to produce the foamed material. The main disadvantages of gas foaming are lack of control of the pore morphology and the tendency of gas bubbles to coalesce because of PEEK's low melt strength.²² Emulsion templating can also be used to produce high porosity high-performance polymer foams (for instance from polyvinylidene fluoride (PVDF), polytetrafluoroethylene (PTFE) and PEEK), however, significant shrinkage of the materials occurs during the final sintering step.²⁹ More recently, Talley et al.^{30–32} described a method to produce porous PEEK aero/xerogels with a foam density of around 0.3 g/cm³ by dissolving PEEK in high boiling solvents (dichloroacetic acid and 4-chlorophenol) followed by precipitating PEEK at temperatures above T_g .

We recently showed that low density (~0.36 g/cm³) monolithic PEEK, polyetherketoneketone (PEKK), and PEI foams with very high E-moduli (97 MPa) can be produced using high temperature thermally-induced phase separation (HT-TIPS).³³ The TIPS method is based on the temperature dependent solubility of polymers in specific solvents. The polymer of interest is dissolved under active mixing until a transparent solution is obtained. Then, the solution is cooled at a specific cooling rate, until liquid-liquid or liquid-solid phase demixing occurs forming a polymer-rich, solvent-poor and a polymer-poor, solvent-rich phase. Subsequent removal of the solvent yields porous polymers.

The research reported herein builds from our previous work, with particular focus on the production of porous PEEK by broadening the scope of polymer/solvent concentrations and cooling rates used in its formation. We will show that it is possible to tailor the foam density and morphology, and thus the mechanical properties of porous PEEK over a wider range than achieved by Talley et al.^{30–32} Most importantly, the mechanical properties of the PEEK foams reported here significantly exceed those reported previously. We will also provide evidence that these improved mechanical properties correlated well with high degrees of crystallinity in our PEEK foams, which are achieved using our HT-TIPS method.

2 | EXPERIMENTAL SECTION

2.1 | Materials

PEEK APC-2 powder with average particle size (SMD or Sauter mean diameter) = 145 μm (see Figure S1 in SI) was kindly supplied by Cytec (Solvay Group). 4-Phenylphenol (melting temperature T_f ~ 166°C, boiling point T_b ~ 321°C) with a purity of 97% was purchased from Sigma-Aldrich and was used as solvent for PEEK.

Iron(III) chloride (anhydrous for synthesis) was purchased from Sigma-Aldrich. Ethanol with a purity of 96% (Brenntag NV, Belgium) was used for purification of porous PEEK. Acetone with 99.5% purity was supplied by Thermo Fisher Scientific. All materials were used as received.

2.2 | Preparation of porous PEEK

Various amounts of PEEK and 4PPH powder were weighed (see Table 1 for formulations and process parameters), and mechanically mixed in a 50 ml borosilicate glass beaker to produce a homogenous mixture of the two powders (PEEK and 4PPH), before a glass-coated magnetic stir bar was added. The beaker containing the blend was then placed into a 250 ml double-walled, round-bottom borosilicate glass vessel (GlasKeller Basel AG, CH) with a two necked glass cap (DN 60), which was connected to a high-temperature thermostat with an active cooling system (Huber Unistat T305W HT, D) with a maximum operating temperature of 300°C using insulated high-temperature resistant hoses. A calibrated precision core thermometer (Erbo TFX 410, Ingolstadt, D) was used to control the temperature inside the PEEK/4PPH mixture. PEEK was dissolved in 4PPH by increasing the vessel temperature until the 4PPH melted (~170–180°C, Figure 1 point A), at which

point stirring commenced. The temperature was further increased until the dissolution temperature (Table 1). Stirring continued for 15 to 25 min until a clear solution was observed (Figure 1, point C). The clear solution point was determined using a green laser pointer (see insert in

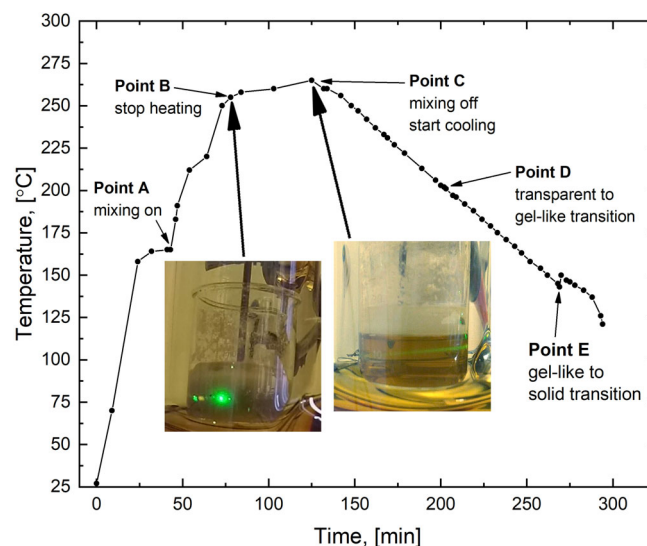


FIGURE 1 Characteristic heating/cooling profile for sample D2. The insert shows how we determined the solution state using a green laser pointer. Insert pictures can also be found in SI Figure S2 [Color figure can be viewed at wileyonlinelibrary.com]

TABLE 1 HT-TIPS process parameters (heating and cooling rates) used for the production of foamed PEEK samples: Cooling rate, β ; temperature, T @ B, at which temperature was kept constant till point C was reached while mixing continued (point B); mixing time, t_{B-C} , at constant temperature required to produce a transparent PEEK solution (see Figure 1); temperature, T_{gel} @ D, where PEEK solution started to become cludy exhibiting a gel-like character; and solvent (4PPH) crystallization temperature, T_f @ E

Sample name	[PEEK]/wt%	β /[°C/min]	T @ B/[°C]	t_{B-C} /[min]	T_{gel} @ D/[°C]	T_f @ E/[°C]
A1	5	0.5	248 ± 4	15	—	146 ± 1
A2	5	1	248 ± 3	15	—	147 ± 1
A3	5	2	249 ± 1	15	—	151 ± 1
A4	5	10	248 ± 4	15	—	150 ± 1
B1	10	0.5	262 ± 8	20	172 ± 4	143 ± 1
B2	10	1	262 ± 4	20	166 ± 3	146 ± 1
B3	10	2	256 ± 3	20	160 ± 2	148 ± 2
B4	10	10	259 ± 2	20	—	150 ± 3
C1	15	0.5	259 ± 4	25	195 ± 5	149 ± 6
C2	15	1	261 ± 3	25	181 ± 9	148 ± 5
C3	15	2	259 ± 1	25	181 ± 1	145 ± 4
C4	15	10	258 ± 1	25	—	150 ± 1
D1	20	0.5	264 ± 3	30	200 ± 4	142 ± 2
D2	20	1	261 ± 1	30	197 ± 8	143 ± 1
D3	20	2	260 ± 3	30	199 ± 7	145 ± 7
D4	20	10	258 ± 3	30	Not visible	151 ± 1

Figure 1). This temperature depended on the PEEK concentration. It was impossible to produce a homogeneous solution when trying to dissolve more than 20 wt% PEEK in 4PPH. After confirming the clear solution point, stirring was stopped and the solution cooled at set cooling rates β (Figure 1 from C, and Table 1). During cooling, the solution started to become turbid and then gel-like (Figure 1 D) in a relatively narrow temperature range (Table 1). After solvent crystallization, observable by the temperature increase recorded due to the release of latent heat of crystallization of 4PPH (Figure 1, E), the vessel temperature was further decreased at the same cooling rate until 120–110°C (inside the samples) to ensure a homogeneous temperature profile of the polymer-solvent mixture. Finally, the samples were removed from the beaker and the crystalline solvent removed by Soxhlet extraction using ethanol for 48 h before being dried until constant weight in a vacuum oven at 60°C for 24 h. At least 5 repeats were performed for porous PEEK samples which were structurally sound to ensure reproducibility.

2.3 | Characterization of porous PEEK

Pore structure: A benchtop scanning electron microscope (JEOL JCM-6000, JEOL Ltd., Japan) was used to investigate the pore morphology of porous PEEK. Pieces of less than 1 cm in longitudinal direction and 1–2 mm in thickness were broken off from the porous PEEK samples and fixed to the sample holder using conductive carbon stickers. Silver paint (Achseon 1415, G 302, Agar Scientific, UK) was applied around the sample edge to increase conductivity prior to gold coating the samples in an argon atmosphere using a fine coater (JEOL JFC-1200, JEOL Ltd, Japan). SEM micrographs were collected at various magnifications from numerous sites on each sample to characterize the pore structure.

Absolute (skeletal) density ρ_s was measured using a helium gas-displacement pycnometer (AccuPyc II 1340, Micromeritics Ltd, Norcross). Porous PEEK samples were cut (for 5 wt% samples) or broken (for 10, 15, and 20 wt% samples) into irregularly shaped pieces (each side of the piece was from 5 to 10 mm) from various positions of the sample, with a total mass of 0.3–0.4 g, then, weighed, and placed into a 3.5 cm³ measurement chamber and its volume determined.

Bulk (foam) density ρ_f was determined using an envelope density analyzer (GeoPyc 1360, Micromeritics Ltd., Norcross). Three pieces of each porous PEEK sample approx. 10 × 10 × 10 mm³ in size were cut from the porous PEEK for individual measurements. The porosity P was calculated using as follows:

$$P = \left(1 - \frac{\rho_f}{\rho_s}\right) \quad (1)$$

Mechanical properties were measured in compression adapting the ISO 844:2001 standard using a dual column universal test frame (Instron 5969, Darmstadt, Germany) equipped with a 50 kN load cell. Porous PEEK samples were cut from their original cylindrical shape using a band saw (PROXXON MBS 240/E) into cubes with dimensions of 10 × 10 × 10 mm³. After cutting, all porous PEEK cubes were carefully polished using a mechanical polishing machine to ensure flat parallel sample surfaces. Samples with obvious cracks or voids were discarded from the measurements. At least 5 samples were compressed to 75% of their original height at a test speed of 1 mm/min, and engineering stress strain curves recorded. The elastic modulus (E) was determined from the linear elastic region of the stress-strain curve. The crush strength (σ_c) is defined as the highest strength at the end of the initial linear elastic region (see SI Figure S3).

The **glass transition temperature** T_g and **degree of crystallinity** X_{DSC} were determined using differential scanning calorimetry (DSC, Discovery series, TA instruments). Between 3 and 6 mg of each sample was analyzed from 50–400°C at a heating rate of 10°C/min. The heat flow was recorded twice for two subsequent heating and cooling runs. X_{DSC} was determined from the area under the melting peak of the first heating run as follows:

$$X_{DSC} = \frac{\Delta H_f^{peak}}{\Delta H^0} \quad (2)$$

where ΔH_f^{peak} is the measured melting enthalpy and ΔH^0 the theoretical enthalpy of melting of a perfectly crystalline PEEK sample (130 J/g).³⁴

Selected samples (A1, B1, B4, C2, and D1) were investigated using ultra-fast calorimetry using a **Flash-DSC** (DSC 2+ Mettler Toledo equipped with UFS 1 MEMS sensors). Such experiments allow for heating and cooling rates of up to 40,000 and 10,000 K/s, respectively, which allows the suppression of secondary crystallization during the experiment.

The critical cooling rate to suppress PEEK crystallization is in the order of 2 K/s.³⁵ Therefore, by melting and subsequent quenching at rates of 5000 K/s fully amorphous PEEK can be created and the step in the heat flux related to the glass transition can be evaluated. The step of the heat flux associated with the glass transition of the fully amorphous state was used to calibrate the mass of the sample. Heat losses are independent of the heating

rate β^{36} and cancel out in the difference of the step height. Hence, these can be used for the determination of the sample mass on the FDSC chip m_{FDSC} :

$$m_{\text{FDSC}} = \frac{\Delta\phi_{\beta}}{\beta \Delta c_p} \quad (3)$$

where $\Delta\phi_{\beta}$ is the step of the heat flux at T_g determined at a heating rate β ($= 5000 \text{ K/s}$) and Δc_p ($= 0.271 \text{ J/g K}^{-1}$) the step of the heat capacity at T_g of PEEK as reported by Cheng et al.³⁷ Sample masses ranged from 5 to 120 ng.

Surface area and mesopore size distribution were determined by nitrogen adsorption at 77 K using the Brunauer–Emmet–Teller (BET) and Barrett–Joyner–Halenda (BJH) methods performed in a surface area analyzer (TriStar II 3020, Micromeritics Ltd., Norcross). Samples with total mass of 0.2 to 0.4 g, were cut or broken into small pieces (roughly 1–2 mm in all dimensions) and dried at 100°C under active nitrogen flow for 12 h prior to measurement.

To determine whether 4PPH remained in PEEK, we performed a **qualitative phenol test**.³⁸ Seven test

tubes with 7 various solutions were prepared. Test tubes were filled with pure acetone or acetone extracted original PEEK as negative controls, 0.5 g of 4PPH were dissolved in acetone as a positive control or extracts from ground PEEK foams (**A1**, **A4**, **D1**, and **D4**). The original or ground PEEK foams were dispersed in acetone and shaken for 24 h. Afterwards, the acetone used to extract the PEEK was collected and added to test tubes and finally 0.3 ml of 1 wt% iron(III) chloride solution was added to each tube and shaken vigorously (see **SI** Figure S4).

3 | RESULTS AND DISCUSSION

Table 1 summarizes our observations during the cooling process. During cooling of 5 wt% PEEK in 4PPH solutions using the HT-TIPS process at all cooling rates, we observed a fast solid–liquid demixing (type 1) in the temperature range of 141–151°C. Typically, solvent crystallization occurred in a few seconds (Table 1), immobilizing the PEEK (Video **S1-A1**, **SI**) and yielding anisotropic,

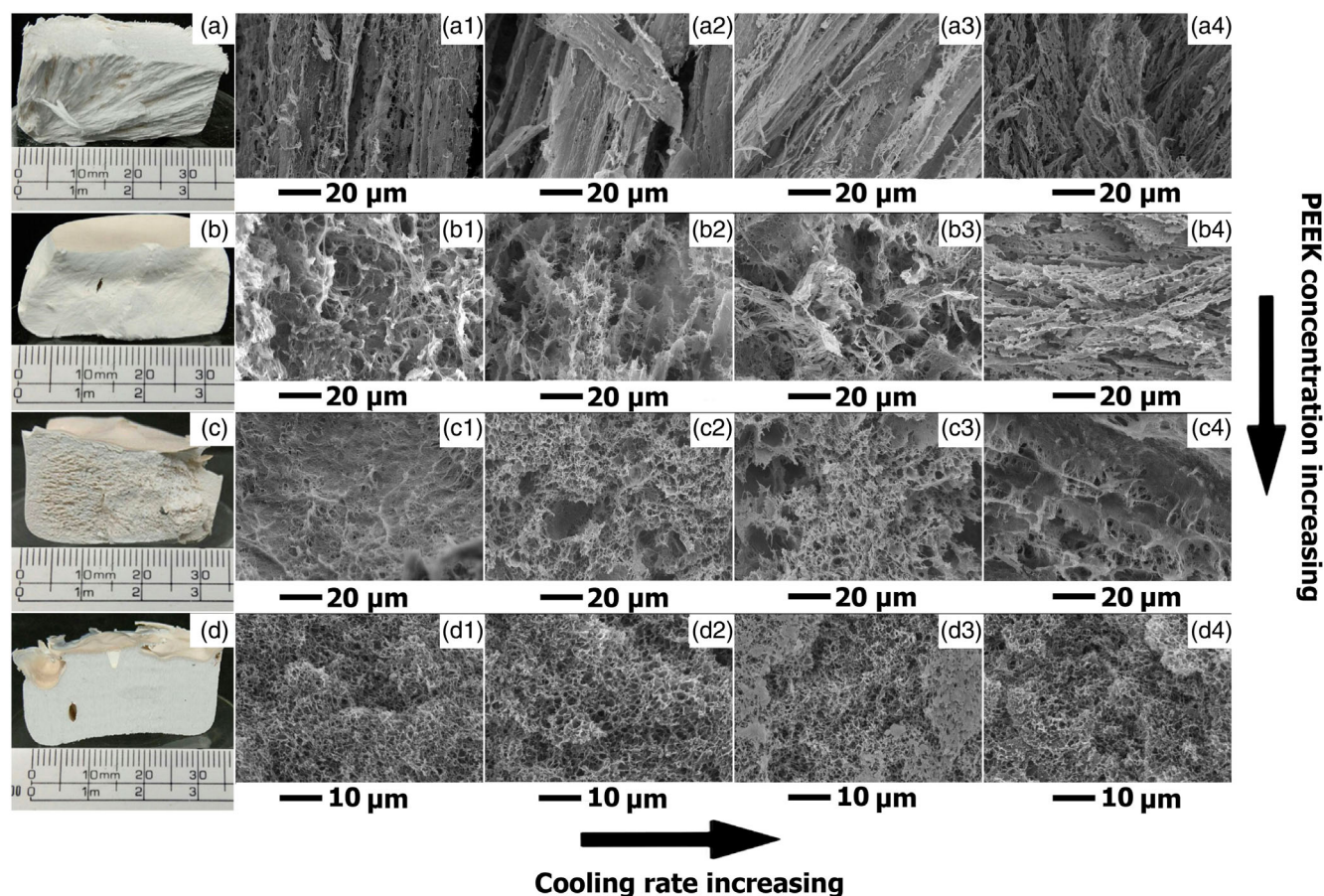


FIGURE 2 Representative photographs and SE micrographs of PEEK foams prepared from PEEK in 4PPH solutions containing 5 wt% (a), 10 (b), 15 (c), and 20 wt% (d) PEEK at cooling rates $\beta = 0.5^\circ\text{C/min}$ (1), 1°C/min (2), 2°C/min (3), and 10°C/min (4). ($\times 3000$ magnification). Please note that for row **D** we used a higher magnification [Color figure can be viewed at wileyonlinelibrary.com]

fiber-like macro- and microscopic structures (photographs and SE micrographs in Figure 2). These samples were feeble and difficult to handle because of weak interactions between the fiber-like features (Figure 2 row A). Solvent crystallization forced the PEEK out of solution and the crystals grew in the freezing direction of the solvent, which formed the anisotropic fiber-like structure, typical for porous polymers obtained by TIPS processes where solvent crystallization occurred before solution gelation.^{42,45} The foams obtained using a cooling rate of 0.5°C/min (**A1**) contained long, thin fibers with no apparent fiber-connectivity. The fiber ends have sharp edges and look as if they were torn apart. Foams prepared at cooling rates of 1 (**A2**) and 2°C/min (**A3**) have a similar morphology, but the fibers appear more densely packed. In foams prepared at a cooling rate of 10°C/min (**A4**) the fibers were much shorter and more chaotically oriented. The foams produced from 5 wt% PEEK in 4PPH solutions had channel-like pores with the largest diameter.

In contrast, slow solid–liquid demixing prior to solvent crystallization (type 2) was observed during cooling of 20 wt% PEEK solutions (Video S2-D1, SI). During this demixing process the PEEK solutions became increasingly turbid and gelled. Gelation is caused by (1) decreasing polymer solubility in solutions with decreasing temperature and (2) polymer crystallization from solution becoming more preferable for semicrystalline polymers as the solution temperature drops below their crystallization temperature.³⁹ The gelation temperature decreased with increasing cooling rates (Table 1). Lower cooling rates provided enough time for PEEK molecules to crystallize from solution thus creating a gel-like structure. The influence of cooling rate on PEEK crystallization process from melt has been well described in the literature^{40,41} and thus it is fair to assume that the same behavior exists for crystallization of PEEK from solution. The gel structure was frozen upon reaching the solvent crystallization temperature of 4PPH. All porous PEEK obtained by HT-TIPS from 20 wt% PEEK in 4PPH solutions had a smooth, white surface (Photo Figure 2 row D) and, at the microscale, a uniform morphology at all cooling rates (Figure 2, D1–D4), producing the smallest pores of all our PEEK foams. The high gelation point (see Table 1) and long time between gelation and solvent crystallization resulted in a homogeneous pore structure (Figure 2, D1–D4).

At concentrations between the two extremes, one observes an overlap of type 1 and 2 solid–liquid demixing processes. As shown in Figure 2 row B and C, the PEEK foams obtained from solutions containing 10 and 15 wt% PEEK had, when produced at low cooling rates ($\beta = 0.5$ and 1°C/min), a typical homogeneous pore structure (Figure 2 B1 and C1, 2). At increased cooling rates ($\beta = 2$ and 10°C/min) a mixed fiber-like/pore structure was

obtained (Figure 2 B2–4 and C3, 4). It is worth noting that at $\beta = 10^\circ\text{C}/\text{min}$, gelation and solution crystallization occurred too fast to visibly distinguish between the two processes (Video S3-A4, SI).

As demonstrated above, the polymer concentration greatly affected the pore structure. Generally, with increasing polymer concentration the pore size decreased, and the foam morphology became more homogeneous (Figure 2).

For all PEEK foams type IV BET isotherms (SI Figure S5) were obtained. Type IV isotherms are indicative of meso/macroporous materials containing pores with diameters ranging from 2 to 100 nm. All foams displayed well-pronounced hysteresis loops and thus it is fair to assume that cylindrical pores were more prominent in the pore walls of the samples than ink-bottle shaped pores. The specific surface areas of porous PEEK produced were in the range of 132–173 m²/g (see Table 2). Three phases form when PEEK crystallization starts from a homogeneous solution: a crystalline PEEK phase, an amorphous PEEK phase still containing solvent, and a solvent-rich phase containing some dissolved polymer. Thus, it is likely that the mesopores in the pore walls of the PEEK foams formed during the extraction of the crystalline 4PPH by ethanol and are the remnants of the polymer remaining in solvent-rich phase. The porosity of the PEEK foams (Table 2) did not significantly affect the surface area. Interestingly, the cooling rate did appear to affect the surface area; lower cooling rates yielded higher specific surface areas within the PEEK foams. This effect could potentially be due to pores collapsing during rapid cooling or solvent crystallization.

The total specific surface area is the sum of the surface areas resulting from large macropores in the foams and mesoscale porosity present in the pore walls of the PEEK foams. The Barrett–Joyner–Halenda (BJH) method was used to determine the pore-size distribution resulting from mesopore scale pores. Besides the macropores visible in the SEM (Figure 2) the foams also contained mesopores with sizes ranging from 2 to 18 nm. Figure 3 shows the pore size distributions for the produced porous PEEK with varying porosities.

The foam density and thus porosity of the PEEK foams is controlled by the PEEK concentration in the solution; increasing the PEEK concentration results in an increased foam density and lower porosity (Table 2), as may be expected. The cooling rate did not significantly affect the foam and skeletal density. However, porous PEEK produced from 5 and 10 wt% solutions obtained at a cooling rate of 10°C/min had a higher porosity than expected. A possible explanation for this could be the high sample anisotropy of all specimens obtained at high cooling rates (Figure 2).

TABLE 2 Skeletal ρ_s and foam density ρ_f , porosity P and BET surface area A_s of PEEK foams

$\beta/^\circ\text{C}/\text{min}$	[PEEK]/wt% Property	5	10	15	20
0.5	ρ_s [g/cm ³]	1.38 \pm 0.03	1.38 \pm 0.02	1.38 \pm 0.02	1.37 \pm 0.01
	ρ_f [g/cm ³]	0.11 \pm 0.02	0.2 \pm 0.04	0.27 \pm 0.07	0.36 \pm 0.06
	P [%]	92 \pm 1	86 \pm 2	81 \pm 5	74 \pm 4
	A_s /m ² /g	159 \pm 7	160 \pm 10	170 \pm 30	140 \pm 10
1	ρ_s [g/cm ³]	1.37 \pm 0.03	1.38 \pm 0.02	1.37 \pm 0.01	1.37 \pm 0.02
	ρ_f [g/cm ³]	0.16 \pm 0.06	0.17 \pm 0.02	0.29 \pm 0.08	0.36 \pm 0.04
	P [%]	89 \pm 4	88 \pm 1	79 \pm 6	73 \pm 4
	A_s /m ² /g	151 \pm 2	150 \pm 10	150 \pm 20	140 \pm 20
2	ρ_s [g/cm ³]	1.37 \pm 0.04	1.37 \pm 0.01	1.37 \pm 0.01	1.38 \pm 0.01
	ρ_f [g/cm ³]	0.12 \pm 0.06	0.15 \pm 0.02	0.24 \pm 0.02	0.32 \pm 0.06
	P [%]	91 \pm 4	89 \pm 3	83 \pm 2	75 \pm 7
	A_s /m ² /g	140 \pm 4	154 \pm 2	149 \pm 3	145 \pm 4
10	ρ_s [g/cm ³]	1.36 \pm 0.01	1.37 \pm 0.01	1.38 \pm 0.01	1.37 \pm 0.01
	ρ_f [g/cm ³]	0.14 \pm 0.04	0.13 \pm 0.03	0.21 \pm 0.08	0.29 \pm 0.06
	P [%]	90 \pm 3	91 \pm 2	85 \pm 5	79 \pm 4
	A_s /m ² /g	130 \pm 20	137 \pm 1	149 \pm 4	141 \pm 5

The measured skeletal densities of porous PEEK produced from solutions containing increasing PEEK concentrations using different cooling rates ranged from 1.36 to 1.38 g/cm³ (Table 2). The amorphous and crystalline phase of PEEK have different densities and thus the absolute density of PEEK depends on the amorphous/crystalline phase ratio. Fully amorphous PEEK has a density of around 1.26 g/cm³,⁴³ while fully crystalline PEEK has a density close to 1.40 g/cm³.⁴⁴ Therefore, our results suggest that the volume fraction degree of crystallinity of the PEEK in our foams ranges from 71% to 86%. This is somewhat surprising as PEEK, when melt processed, has typically a degree of crystallinity of ~30%–40%, which is primarily influenced by processing conditions and thermal history.⁴⁰

However, in our study PEEK (powder) was fully dissolved at ~250–270°C in the high boiling solvent 4PPH and then crystallized from solution during the cooling process. The thermal properties were characterized by DSC, shown in Figure 4.

The glass transition temperature of (APC-2) PEEK, according to the manufacturer, ought to be +143°C with minor variations and should be evident as a step in the DSC heating curve.¹⁵ However, for semicrystalline polymers with a high degree of crystallinity, T_g can be difficult to define. Our porous PEEK, which crystallized from 4PPH solution during cooling (see Table 1), possessed rather high degrees of crystallinities, higher than those reported in the literature,^{40,41,50} with values exceeding 50% and, therefore, no well-visible glass transition step was discernible in the

heating run (Figure 4(a)). The degree of crystallinities determined from the recrystallisation peak (now from the melt) during the cooling run, were below 40%, as expected. In addition, the glass transition step during cooling was visible (Figure 4(a)). To ensure that these high degrees of crystallinity determined by standard DSC experiments were correct they were remeasured by Flash-DSC (Figure 4(b)). Degrees of crystallinity, X_{DSC} , for our porous PEEKs are listed in Table 3.

No substantial recrystallisation is possible when heating with rates of 5000 K/s as the heating curve of the fully amorphous state clearly shows (no endothermic peak in the red curve in Figure 4(b)). Also, no melting or recrystallisation is discernible in the as-crystallized state (black curve in Figure 4(b)). The degree of crystallinity of the five selected samples was determined from the heat of fusion of as-crystallized samples with good precision by division with the heat of fusion of the fully crystalline state ($\Delta H_f = 130$ J/g). The crystallinity determined by FDSC confirms the high crystallinities obtained by standard DSC measurements (Table 3). However, FDSC also shows that the crystallinity was underestimated by 10%–15% during standard DSC measurements (Table 4). FDSC allows for the inhibiting of dynamic melting-recrystallization during heating, which affects the reliability of the interpretation of the melting peak in standard DSC. Flash-DSC, therefore, better reflects the crystallinity of the as-produced state, which is in much better agreement with the volumetric crystallinities estimated from measured densities. The high

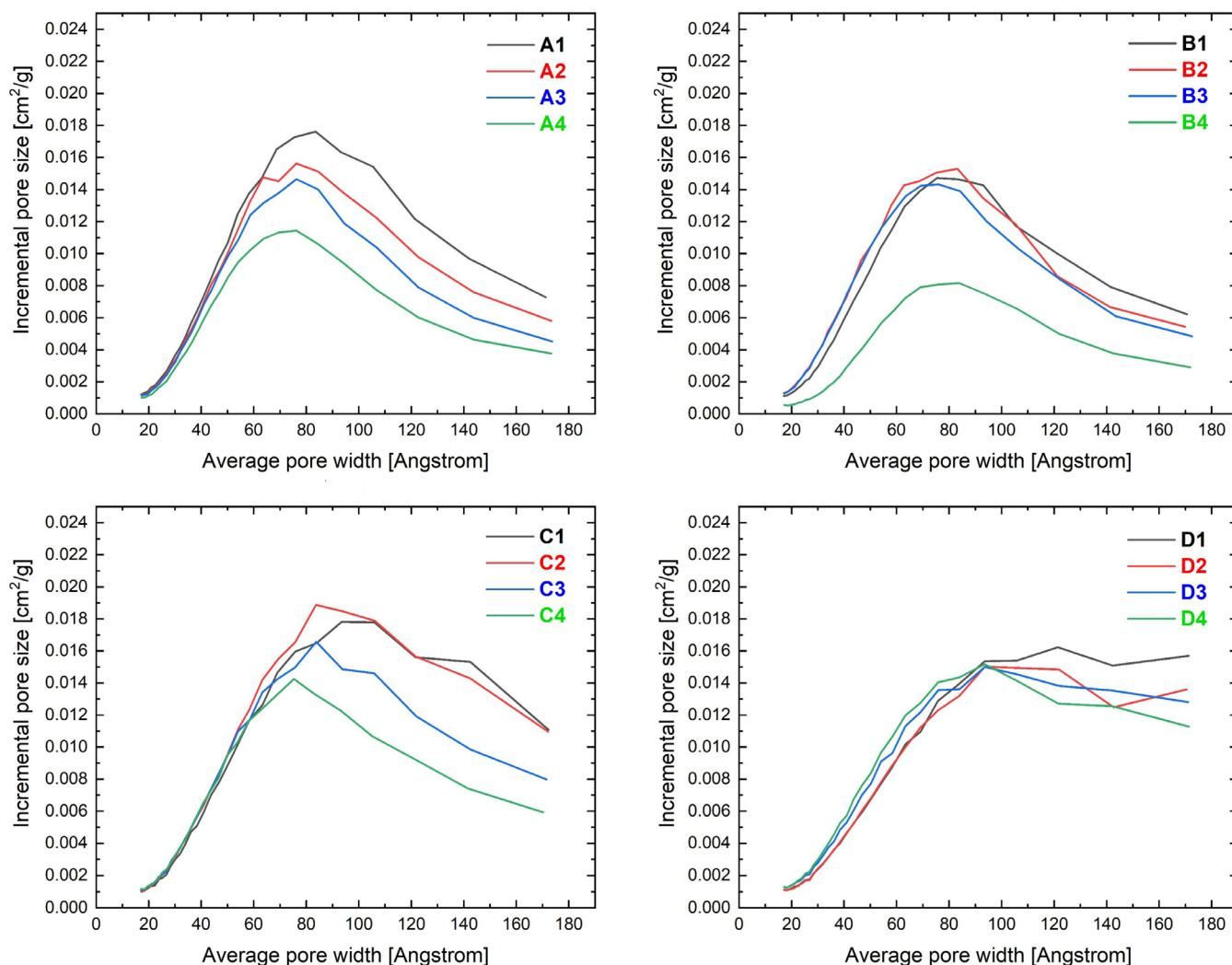


FIGURE 3 Incremental pore size distribution as function of average pore width for 5 wt% (A1-A4), 10 wt% (B1-B4), 15 wt% (C1-C4), and 20 wt% (D1-D4) foamed PEEK [Color figure can be viewed at [wileyonlinelibrary.com](#)]

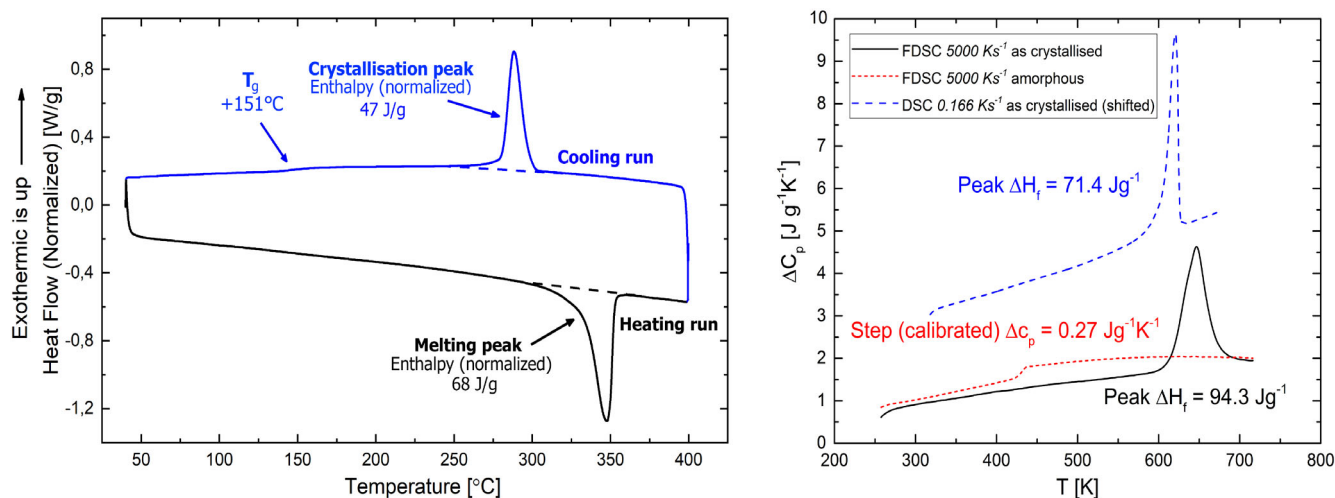


FIGURE 4 DSC (left figure) and flash DSC (right figure) evaluation of crystallinity sample A1 [Color figure can be viewed at [wileyonlinelibrary.com](#)]

TABLE 3 Measured change in melt and crystallization enthalpies ΔH_f and degrees of crystallinity X_{DSC} , calculated using equation 3, obtained by standard DSC of porous PEEK

Sample	ΔH_f [J/g]		X_{DSC} [%]	
	Heating run	Cooling run	Heating run	Cooling run
A1	70 ± 2	47 ± 2	54 ± 2	40 ± 1
A2	70 ± 2	48 ± 1	54 ± 2	40 ± 1
A3	66 ± 2	49 ± 1	50 ± 2	38 ± 1
A4	64 ± 1	49 ± 2	49 ± 1	38 ± 2
B1	71 ± 2	49 ± 2	54 ± 2	38 ± 1
B2	71 ± 2	52 ± 1	55 ± 1	40 ± 1
B3	69 ± 4	53 ± 1	53 ± 3	41 ± 1
B4	63 ± 4	50 ± 3	48 ± 3	38 ± 3
C1	72 ± 1	47 ± 1	55 ± 1	36 ± 1
C2	71 ± 1	53 ± 1	55 ± 1	41 ± 1
C3	71 ± 1	53 ± 1	55 ± 1	41 ± 1
C4	66 ± 2	53 ± 2	51 ± 2	41 ± 2
D1	73 ± 3	52 ± 1	56 ± 2	41 ± 1
D2	74 ± 1	54 ± 1	57 ± 1	42 ± 1
D3	71 ± 2	52 ± 1	55 ± 1	40 ± 1
D4	68 ± 5	51 ± 1	52 ± 4	39 ± 1

TABLE 4 Degree of crystallinity X_{FDSC} calculated from ΔH_f data, determined by FDSC measurements

Sample	X_{FDSC} [%]	Sample mass [ng](calibrated through $\Delta\phi\beta$)
A1	72	38.4
B1	64	5.3
B4	61	46.1
C2 (small load)	59	8.5
C2 (heavy load)	61	118.1
D1	76	40.4

degree of crystallinity X_{FDSC} did positively influence the mechanical strength of the produced PEEK foams.

The PEEK amorphous phase tends to transform to a crystalline phase at temperatures above T_g , a well-known effect called polymer annealing. Annealing of PEEK is well documented in the literature and occurs at temperatures between T_g and the melting point.^{47,48} In this temperature range, polymer chains become more mobile and tend to assume a more compact state to reduce the system energy, joining the crystal lattice at temperatures above T_g . PEEK annealing generally starts at temperatures above 200°C with annealing time being an important parameter due to the slow polymer chain rearrangement process.⁴⁹ In general, longer annealing times result in a higher degree of crystallinity.

Based on these facts and our findings, we hypothesize the following explanation of the observed effects: (i) dissolving PEEK in 4PPH at temperatures above T_g is increasing the mobility of polymer chains during cooling, which is the main factor for the high degree of crystallinity (Table 4), (ii) cooling PEEK in 4PPH solution during the HT-TIPS process, leads to PEEK crystallization from solution; lower cooling rates allow for longer crystallization times at temperatures above T_g , which results in a higher degree of crystallinity.

The amorphous/crystalline phase ratio of a polymer affects density, thermal behavior, solvent resistance, processability, and mechanical properties. Higher degrees of crystallinity result in close packing of the PEEK molecules, which results in a higher skeletal density and correspondingly higher elastic moduli, as our results confirm.

The mechanical properties of the foams prepared from 5 wt% PEEK in 4PPH solutions could not be determined due to their feeble, anisotropic, fiber-like structure, which made it impossible to prepare test specimens. Of the foams prepared from 10 wt% PEEK in 4PPH solutions, only the sample produced using a cooling rate of 0.5°C/min could be cut and tested. This sample had a crush strength of 0.8 MPa and an elastic modulus of 13 MPa (Table 5) despite its low foam density and high porosity (88%), which was caused by its relatively homogeneous morphology (Figure 2, **B1**). The foams produced from 15 wt% PEEK in 4PPH solutions had similar porosities (ranging between 79% and 85%) but much higher

$\beta/^\circ\text{C}/\text{min}$	[PEEK]/wt% Property	10	15	20
0.5	E [MPa]	13 ± 4	40 ± 10	130 ± 20
	σ [MPa]	0.8 ± 0.1	1.8 ± 0.6	6.6 ± 0.8
1	E [MPa]	n/a	40 ± 10	100 ± 20
	σ [MPa]	n/a	1.9 ± 0.1	7 ± 1
2	E [MPa]	n/a	17 ± 6	n/a
	σ [MPa]	n/a	1.9 ± 0.1	n/a

TABLE 5 Mechanical properties of the foamed PEEK samples obtained from various PEEK concentrations (5 wt% samples are not possible to cut for compression tests) and cooling rates (10°C/min samples are not available because of thermo-residual stress cracks presents), where E represents elastic modulus and σ is crush strength

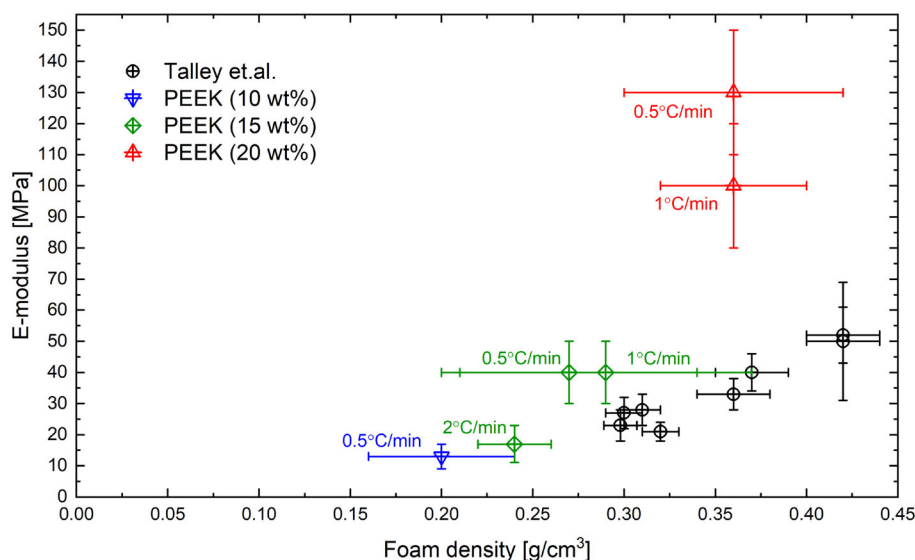


FIGURE 5 Elastic moduli of our porous PEEK obtained using various cooling rates and polymer concentrations compared with literature data.³¹ Detailed graphs showing E-moduli and crush strengths as a function of foam density and porosity of our PEEK samples can be found in figure S7 (SI) [Color figure can be viewed at wileyonlinelibrary.com]

E-moduli and crush strengths compared to the foams prepared from 10 wt% solutions. The mechanical properties of the samples produced using cooling rates of 0.5 (C1) and 1°C/min (C2) were considerably higher than those of foams produced with a cooling rate of 2°C/min (C3) (Figure 5). This behavior can be explained by the change of the foam morphology; the PEEK foam C1 and C2 were obtained by type 2 solid/liquid demixing and had, therefore, homogeneous pore structures while for C3 the shorter gelation time caused it to demix in a type 1/2 mixed-mode resulting in a mixed fiber-like/pore structure. The foams (C4) produced using 15 wt% PEEK in 4PPH using a cooling rate of 10°C/min contained large cracks (see Figure S6, C4), which did not allow for the preparation of test specimens.

The foams prepared from 20 wt% PEEK solutions possessed the highest mechanical properties of all porous PEEK samples; those foams made with cooling rates of 0.5 (D1) and 1°C/min (D2) had elastic moduli up to 125 MPa and crush strength of 6–7 MPa. Note that the foam density, porosity (Table 2) and morphology of D1 and D2 (Figure 2, D1-2) were rather similar and, therefore, also their mechanical properties. However,

compared to the B and C-series the foam density increased significantly, and even more importantly, the degree of crystallinity increased by about 12% (Table 4), which led to the much-improved mechanical performance. Unfortunately, it was impossible to produce test specimens from foams produced at higher cooling rates (2 and 10°C/min) as they contained many internal cracks, likely caused by residual thermal stresses⁴⁶ (Figure S6, D3-4).

Figure 5 shows also the elastic moduli of PEEK foams reported by Talley et al.³¹ The porous PEEK produced by us had at much lower foam densities, yet similar elastic moduli compared to those reported by Talley et al. This is possibly due to the higher degree of crystallinity of PEEK crystallized from 4PPH solution as compared to PEEK processed from dichloroacetic acid (maximum crystallinity = 51%).³¹

4 | CONCLUSIONS

High porosity PEEK foams with controllable porosity were produced using an HT-TIPS process. The influence


of polymer concentration and cooling rate was investigated. Based on the findings, two main conclusions can be drawn: (1) polymer concentration significantly affects the demixing process – at PEEK concentrations in 4PPH below 10 wt%, solvent solidification occurs prior to polymer demixing while at higher polymer concentrations, solution gelation caused by PEEK crystallization takes place before solvent crystallization. The nature of the liquid–solid phase separation process determines the pore structure and morphology. The foam density (110 to 360 kg/m³) and thus porosity (92% to 73%) of our PEEK foams can be controlled by the amount (up to 20 wt%) of PEEK dissolved in 4PPH. The crystallization time of PEEK from 4PPH solutions is controlled by the cooling rate and results in very high crystallinity PEEK in our foams, which both lead to much higher skeletal PEEK densities (1360–1380 kg/m³) and elastic moduli of up to 125 MPa (as well as crush strengths).

ACKNOWLEDGMENTS

We greatly acknowledge funding from the Austrian Research Council FWF through the grant I1800. The authors also gratefully acknowledge the help of Lisa Panzenboeck (UniVie, A), Manon Goubet and Alice Charton (both Ecole des Mines d'Alès, F) for their help in preparing and analyzing samples. We also thank the reviewers for their helpful feedback, which helped to improve our manuscript.

ORCID

Dmitrii Rusakov  <https://orcid.org/0000-0002-2155-4833>

Angelika Menner  <https://orcid.org/0000-0002-3931-9882>

Florian Spieckermann  <https://orcid.org/0000-0003-4836-3284>

Harald Wilhelm  <https://orcid.org/0000-0001-9290-5760>

Alexander Bismarck  <https://orcid.org/0000-0002-7458-1587>

REFERENCES

- [1] J. Da Silva Burgal, L. G. Peeva, S. Kumbharkar, A. Livingston, *J. Membr. Sci.* **2015**, 479, 105.
- [2] G. Wang, *High Performance Polymers and Engineering Plastics* (Eds: Vikas Mittal), John Wiley & sons, Hoboken, New Jersey **2011**. <https://onlinelibrary.wiley.com/doi/10.1002/9781118171950.ch10>.
- [3] V. Mylläri, T.-P. Ruoko, J. Vuorinen, H. Lemmetyinen, *Polym. Degrad. Stab.* **2015**, 120, 419.
- [4] D. Li, D. Shi, K. Feng, X. Li, H. Zhang, *J. Membr. Sci.* **2017**, 530, 125.
- [5] H. N. Beck, *J. Appl. Polym. Sci.* **1992**, 45, 1361.
- [6] M. F. Sonnenschein, *J. Polym. Sci., Part B: Polym. Phys.* **2003**, 41, 1168.
- [7] P. Venkatraman, C. Rader, N. Bohmann, E. J. Foster, *Polymer* **2019**, 169, 154.
- [8] F. Li, Y. Hu, X. Hou, X. Hu, D. Jiang, *High Perform. Polym.* **2017**, 30, 657.
- [9] C. Y. Hsu, K. Scraftford, C. Ni, F. Deng, *Polym. Eng. Sci.* **2019**, 59, 1209.
- [10] L. Q. Cortes, A. Lonjon, E. Dantras, C. Lacabanne, *J. Non-Cryst. Solids* **2014**, 391, 106.
- [11] J. Cao, Y. Lu, H. Chen, L. Zhang, C. Xiong, *Int. J. Polym. Mater. Polym. Biomater.* **2018**, 68, 433.
- [12] S. Najeeb, M. S. Zafar, Z. Khurshid, F. Siddiqui, *J. Prosthodont. Res.* **2016**, 60, 12.
- [13] I. V. Panayotov, V. Orti, F. Cuisinier, J. Yachouh, *J. Mater. Sci. Mater. Med.* **2016**, 27, 118.
- [14] M. F. Sonnenschein, *J. Appl. Polym. Sci.* **1999**, 72, 175.
- [15] D. Parker, J. Bussink, H.T. Van De Grampel, G.W. Wheatley, E.-U. Dorf, E. Ostlinning, K. Reinking, F. Schubert, O. Jünger, *Ullmann's Encyclopedia of Industrial Chemistry*. John Wiley & Sons, Hoboken, New Jersey **2012**. https://onlinelibrary.wiley.com/doi/10.1002/14356007.a21_449.pub4.
- [16] C. Barile, C. Casavola, F. De Cillis, *Composites, Part B* **2019**, 162, 122.
- [17] A. A. Stepashkin, D. I. Chukov, F. S. Senatov, A. I. Salimon, A. M. Korsunsky, S. D. Kaloshkin, *Compos. Sci. Technol.* **2018**, 164, 319.
- [18] Q. Liu, Z. Tang, B. Ou, L. Liu, Z. Zhou, S. Shen, Y. Duan, *Mater. Chem. Phys.* **2014**, 144, 213.
- [19] I. Pulko, V. Smrekar, A. Podgornik, P. Krajnc, *J. Chromatogr. A* **2011**, 1218, 2396.
- [20] M. Tebbth, A. Menner, A. Kogelbauer, A. Bismarck, *Curr. Opin. Chem. Eng.* **2014**, 4, 114.
- [21] N. T. Evans, F. B. Torstrick, C. S. Lee, K. M. Dupont, D. L. Safranski, W. A. Chang, A. E. Macedo, A. S. Lin, J. M. Boothby, D. C. Whittingslow, R. A. Carson, R. E. Guldborg, K. Gall, *Acta Biomater.* **2015**, 13, 159.
- [22] P. Werner, R. Verdejo, F. Wöllecke, V. Altstädt, J. K. W. Sandler, M. S. P. Shaffer, *Adv. Mater.* **2005**, 17, 2864.
- [23] A. R. Siddiq, A. R. Kennedy, *Mater. Sci. Eng. C Mater. Biol. Appl.* **2015**, 47, 180.
- [24] R. Verdejo, P. Werner, J. Sandler, V. Altstädt, M. S. P. Shaffer, *J. Mater. Sci.* **2009**, 44, 1427.
- [25] L. Cai, Y. Pan, S. Tang, Q. Li, T. Tang, K. Zheng, A. R. Boccaccini, S. Wei, J. Wei, J. Su, *J. Mater. Chem. B* **2017**, 5, 8337.
- [26] K. H. Tan, C. K. Chua, K. F. Leong, M. W. Naing, C. M. Cheah, *Proc. Inst. Mech. Eng. H* **2005**, 219, 183.
- [27] Q. Yang, G. Zhang, Z. Ma, J. Li, X. Fan, *J. Appl. Polym. Sci.* **2015**, 132, 42576.
- [28] L. Cafiero, S. Iannace, L. Sorrentino, *Eur. Polym. J.* **2016**, 78, 116.
- [29] I. Akartuna, E. Tervoort, J. C. H. Wong, A. R. Studart, L. J. Gauckler, *Polymer* **2009**, 50, 3645.
- [30] S. J. Talley, X. Yuan, R. B. Moore, *ACS Macro Lett.* **2017**, 6, 262.
- [31] S. J. Talley, C. L. Anderson-Schoepe, C. J. Berger, K. A. Leary, S. A. Snyder, R. B. Moore, *Polymer* **2017**, 126, 437.
- [32] S. J. Talley, S. L. Vivod, B. A. Nguyen, M. A. B. Meador, A. Radulescu, R. B. Moore, *ACS Appl. Mater. Interfaces* **2019**, 11, 31508.
- [33] D. Rusakov, A. Menner, A. Bismarck, *Macromol. Rapid Commun.* **2020**, 41, 2000110.

- [34] D. J. Blundell, B. N. Osborn, *Polymer* **1983**, 24, 953.
- [35] Y. Furushima, A. Toda, V. Rousseaux, C. Bailly, E. Zhuravlev, C. Schick, *Polymer* **2016**, 99, 97.
- [36] C. R. Quick, J. E. K. Schawe, P. J. Uggowitzer, S. Pogatscher, *Thermochim. Acta* **2019**, 677, 12.
- [37] S. Z. D. Cheng, M. Y. Cao, B. Wunderlich, *Macromolecules* **1986**, 19, 1868.
- [38] W. B. Deichmann, *Ind. Eng. Chem. Anal. Ed.* **1944**, 16, 37.
- [39] D. R. Lloyd, K. E. Kinzer, H. S. Tseng, *J. Membr. Sci.* **1990**, 52, 239.
- [40] L. Jin, J. Ball, T. Bremner, H.-J. Sue, *Polymer* **2014**, 55, 5255.
- [41] Vasconcelos, G.d.C., R.L. Mazur, E.C. Botelho, M.C. Rezende, and M.L. Costa, *J. Aerospace Technol. Manage.* **2010**, 2, 155.
- [42] F. Yang, X. Qu, W. Cui, J. Bei, F. Yu, S. Lu, S. Wang, *Biomaterials* **2006**, 27, 4923.
- [43] D. P. Jones, D. C. Leach, D. R. Moore, *Polymer* **1985**, 26, 1385.
- [44] C. N. Velisaris, J. C. Seferis, *Polym. Eng. Sci.* **1986**, 26, 1574.
- [45] Ö. C. Önder, E. Yilgör, I. Yilgör, *Polymer* **2016**, 107, 240.
- [46] W. J. Unger, J. S. Hansen, *J. Compos. Mater.* **1993**, 27, 108.
- [47] D. Veazey, T. Hsu, E. D. Gomez, *J. Appl. Polym. Sci.* **2019**, 136, 47727.
- [48] Z. Jiang, P. Liu, H.-J. Sue, T. Bremner, *Polymer* **2019**, 160, 231.
- [49] J. Audoit, L. Rivière, J. Dandurand, A. Lonjon, E. Dantras, C. Lacabanne, *J. Therm. Anal. Calorim.* **2018**, 135, 2147.
- [50] S.-L. Gao, J.-K. Kim, *Compos. Part A: Appl. Sci. Manuf.* **2000**, 31, 517.

SUPPORTING INFORMATION

Additional supporting information may be found online in the Supporting Information section at the end of this article.

How to cite this article: D. Rusakov, A. Menner, F. Spieckermann, H. Wilhelm, A. Bismarck, *J. Appl. Polym. Sci.* **2022**, 139(1), e51423. <https://doi.org/10.1002/app.51423>

Morphology and properties of foamed high crystallinity PEEK prepared by high temperature thermally induced phase separation

Dmitrii Rusakov^a, Angelika Menner^a, Florian Spieckermann^b, Harald Wilhelm^c and Alexander Bismarck^{a,d,*}

^a Institute of Material Chemistry and Research, Polymer and Composite Engineering (PaCE) Group, Faculty of Chemistry, University of Vienna, Währinger Straße 42, 1090 Vienna, Austria

^b Materials Physics, Department Materials Science, University of Leoben, 8700 Leoben, Jahnstrasse 12/I

^c Laboratory of Polymer Engineering (LKT-TGM), Wexstraße 19-23, 1200 Vienna, Austria

^d Department of Chemical Engineering, Imperial College London, South Kensington Campus, London, SW7 2AZ, UK

* corresponding author: alexander.bismarck@univie.ac.at

Supporting Information

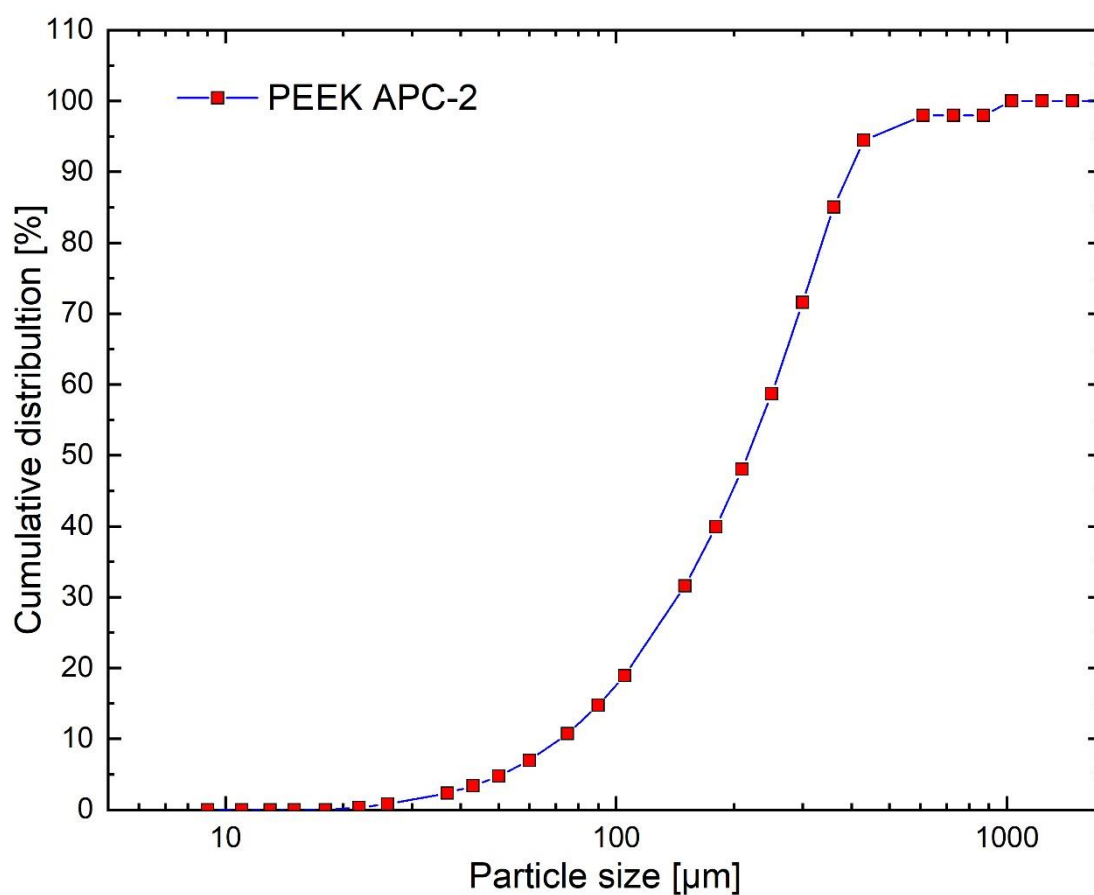


Fig. S1. PEEK APC-2 powder cumulative particles size distribution.

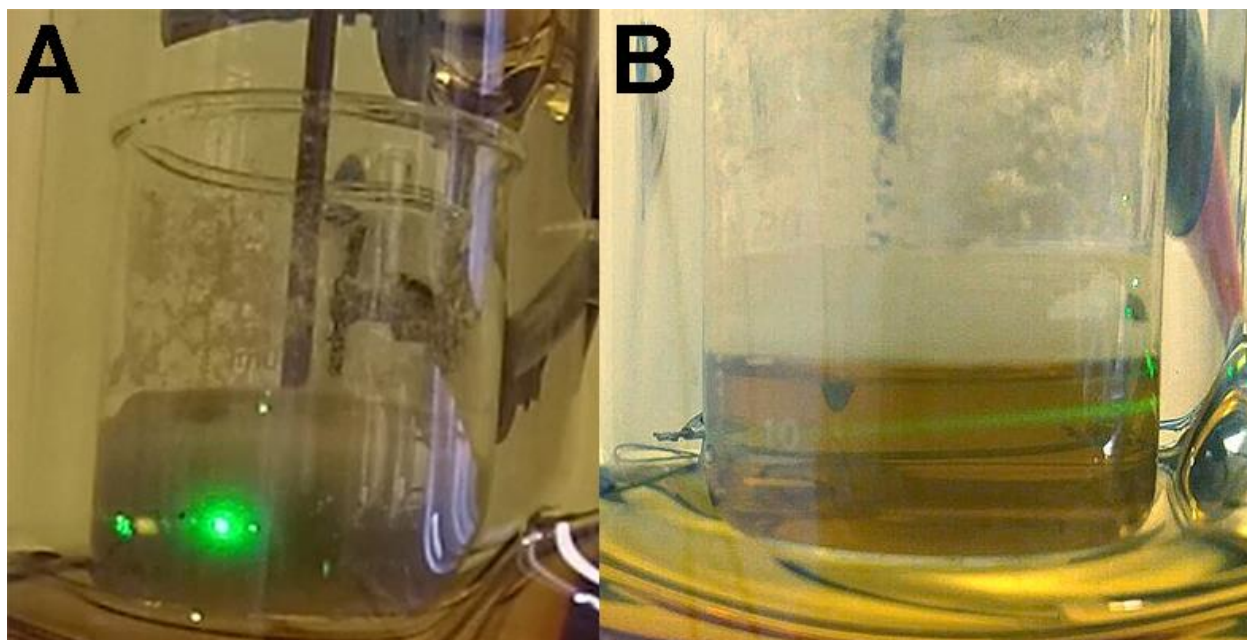


Fig. S2. Image (A) represent non-transparent PEEK/4PPH solution with scattered laser pointer spot (**Fig.1** point **B**, +254°C/77 min of the process); and image (B) with transparent solution, where laser pointer beam going through it without scattering (**Fig.1** point **C**, +265°C/125 min).

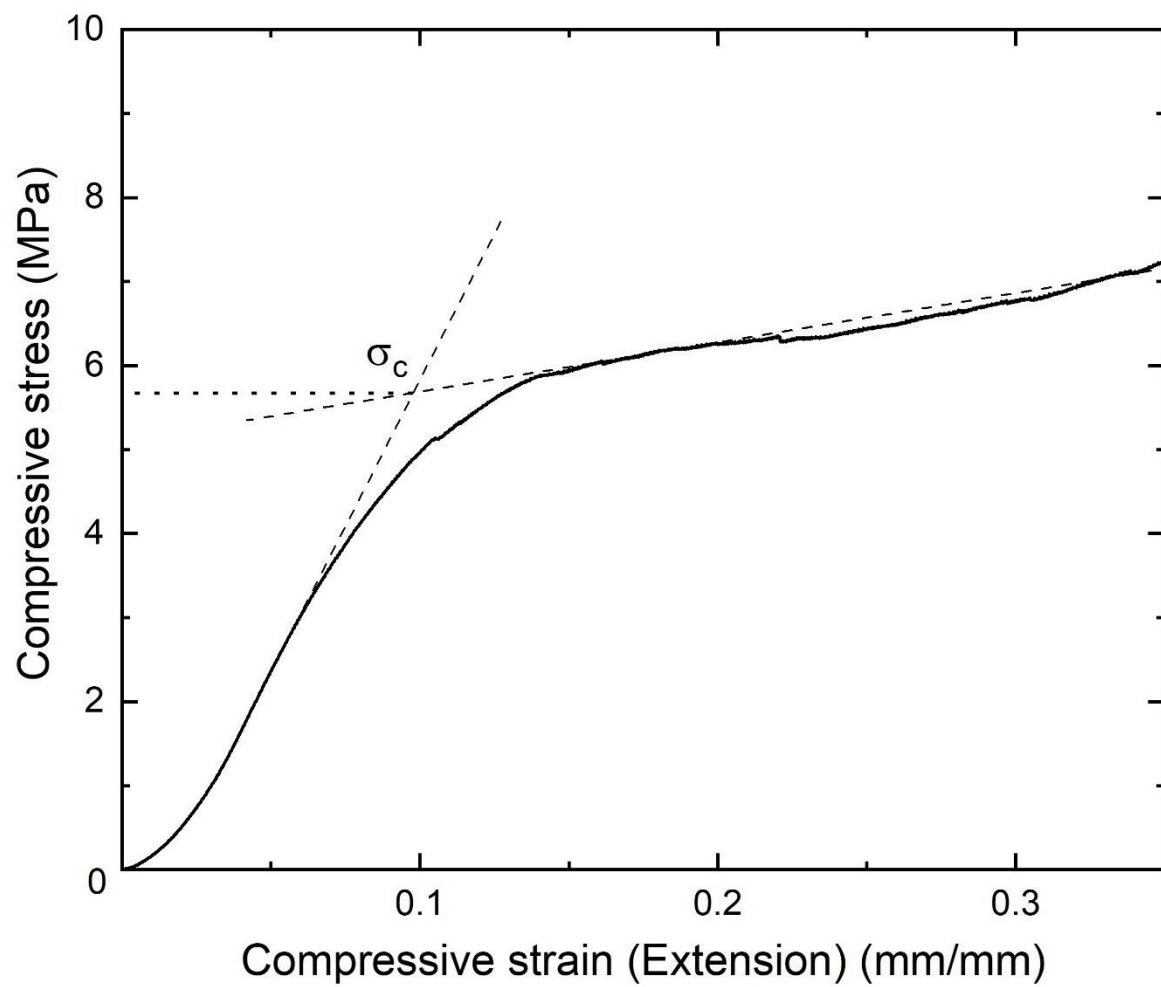


Fig. S3. Illustration of the determination of crush strength (σ_c) for **D2** sample.

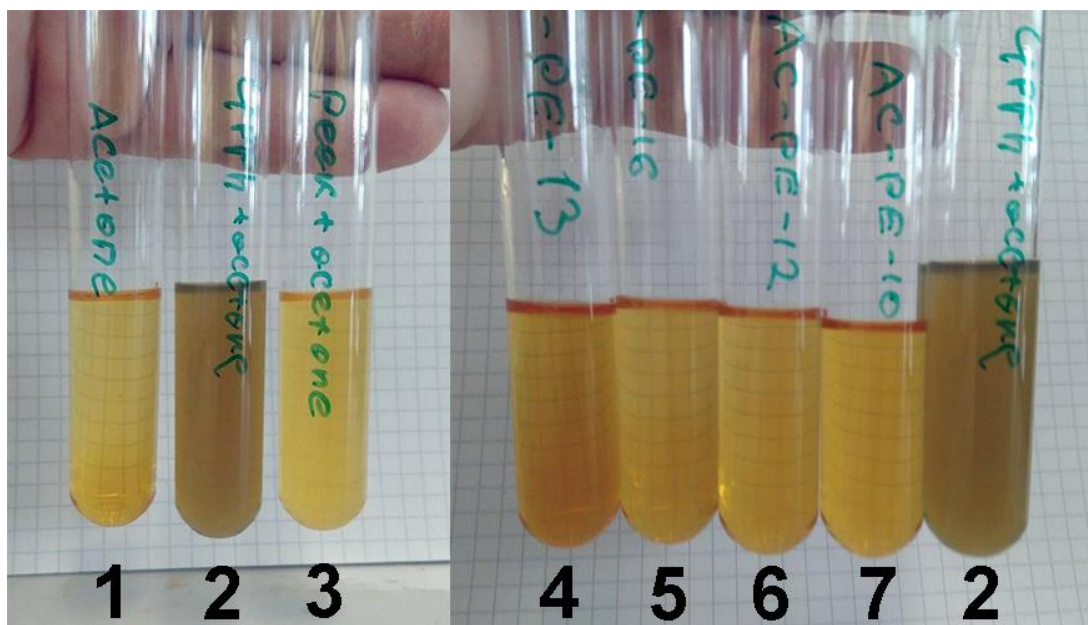


Fig. S4. Ferric Chloride Test to define phenol presence.

7 samples were prepared for the ferric chloride test:

- 1) Pure acetone
- 2) 0.5 g 4PPH with 5 g of acetone
- 3) 0.5 g of PEEK APC-2 (original PEEK powder) with 5 g of acetone
- 4) 0.5 g of ground PE-5-10 sample with 5 g of acetone
- 5) 0.5 g of ground PE-5-0.5 sample with 5 g of acetone
- 6) 0.5 g of ground PE-20-0.5 sample with 5 g of acetone
- 7) 0.5 g of ground PE-20-10 samples with 5 g of acetone

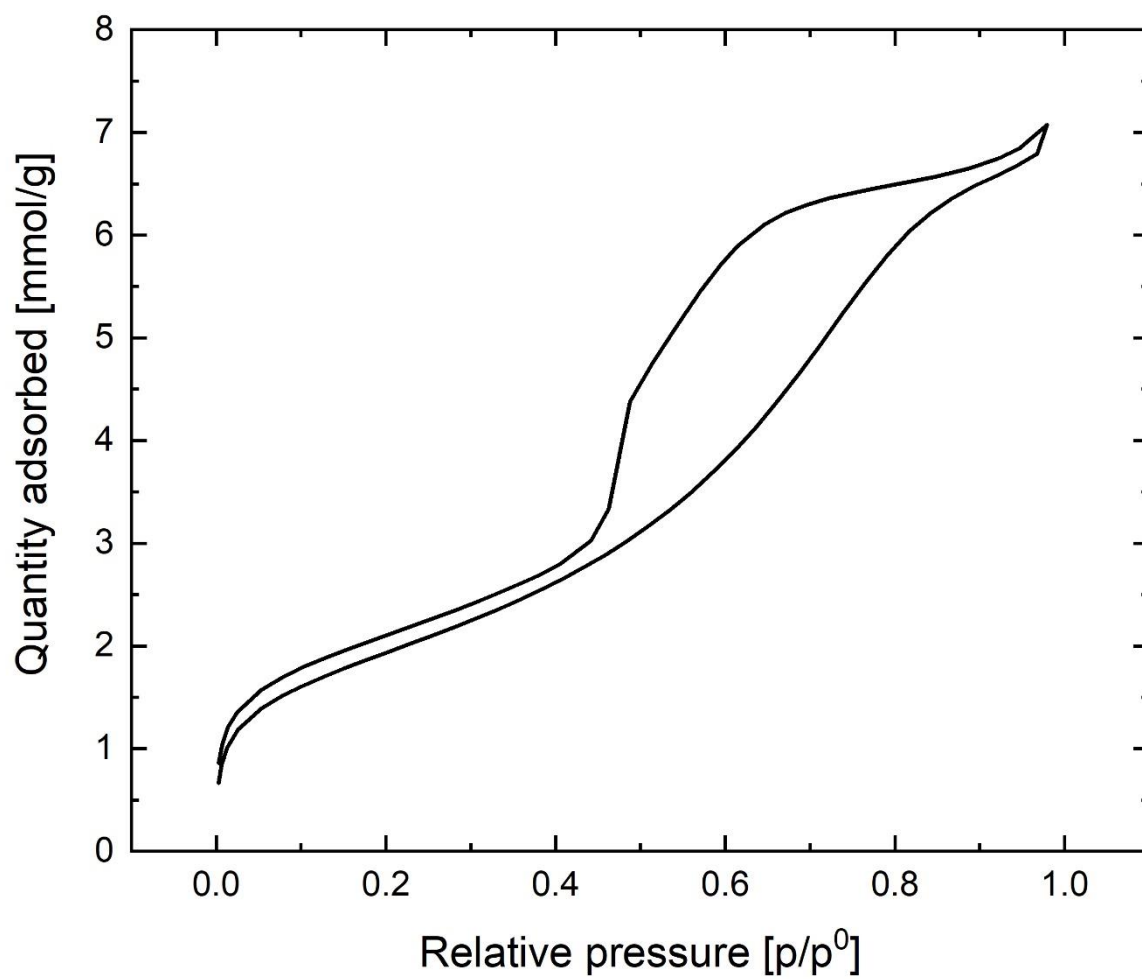


Fig. S5 Characteristic nitrogen adsorption isotherm for **B2** sample.

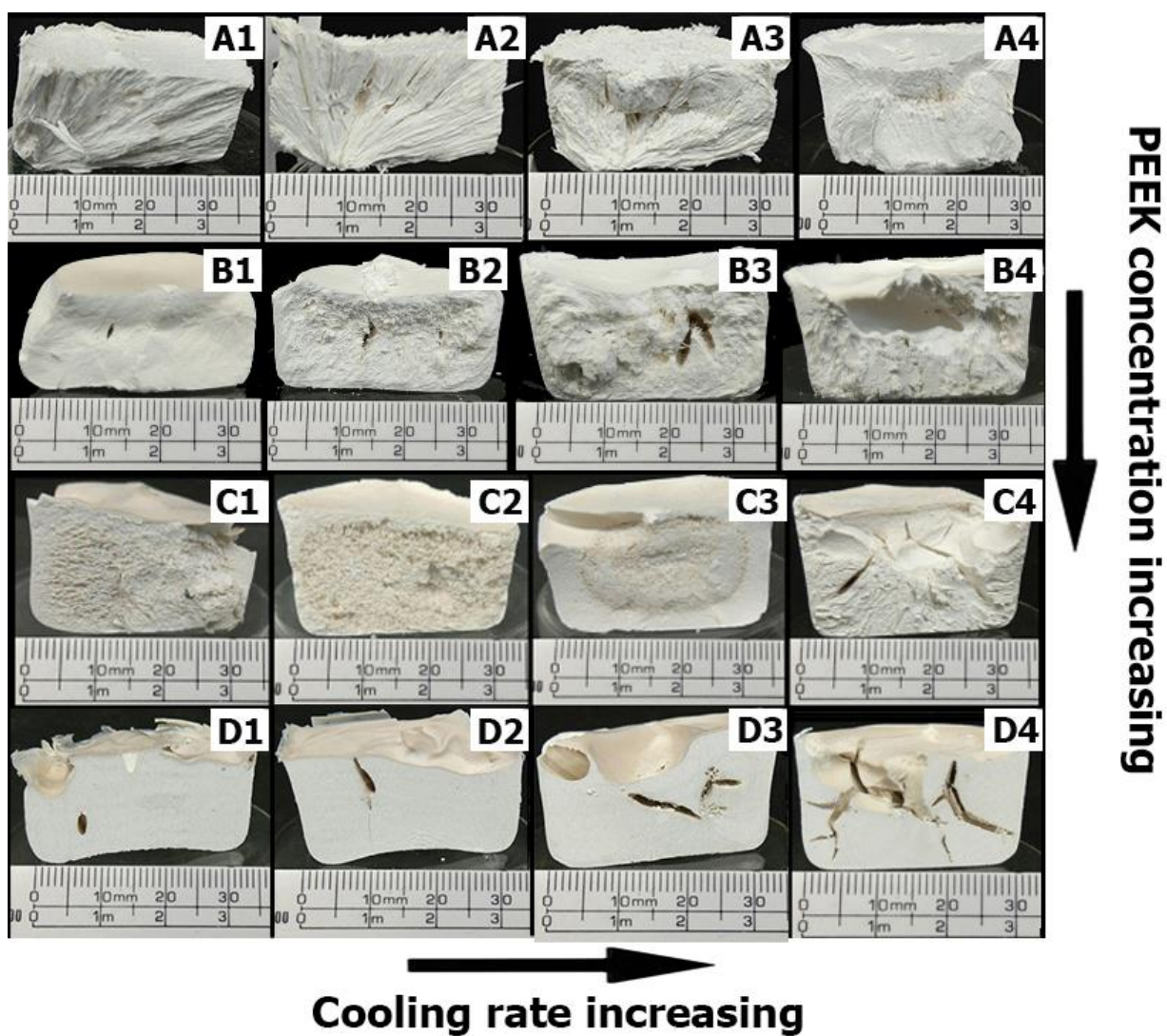


Fig. S6. Photographs of PEEK foams after purification, produced by HT-TIPS from 5 wt% (row A), 10 wt% (row B), 15 wt% (row C) 20 wt% (row D) PEEK in 4PPH solutions, at cooling rates β of 1) 0.5 °C/min, 2) 1 °C/min, 3) 2 °C/min, and 4) 10 °C/min.

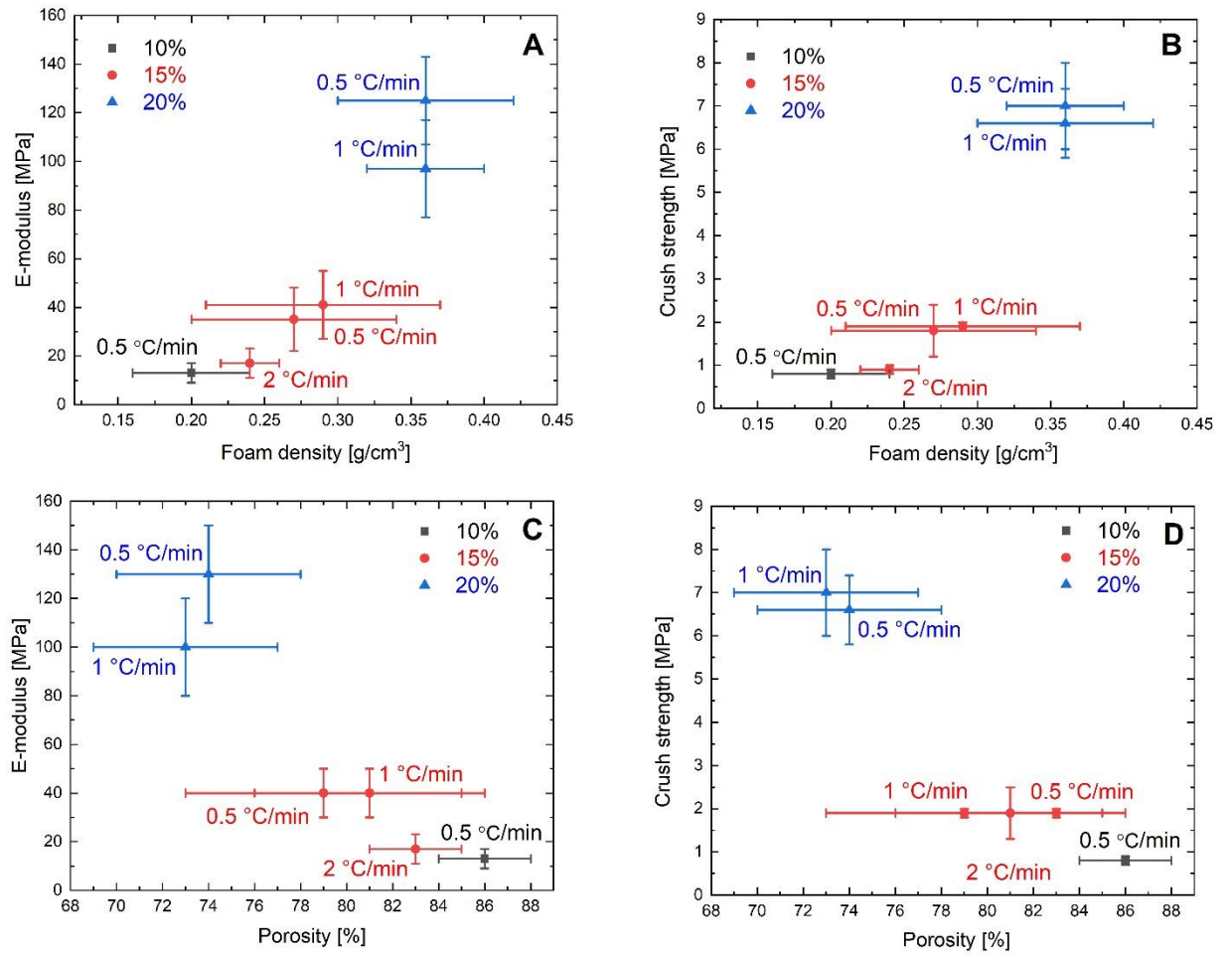


Fig. S7. Elastic modulus (left) and crush strength (right) of our PEEK foams at the different cooling rates as a function of foam density (A and B); and as a function of porosity (C and D respectively).

Publication 3

Rusakov, D., Steffny, I., Spieckermann, F., Menner, A., Bismarck, A., High porosity poly (ether ketone ketone): Influence of solvents on foam properties. Submitted in 2022.

High porosity poly (ether ketone ketone): Influence of solvents on foam properties

Dmitrii Rusakov¹, Innozenz Steffny², Florian Spieckermann³, Angelika Menner¹ and Alexander Bismarck^{1,4}

¹ Polymer and Composite Engineering (PaCE) Group, Institute of Materials Chemistry, Faculty of Chemistry, University of Vienna, Währinger Str. 42, 1090 Vienna, Austria.

² Erich Schmid Institute of Materials Science of the Austrian Academy of Sciences, Jahnstrasse 12/I, 8700 Leoben, Austria.

³ Chair of Materials Physics, Department of Materials Science, Montanuniversität Leoben, Jahnstrasse 12/I, 8700 Leoben, Austria.

⁴ Department of Chemical Engineering, Imperial College London, South Kensington Campus, London, SW7 2AZ, UK.

Abstract: Poly (ether ketone ketone) (PEKK) is semicrystalline high-performance polymer with exceptional mechanical properties, high continuous operation temperature and is insoluble in most common solvents. Porous PEKK is desired for biomedical applications. PEKK was dissolved in two high boiling aprotic solvents, 4-phenylphenol (4PPH) and 9-fluorenone (9FN), and foams were manufactured using a high-temperature thermally induced phase separation (HT-TIPS) process. We demonstrated that the solvent has a pronounced influence on the phase separation behaviour, which determines the foam morphology, physical and mechanical properties of PEKK foams. Porous PEKK with porosities ranging from 70% to 90% and specific surface areas up to 194 m²/g and elastic moduli ranging from 35 MPa to 100 MPa were produced.

Keywords: Polyetherketoneketone, PEKK, porous polymers, thermally induced phase separation

Introduction

High performance polymers are polymers with a unique combination of outstanding mechanical properties, high chemical resistance, and good biocompatibility. Amongst high-performance polymers polyaryletherketones (PAEKs) stand out because of their high continuous service temperature (250°C), excellent mechanical properties and chemical resistance. The combination of stable aryl rings and rigid keto- and ether-groups in the polymer backbone impart PEAKs with this unique property profile [1, 2]. One polymer of the PEAK family is the poly (ether ketone ketone) (PEKK) – a linear, semicrystalline thermoplastic with a glass transition temperature (T_g) of around 153°C and a melting point close to 350°C. The physical properties of PEKK, such as its degree of crystallinity, are related to the para/meta phenyl isomer ratio [3, 4]. Because of the good compatibility of PEKK with reinforcement agents, such as glass and/or carbon fibres, nanowires and hydroxyapatite particles [5-8] its mechanical properties can be further improved. Unfortunately, PEKK requires high processing temperatures (around 400°C) [9]. However, not all applications do require bulk PEKK material. Weight critical applications for instance in the biomedical and aerospace fields, require low density but high mechanical property materials.

In general terms, porous polymers are combining low density, good thermal, impact and sound insulation properties with sufficient mechanical properties and high surface area [10]. Several methods exist to produce thermoplastic porous high-performance polymers, such as foam injection moulding [11], porogen leaching [12], emulsion templating [13] and phase separation/inversion methods [14]. Porous PEKK has been produced using a combination of compression moulding and particle leaching [15]. The limitation of the particle leaching method is the difficulty to control the pore morphology, the degree of pore interconnectivity, limitations maximum porosity and porogen extraction.

An alternative route to produce porous polymers are phase separation/inversion methods, which are often used to produce 2D materials, such membranes [16]. A commonly used method to produce polymer foams and membranes is thermally induced phase separation (TIPS) [17-19]. The main principle of the TIPS method is based on polymer solubility, which varies with temperature. The TIPS process typically involves: i) polymer dissolution in a suitable solvent at a given temperature, until a homogeneous solution is obtained, ii) the temperature of this polymer solution is lowered at a defined cooling rate until iii) liquid-liquid or liquid-solid polymer demixing takes place at a specific temperature either at the cloud point, respectively, which results in two distinct phases after demixing: a polymer-rich and the polymer poor phase. After solvent extraction, exchange or evaporation, a porous polymer is obtained from the polymer-rich phase

[20]. In addition to the methods simplicity, TIPS has a several advantages, as its requires a rather simple experimental setup, allows for the control of morphology, is reproducible, and it offers the possibility to reuse solvents [19]. Unfortunately, PEKK only can be dissolved at room temperature in concentrated sulfuric or methylsulfuric acid.

We recently demonstrated a high temperature TIPS process to produce porous poly (ether ether ketone) (PEEK) using high boiling aprotic solvent [21, 22]. In analogy we expected that also PEKK is soluble in high boiling point aprotic solvents above its T_g . In this study, we investigated the preparation of high porosity bulk PEKK foams with controllable porosity and pore morphology. The influence of cooling rate, polymer concentration and solvent type on PEKK foam morphology, physical and mechanical properties was studied.

2. Experimental part

2.1. Materials

Poly (ether ketone ketone) (PEKK) powder was kindly supplied by Cytec (Solvay Group). 4-phenylphenol (melting temperature $T_f \sim 166$ °C, boiling point $T_b \sim 321$ °C) with a purity of 97% and 9-fluorenone ($T_f \sim 84$ °C, $T_b \sim 342$ °C) with a purity of 98% were purchased from Sigma-Aldrich. Ethanol (96% purity) was purchased from Brenntag NV (Belgium). All materials were used as received.

2.2. Preparation of foamed PEKK

For the HT-TIPS process, a thermostat (Unistat T305W HT, Huber, Germany) with an active water-cooling system was used. A 250 mL round-bottom double-walled borosilicate glass vessel (GlassKeller, Basel AG, Switzerland) with a two-necked glass cover (DN 60) was connected to the thermostat. Various amounts of PEKK and 4PPH or 9FN powder (**Table 1**) were placed and mechanically mixed in 50 mL borosilicate beakers. Afterwards, a glass-coated magnetic stirrer bar was added into the beaker containing the PEKK/solvent mixture. An external precision thermometer (Erbo TFX 410, Ingolstadt D) was placed into the polymer solvent mixture, which allowed for precise temperature control of the process.

The temperature of the PEKK/solvent mixture was increased until all 4PPH or 9FN melted (**Fig. 1, point A**). At this point, the magnetic stirring was started. Afterwards, the solution temperature was increased until the dissolution temperature, which was determined in preliminary experiments (**Fig. 1, point B; Table 1, T_{transp}**). At this temperature the solution was stirred for 10 – 30 min to obtain a clear solution (**Fig. 1, plateau B \rightarrow C; Table 1, t_{mix}**). The transparency of the polymer

solution was determined using a green laser pointer. The only exception was PEKK in 9FN solutions containing 20 wt% polymer; in this case the clear solution point was not obvious to obtain as the solutions always had a non-transparent layer on the top as result of a small temperature gradient between solution and environment. Prior to starting cooling, stirring was stopped and the stirring bar removed. Subsequently, the solution was cooled at certain cooling rates β (**Table 1**). During cooling two phenomena were observed either in succession or simultaneously – PEKK gelation/crystallisation from solution (**Fig.1, point D; Table 1, T_{gel}**) and/or only solvent solidification. Solvent crystallisation was apparent by the recorded temperature increase inside the vessel due to the release of the latent heat of crystallisation (**Fig. 1, point E; Table 1, T_{solid}**). After T_{solid} cooling continued at the same rate to 70°C for samples containing 4PPH or until 50°C for the samples with 9FN. Finally, the samples were removed from the beaker and the solvent extracted using ethanol in a Soxhlet apparatus for 48 h followed by drying in a vacuum oven at 40 °C for 24 h.

Table 1. Characteristic HT-TIPS heating and cooling profiles for PEKK in 4PPH and 9FN solutions. β is the cooling rate; T_{transp} the temperature range, during which PEKK dissolves; t_{mix} the mixing time at the dissolution temperature T_{transp} ; T_{gel} the temperature range in which the PEKK solution undergoes phase transition – the solution changes from transparent to turbid; T_{solid} the temperature range in which solution crystallisation takes place (which depends on [PEKK] and the cooling rate β).

Sample name	Solvent	[PEKK] wt%	β [°C/min]	T_{transp} [°C]	t_{mix} [min]	T_{gel} [°C]	T_{solid} [°C]
PH-1	4PPH	10	0.5	246 ± 3	10	*	145 ± 2
PH-2	4PPH	10	1	246 ± 10	10	*	148 ± 2
PH-3	4PPH	10	2	242 ± 2	10	*	148 ± 10
PH-4	4PPH	10	10	240 ± 3	10	*	175 ± 1
PH-5	4PPH	20	0.5	258 ± 9	20	187 ± 7	158 ± 13
PH-6	4PPH	20	1	258 ± 7	20	190 ± 17	152 ± 9
PH-7	4PPH	20	2	258 ± 9	20	156 ± 1	145 ± 1
PH-8	4PPH	20	10	258 ± 10	20	*	170 ± 8
FN-1	9FN	10	0.5	252 ± 2	20	183 ± 12	70 ± 3
FN-2	9FN	10	1	253 ± 2	20	185 ± 8	65 ± 4
FN-3	9FN	10	2	252 ± 4	20	191 ± 1	66 ± 6
FN-4	9FN	10	10	252 ± 4	20	185 ± 7	71 ± 6
FN-5	9FN	20	0.5	233 ± 6	30	190 ± 9	56 ± 2
FN-6	9FN	20	1	232 ± 7	30	181 ± 6	60 ± 1
FN-7	9FN	20	2	240 ± 8	30	187 ± 10	71 ± 5
FN-8	9FN	20	10	232 ± 2	30	203 ± 9	78 ± 1

* in this case no separate PEKK gelation was observed only solvent crystallization occurred.

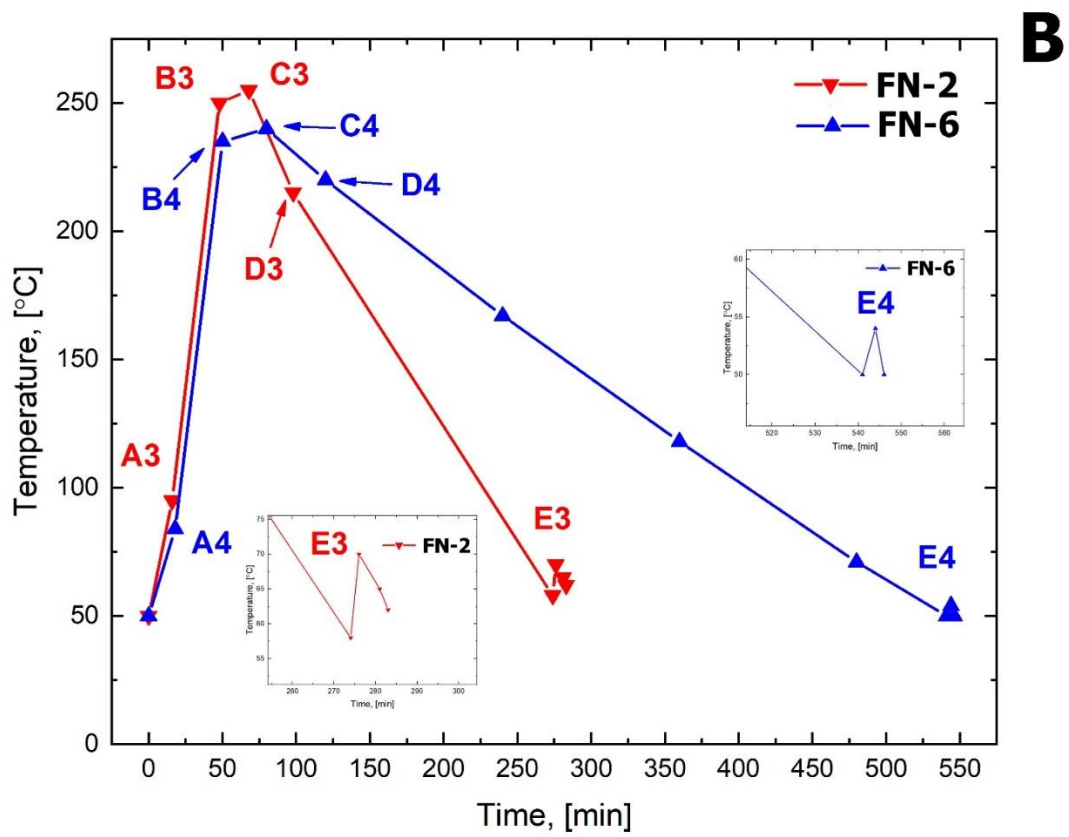
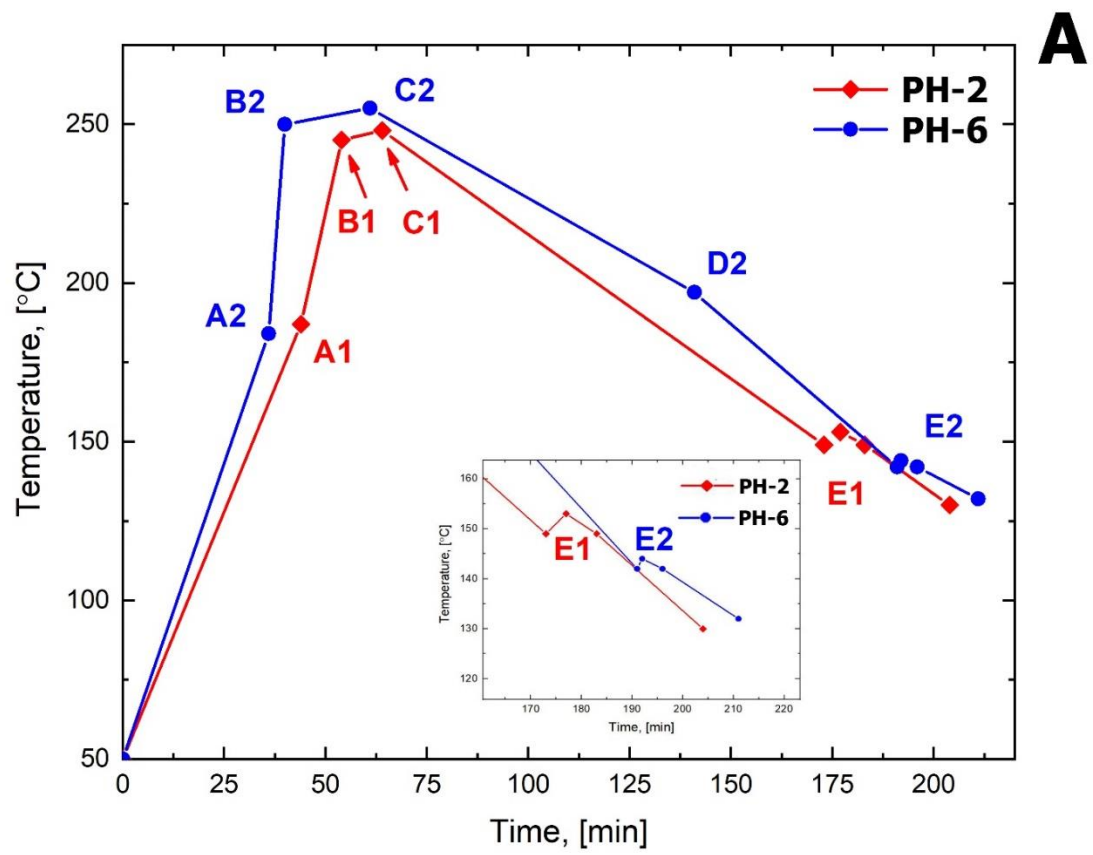


Fig.1. Characteristic heating/cooling profiles for A) 4PPH and B) 9FN solutions containing 10 (PH-2/FN-2) and 20 wt% (PH-6/FN-6) PEKK, respectively.

2.3. Characterization of foamed PEKK

The **pore morphology** of porous PEKK was characterised using a benchtop scanning electron microscope (JEOL JCM-6000, JEOL Ltd, Japan and CARL ZEISS SUPRA VP55, CARL ZEISS AG, Germany). Each polymer foam was either cut or broken into small pieces (ca. 1 cm length and 1-2 mm thickness), fixed onto the sample holder using carbon sticky tape. To ensure sufficient electrical contact between samples and the carbon sticker silver paint (Achseon 1415 G 302, Agar scientific, UK) was applied around them. Then, the samples were gold coated in argon atmosphere using a gold-coater (JEOL JFC-1200, JEOL Ltd, Japan).

Skeletal volume was measured using a helium gas-replacement pycnometer (AccuPyc II 1340, Micromeritics Ltd, Norcross, USA). Each sample for pycnometry was cut or broken into pieces (with 5 – 10 mm each side of the piece), weighted (0.2 – 0.4 g), and placed into the 3.5 cm³ measurement chamber. The **skeletal density** ρ_s was calculated by taking the ratio of measured volume and mass. The **foam density** ρ_f was determined by using a powder pycnometer (GeoPyc 1360, Micromeritics Ltd, Norcross, USA). At least three pieces (10x10x10 mm³) of each foamed PEKK sample were characterized. The resulting porosity P was calculated using the following equation:

$$P = \left(1 - \frac{\rho_f}{\rho_s}\right) \cdot 100\%$$

The **mechanical properties** of porous PEKK were determined in compression using a dual column universal testing frame (Instron 5969, Darmstadt, Germany) quipped with a 50 kN load cell adapting standard ISO 844:2001. The foamed PEKK samples were cut using a band saw (PROXXON MBS 240/E) into 1 x 1 x 1 cm³ cubes and mechanically polished to obtain parallel surfaces. Each sample cube was compressed to 75% of their original height at a test speed of 1 mm/min, while stress-engineering strain curves were recorded. The linear region of the curve was used to determine the elastic modulus (E) and the crush strength (σ_c) was determined as shown on **Fig. S1**.

The **specific surface area** of the foamed PEKK was determined by measuring nitrogen adsorption isotherms at 77K using Brunauer–Emmet–Teller (BET) and Barrett-Joyner-Halenda (BJH) methods. A surface area analyser (TriStar II 3020, Micromeritics Ltd., Norcross, USA) was used. Prior to the measurements each sample was cut into 1-2 mm sized pieces, weighted (from 0.2 to 0.4 g), placed inside a measurement vial and dried at 100 °C under active nitrogen flow for 12 h.

The **thermal properties** were investigated by differential scanning calorimetry (DSC, TA Instruments, Discovery series). 2-6 mg of each foamed PEKK sample was analysed in a temperature range from 50 to 400 °C at a heating/cooling rate of 10°C/min. The heat flow was recorded twice for heating and cooling runs. The degree of crystallinity was calculated from the measured melting enthalpy ΔH_f^{peak} :

$$X_{DSC} = \frac{\Delta H_f^{peak}}{\Delta H^0}.$$

where ΔH^0 the theoretical enthalpy of melting of a perfectly crystalline PEKK sample (130 J/g) [3].

Selected porous PEKK samples were also examined using flash DSC (Mettler Toledo Flash DSC 2+, with UFS 1 MEMS sensors). Flash DSC (FDSC) is a chip calorimetry technique that allows to reach heating rates up to 40.000 K/s and cooling rates up to 10.000 K/s. Hence secondary crystallisation that might occur in conventional DSC in many polymeric materials can be effectively suppressed. By this mean the crystallinity of the foam can be determined while excluding recrystallisation effects.

Fully amorphous PEKK can be produced in the flash DSC by melting and quenching with cooling rates exceeding the critical cooling rate. The mass of the PEKK sample deposited on the Flash DSC sensor was determined by the change in heat capacity related to the glass transition of a fully amorphous sample. The following equation was used for this purpose:

$$m_{FDSC} = \frac{\Delta\phi_\beta}{\beta \Delta c_p}$$

with $\Delta\phi_\beta$ the step of the heat flux at the glass transition for a certain heating rate β , Δc_p the change in heat capacity for a fully amorphous sample at the glass transition as determined from standard DSC and m_{FDSC} the mass of the sample placed on the chip of the FDSC. The sample mass ranged from 120 to 697 ng.

3. Results and discussion

3.1. Influence of solvent type and PEKK concentration on the pore morphology

The solvent type significantly affected the polymer solution demixing behaviour and the morphology of foamed PEKK as well as its properties. For PEKK/4PPH solutions two types of demixing were observed during cooling: i) solvent solidification took place prior to PEKK gelation

and ii) PEKK gelation occurred first during the cooling process followed by solvent crystallisation. The first type of demixing (i) was observed for 10 wt% PEKK in 4PPH solutions for which polymer gelation must have occurred simultaneously with solvent crystallisation [23, 24]. In this case, due to solvent crystallisation, the transition from liquid to solid state took place only in few seconds and immobilizes the polymer structure inside the solidified solvent (**Fig. 1 A, curve PH-2, Video S1**). Moreover, a significant temperature increase was measured at the point when 4PPH started to crystallise. The second type of demixing (ii), in which gelation was detected prior to solvent crystallization, was observed when using 20 wt% PEKK in 4PPH to prepare PEKK foams. During the cooling procedure the polymer solubility started to decrease with decreasing temperature resulting in gelation (**Fig. 1A, point D, Video S2**). At this point solid-liquid demixing started and the polymer forms a gel phase. Only afterwards, the solvent crystallization point was reached immobilizing the already formed PEKK gel.

When using 9FN as PEKK solvent only the second type of demixing (ii) was observed. During the cooling procedure, the polymer solution became turbid at the gelation point and later crystallised (**Video S3**). In addition, we noted that in general to dissolve PEKK in 9FN required longer dissolution times as compared to the 4PPH solvent (**Table 1**). Despite this, it appears that PEKK gelation from 9FN occurred around the same temperatures as in 4PPH solutions (**Table 1**).

3.2. Density and porosity of PEKK foams

PEKK, as all other members of the PEAK family, consists of amorphous and crystalline phases, which have different densities. The PEKK bulk density depends on the crystalline-to-amorphous phase ratio; the amorphous PEKK phase was reported to have a density of about 1.26-1.27 g/cm³ while that of the crystalline phase density was reported to be ~ 1.42 g/cm³ [25]. Moreover, the degree of crystallinity of PEKK is dependent of the terephthalic and isophthalic monomers ratio in the polymer [26, 27]. A higher terephthalic monomer ratio leads to a higher crystallinity ratio and, therefore, to a higher bulk density. The measured bulk densities ranged from 1.38 to 1.40 g/cm³ (see **Table 2**), which indicates a high-volume fraction of the crystalline phase in our porous PEKK.

The foam density and porosity for all PEKK foams produced from 4PPH (and to a lesser extent for 9FN) was determined by the polymer concentration used. Increasing the polymer concentration resulted in higher foam densities and thus a lower porosity. PEKK foams produced from 10 wt% PEKK dissolved in 9FN had a much higher density than expected, which was because the foam precursor shrunk drastically by 25-30% after purification in EtOH and during drying (**Video S4**, where the left sample is the sample obtained from 20 wt% PEKK dissolved in 9FN and right

sample is the samples obtained from 10 wt% dissolved in 9FN), which was likely due to the capillary pressure exerted by EtOH in combination with the limited mechanical properties of the PEKK foam as a result of its low initial density. For all PEKK foams produced from 4PPH and 9FN the cooling rate does not affect the foam density and thus the porosity.

Table 2. Bulk ρ_s and foam density ρ_f , porosity P and BET surface area A_s of PEKK foams

Sample name	Bulk density [g/cm ³]	Foam density [g/cm ³]	Porosity [%]	Surface area [m ² /g]
PH-1	1.39 ± 0.02	0.19 ± 0.03	86 ± 2	87 ± 13
PH-2	1.38 ± 0.01	0.18 ± 0.04	87 ± 3	75 ± 17
PH-3	1.40 ± 0.01	0.15 ± 0.02	89 ± 1	39 ± 2
PH-4	1.38 ± 0.01	0.19 ± 0.02	87 ± 2	35 ± 3
PH-5	1.38 ± 0.02	0.33 ± 0.07	76 ± 5	86 ± 15
PH-6	1.39 ± 0.02	0.30 ± 0.05	78 ± 4	75 ± 14
PH-7	1.40 ± 0.01	0.24 ± 0.05	83 ± 3	69 ± 11
PH-8	1.39 ± 0.04	0.22 ± 0.06	84 ± 5	29 ± 3
FN-1	1.40 ± 0.02	0.41 ± 0.02	71 ± 2	181 ± 10
FN-2	1.40 ± 0.01	0.29 ± 0.06	81 ± 7	183 ± 11
FN-3	1.40 ± 0.02	0.34 ± 0.1	76 ± 10	194 ± 8
FN-4	1.40 ± 0.01	0.38 ± 0.05	73 ± 4	184 ± 3
FN-5	1.40 ± 0.01	0.31 ± 0.03	78 ± 3	178 ± 12
FN-6	1.39 ± 0.01	0.30 ± 0.05	79 ± 4	178 ± 16
FN-7	1.40 ± 0.01	0.27 ± 0.03	81 ± 2	163 ± 7
FN-8	1.40 ± 0.02	0.31 ± 0.02	78 ± 2	166 ± 6

3.3. Macro- and microscale foam morphology

After 4PPH extraction and drying, all 10 wt% PEKK/4PPH samples have an anisotropic fibre-like structure (**Fig. 2**), which is typical for solid-liquid demixing occurs when the solvent crystallises during cooling without any other visible demixing [24, 28]. Thus, the cooling rate did not have a significant effect on the resulting structure. All porous PEKK (PH1-4) possess elongated pores, oriented in the direction the solvent crystallisation front. These porous PEKK samples contain long fibres without much interconnectivity between fibre layers, which allowed for the samples to be pulled apart without much effort perpendicular to the fibre direction (which made impossible to quantify their mechanical properties in compression). The only visible difference between porous PEKKs produced from 10 wt% 4PPH solutions with increasing cooling rates was that solution crystallisation started in various points. Only the porous PEKK produced from a 10 wt% PEKK in 4PPH solution using a cooling rate of 10 °C/min (PH-4) did contain a large void (an unintentional pore). This observation could be explained by the residual thermal stresses inside the material

resulting from the fast cooling process; the solvent starts crystallising from the outside while the centre is still liquid (**Video S5**).

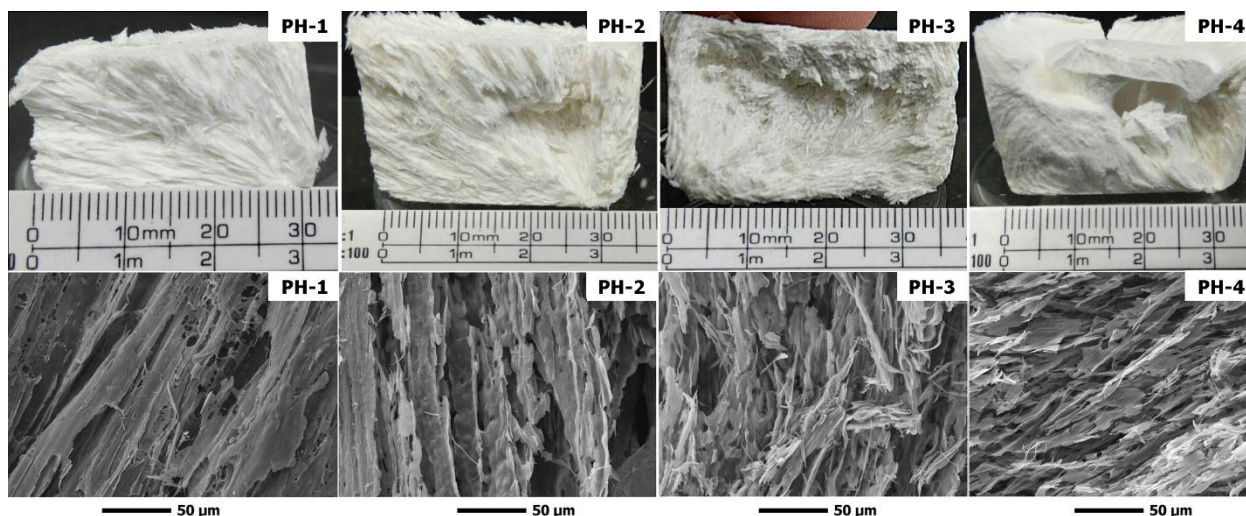


Fig. 2. Representative photos and SEM images ($\times 3000$ magnification) of PEKK foams produced from a 10 wt% PEKK in 4PPH solution.

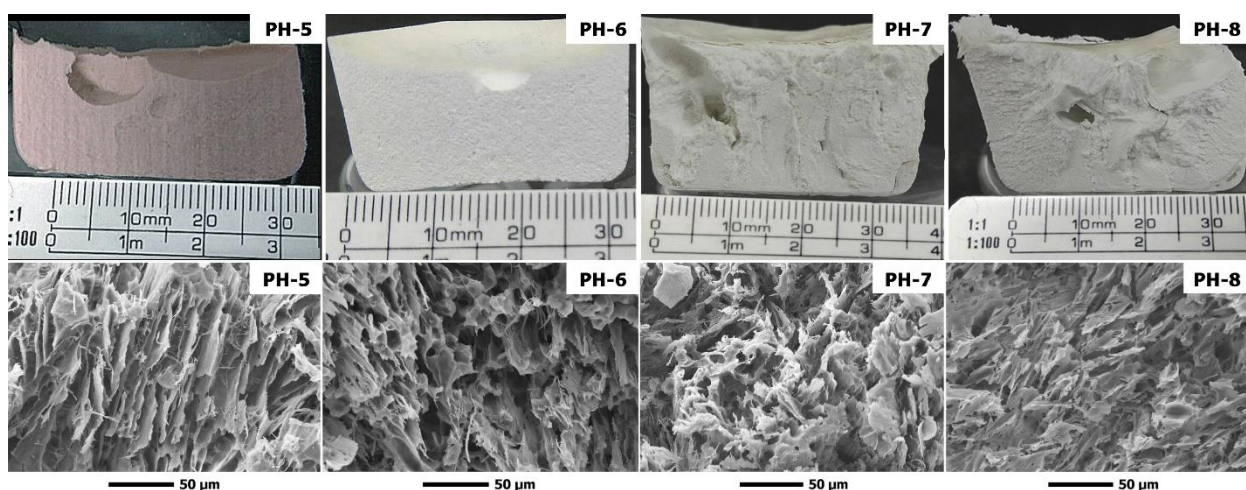


Fig. 3. Representative photos and SEM images ($\times 3000$ magnification) of PEKK foams produced from 20 wt% PEKK in 4PPH solutions.

In contrast to the 10 wt% PEKK in 4PPH, the foams produced from 20 wt% PEKK in 4PPH solutions did not possess such a pronounced fibre-like structure (**Fig. 3**). This difference between the PEKK foams produced from 10 and 20 wt% solutions can be explained by the fact that in this case PEKK did precipitate before the solvent crystallisation occurred. Also, for the porous PEKK produced from 20 wt% PEKK in 4PPH solutions, the cooling rate did not have a significant effect on the resulting morphology, with the exception of the sample produced at a cooling rate of 10 °C/min, which again contained large voids and cracks inside. In the porous PEKKs produced from 20 wt% PEKK in 4PPH solutions, in which polymer gelation took place prior to solvent

crystallisation, the microscale structure was much more homogeneous than for porous PEKK produced from 10 wt% PEKK in 4PPH.

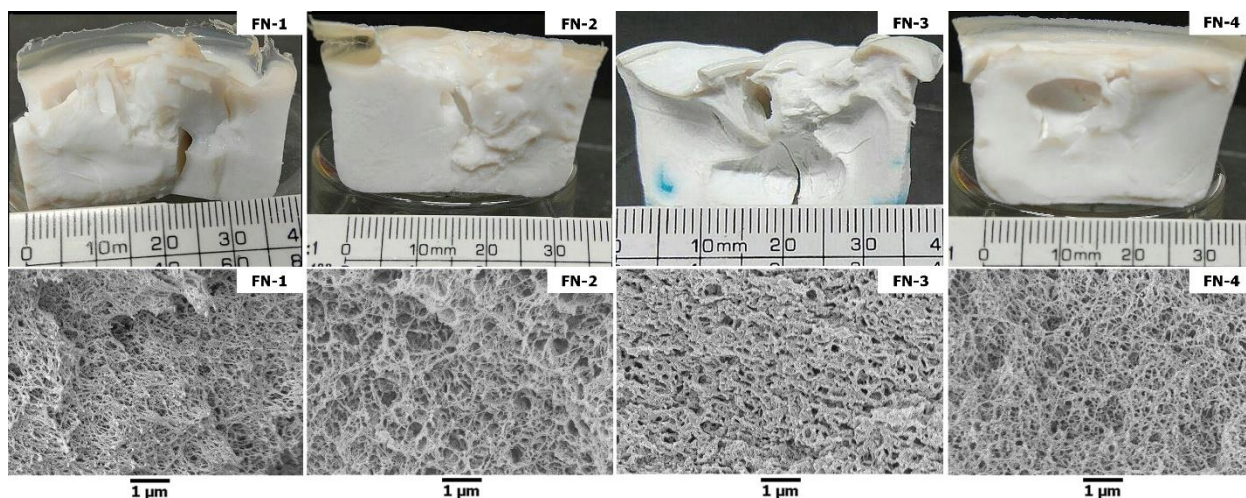


Fig. 4. Representative photos of EtOH filled PEKK foams prior to drying and SEM images ($\times 15000$ magnification) of PEKK foams produced from 10 wt% PEKK in 9FN solutions.

Porous PEKK produced from 10 wt% PEKK in 9FN solutions still containing EtOH after removal of 9FN experienced massive shrinkage in all directions after drying (**Fig. 4**, see also **Video S4**). The microstructure of these PEKK foams looks a mesh of nanoscale interconnected fibres, which could be the results of pores collapsing during EtOH removal.

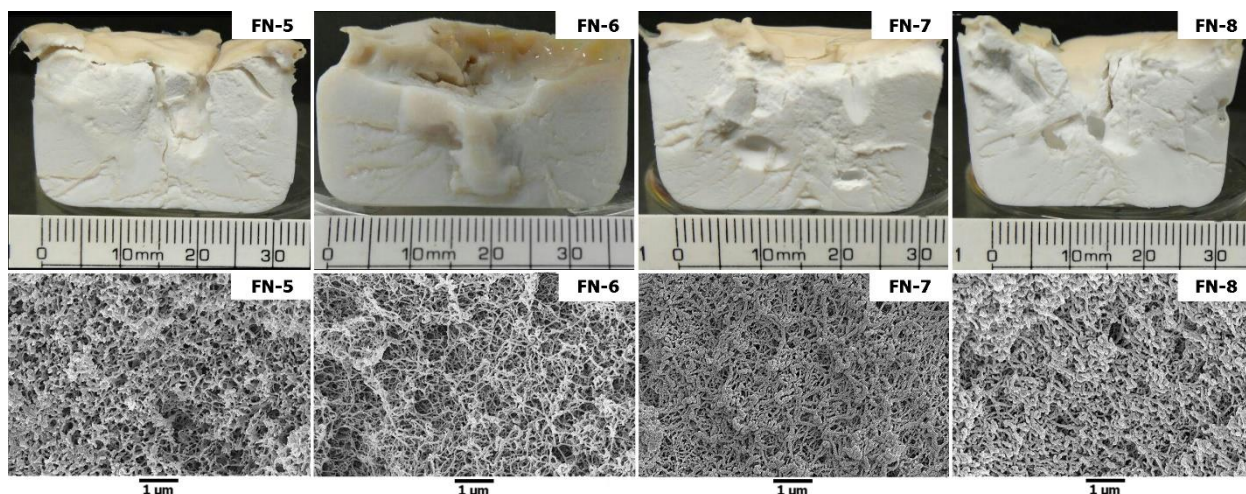


Fig. 5. Representative photos of PEKK foams and SEM images ($\times 15000$ magnification) of PEKK foams obtained from 20 wt% 9FN solutions after solvent removal and drying.

Unlike the PEKK foams produced from 10 wt% PEKK in 9FN solutions, those obtained from 20 wt% solutions did not experience any shrinkage (**Fig. 5**). These foams have a much more homogeneous macroscopic appearance as those produced from 4PPH solutions. Also, in this case, the cooling rate did not have a significant influence on the macroscale morphology. SEM micrographs of foams produced from 20 wt% PEKK in 9FN solution also consist of a network of

fine interconnected fibres, which is, however, much denser as in the case of PEKK foams produced from 10 wt% in 9FN solutions.

The specific surface area of PEKK foams was determined by nitrogen adsorption at 77K. Type IV BET isotherms with hysteresis loops were observed (**Fig. 6**). This isotherm type is typical for meso- and microporous materials, with pore diameters ranging from 2 nm to about 50 nm. The presence of a hysteresis loop indicates multilayer adsorption with subsequent capillary condensation in pores [29]. However, samples produced from 4PPH and 9FN have various shaped hysteresis loops – hysteresis type II (H2) for PEKK/4PPH and hysteresis type III (H3) for PEKK/9FN samples. H2 hysteresis is typical for ink-bottle type pores with a narrow neck and a wide bottom, whereas H3 hysteresis is characteristic for slit-like uniform pores [30]. These nanometre-sized pores formed in the macroscale pore network on the pore walls during the TIPS process in which PEKK phase separated from the solvent resulting in a polymer-rich phase surrounded by a polymer-poor solvent-rich phase, which after removal of the solvent caused the formation of such nanometre-scale pores on the pore walls of the foams.

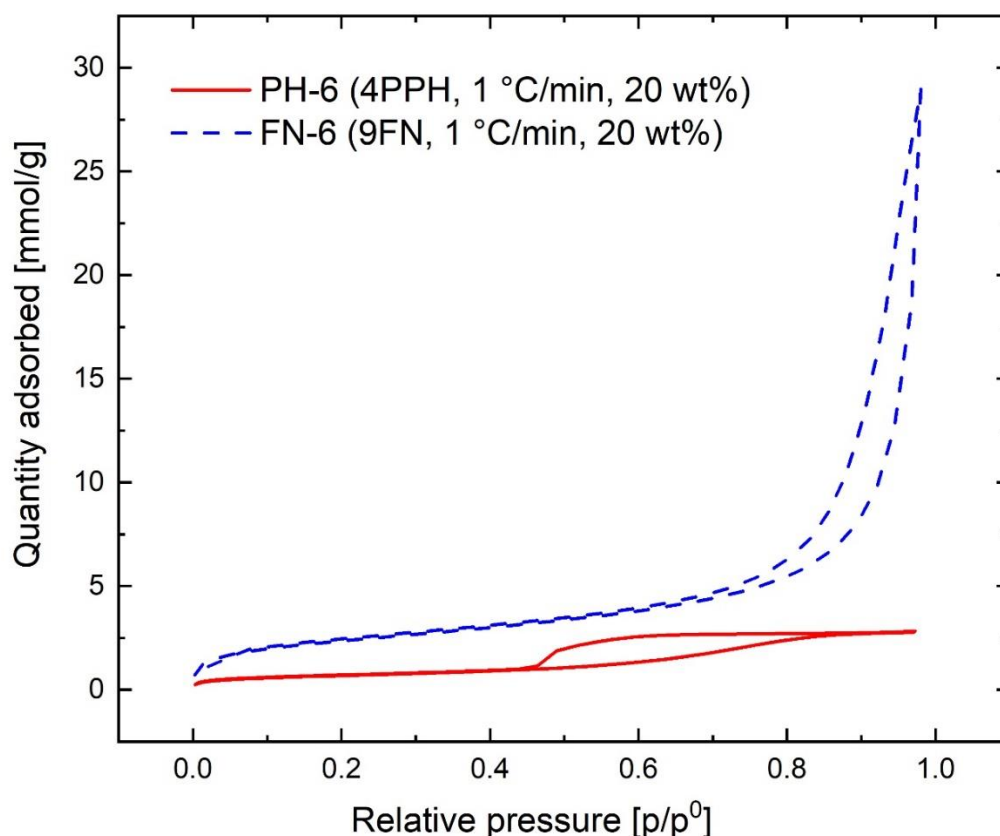


Fig.6. Characteristic nitrogen ad/desorption isotherms of porous PEKK PH-6 (red solid line - 4PPH, 1 °C/min, 20 wt%) and FN-6 (blue dash line - 9FN, 1 °C/min, 20 wt%). Individual nitrogen ad/desorption isotherms for the samples PH-6 and FN-6 could be found in SI Fig S2.

The specific surface areas for all PEKK foams produced from 4PPH decreased with increasing cooling rate from 87 to 29 m²/g (see **Table 2**) while those produced from PEKK in 9FN solutions were twice as large, around 180 m²/g but independent of the cooling rate used. The higher surface area of the PEKK foams produced from 9FN can be explained by the finer interconnected fibre network structure as compared to those produced from 4PPH solutions. The specific surface area of the PEKK foams produced from 4PPH likely decreased with increasing cooling rate because of pore collapse caused by the faster solvent crystallisation.

3.4. Mechanical properties of PEKK foams

For reasons related to the fragile nature and anisotropy of PEKK foams produced from 10 wt% PEKK solutions it was impossible to characterise their mechanical properties. Thus, it was only possible to measure mechanical properties of porous PEKKs produced from 20 wt% solutions at cooling rates of 0.5 and 1 °C/min. The compression strain-stress curves obtained are typical for porous polymers (see **Fig. S3**). The stress-strain curves contained the three regions commonly observed; the elastic deformation region at low applied strains followed by the plastic deformation plateau in which pore walls are being deformed and the densification region in which pore collapse takes place.

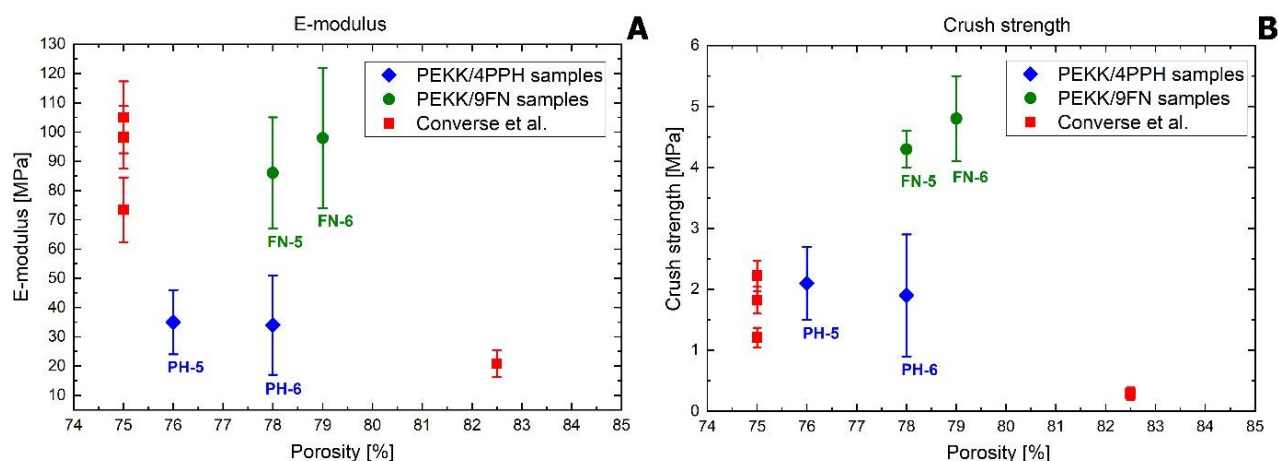


Fig. 7. Elastic modulus (A) and crush strength (B) of porous PEKKs produced from 20 wt% PEKK dissolved in 4PPH and 9FN using cooling rates $\beta = 0.5$ and 1 °C/min as function of porosity in order to compare our data with those reported by Converse et al.[15].

Both samples obtained from PEKK in 4PPH solution have E-moduli ranging between 30 to 40 MPa and crush strength around 2 MPa. The low elastic moduli were likely due to the macro- and microscale anisotropy and irregular pore morphology (**Fig. 3**). However, porous PEKK samples obtained from PEKK in 9FN solutions had much better mechanical properties compared to the PEKK foams made from 4PPH solutions (**SI, Table S1**). The much higher elastic moduli and crush

strengths of the PEKK foams made from 9FN was caused by the much more homogenous interconnected fibre-network structure in comparison with the anisotropic fibre-like structure of the foams made from 4PPH. Converse et al. [15] were the only other authors reporting mechanical properties of high porosity PEKK foams. However, their foams were produced by particle leaching from compression moulded PEKK composites. Despite a higher porosity of our PEKK foams produced from 20 wt% 9FN solutions the modulus of our foams was comparable but the crush strength exceeded their reported values, which could be due to the change in pore morphology or in degree of crystallinity of PEKK crystallised from the melt or solution.

3.5. Thermal properties of porous PEKK

For semi-crystalline polymers crystallinity is a crucial parameter, which affects their thermo-mechanical properties, solvent resistance and processability. In general, completely amorphous PEKK compared to its same semi-crystalline counterpart has much lower mechanical properties. Compact crystalline packaging leads to a denser and more thermo-mechanically stable structure. Typically, PEKK has a degree of crystallinity ranging from 20 to 40% [3, 4, 26]. The degree of crystallinity of PEKK crystallised from 4PPH solution were at the high end of those reported for melt crystallised PEKK while those produced from 9FN solutions are even slightly higher. PEKK recrystallised from the melt has degrees of crystallinity falling into the literature range.

Table 3. Glass transition temperature (T_g) and degree of crystallinity (X_{DSC}) of porous PEKK obtained by standard DSC.

	1st heating run	1st cooling run		2nd heating run	
Sample name	X_{DSC} [%]	X_{DSC} [%]	T_g [°C]	X_{DSC} [%]	T_g [°C]
PH-1	40 ± 3	36 ± 1	154 ± 2	34 ± 3	159 ± 1
PH-2	42 ± 1	35 ± 2	153 ± 1	34 ± 3	157 ± 2
PH-3	43 ± 3	34 ± 3	156 ± 1	35 ± 4	160 ± 2
PH-4	40 ± 2	34 ± 1	156 ± 1	36 ± 3	160 ± 1
PH-5	44 ± 1	35 ± 1	152 ± 1	35 ± 2	156 ± 2
PH-6	44 ± 2	36 ± 1	153 ± 2	36 ± 1	157 ± 1
PH-7	44 ± 5	33 ± 1	154 ± 1	34 ± 2	159 ± 1
PH-8	40 ± 1	35 ± 2	153 ± 2	34 ± 1	157 ± 1
FN-1	49 ± 4	27 ± 1	155 ± 2	27 ± 1	158 ± 1
FN-2	48 ± 2	27 ± 1	154 ± 2	27 ± 2	159 ± 2
FN-3	48 ± 1	27 ± 1	155 ± 1	27 ± 1	158 ± 1
FN-4	45 ± 4	26 ± 1	155 ± 1	26 ± 2	160 ± 1
FN-5	45 ± 1	27 ± 1	157 ± 2	26 ± 1	160 ± 1
FN-6	47 ± 4	27 ± 1	155 ± 1	27 ± 1	159 ± 1
FN-7	44 ± 2	26 ± 1	156 ± 1	28 ± 2	159 ± 2
FN-8	45 ± 3	27 ± 1	154 ± 1	27 ± 2	159 ± 1

Only little or no recrystallisation, depending on the sample used, was observed during the first heating run with heating rates as low as 500 K/s. To create fully amorphous samples a cooling rate of 10 K/s was sufficient and in heating curves no endothermic peaks were observed. The degree of crystallinity of the as produced PEKK foams from the measured melting enthalpies ΔH_f .

Table 4. Degree of crystallinity (X_{FDSC}) data obtained by Flash-DSC.

Sample	X_{FDSC} , [%]	Sample Mass [ng] (determined using $\Delta\varphi_\theta$)
PH-1	43	120.1
PH-2	35	624.0
PH-3	28	238.4
PH-5	39	697.9
PH-7	30	624.0
FN-1	42	440.5
FN-3	35	309.5
FN-5	32	178.5
FN-7	30	315.7
FN-8	24	440.5

The degree of crystallinity determined by FDSC ranges from 0.24 to 0.43 confirming the observed crystallinities derived from standard DSC (**Table 3**) for most samples. For the base material a crystallinity of 0.3 using standard DSC and FDSC. Because FDSC allows to prevent dynamic recrystallization during heating it allows to portray the crystallinity of the as produced state independently of such effects. The samples, for which the E-modulus was measured, show a lower crystallinity in FDSC than in conventional DSC. These differences may result from the different measuring method of the FDSC as the thermal contact of the very porous samples may be bad during the first heating run. Especially for samples PH-3 and PH-7, the fragile and highly porous nature of the PEKK foam may have an impact leading to poor thermal contact with the FDSC-chip.

The mechanical strength of PEKK foam samples may be positively influenced by high crystallinities. However, there is no necessity that a high crystallinity results in a much higher E-modulus as also the microstructure of the foam plays an important role [3]. Crumbling can be excluded for samples FN-5, FN-7 and FN-8, leading to the conclusion that those samples are more amorphous than the data from standard DSC might suggest. Hence it can be concluded that enhanced stiffness is mainly associated with the foam and fibre network structure and less with the inherent crystallinity in the present work.

4. Conclusion

We demonstrated that high porosity bulk PEKK foams can be produced using TIPS from PEKK in 4-phenylphenol or 9-fluorenone solutions. The porosity of the PEKK foams can be controlled using the polymer concentration. The type of polymer solvent demixing depended on the polymer concentration and type of solvent used; 9FN has a much lower melting temperature as compared to 4PPH and thus polymer-solvent demixing always occurred prior to solvent crystallisation, which influenced the pore structure. PEKK foams produced from 4PPH had an anisotropic fibre structure while those produced from 9FN had an interconnected nanofibre network structure. Unfortunately, the foams produced from 10 wt% PEKK in 9FN were not sufficiently mechanically robust to withstand the drying procedure during which they shrunk massively. PEKK foams with porosities ranging from 76-79% had elastic moduli ranging from 34 to 98 and crush strength ranging from 1.9 to 4.8 MPa. The PEKK foams produced from 9FN outperformed those made from 4PPH, which is likely due to their different pore morphologies. The degree of crystallinity of PEKK crystallised from solutions exceeded those obtained for melt crystallised PEKK.

Acknowledgements

We greatly acknowledge funding from the Austrian Research Council FWF through the grant I1800. The authors also gratefully acknowledge the help of Lisa Panzenboeck (UniVie, A), Manon Goubet and Alice Charton (both Ecole des Mines d'Alès, F) for their help in preparing and analysing samples. We also thank the reviewers for their helpful feedback, which helped to improve our manuscript.

References:

1. Attwood, T.E., P.C. Dawson, J.L. Freeman, L.R.J. Hoy, J.B. Rose, and P.A. Staniland, *Synthesis and properties of polyaryletherketones*. Polymer, 1981. **22**(8): p. 1096-1103.
2. Krishnaswamy, R.K. and D.S. Kalika, *Glass transition characteristics of poly(aryl ether ketone ketone) and its copolymers*. Polymer, 1996. **37**(10): p. 1915-1923.
3. Quiroga Cortés, L., N. Caussé, E. Dantras, A. Lonjon, and C. Lacabanne, *Morphology and dynamical mechanical properties of poly ether ketone ketone (PEKK) with meta phenyl links*. Journal of Applied Polymer Science, 2016. **133**(19): p. 43396.
4. Ho, R.-M., P. Honigfort, H.-M. Lin, S.Z.D. Cheng, B.S. Hsiao, and K.H. Gardner, *Crystal morphological investigation in thin films of poly(aryl ether ketone ketone) having a meta-linkage*. Polymer, 1997. **38**(20): p. 5051-5058.
5. Tadini, P., N. Grange, K. Chetehouna, N. Gascoin, S. Senave, and I. Reynaud, *Thermal degradation analysis of innovative PEKK-based carbon composites for high-temperature aeronautical components*. Aerospace Science and Technology, 2017. **65**: p. 106-116.
6. Nassir, N., R.S. Birch, W.J. Cantwell, Q.Y. Wang, L.Q. Liu, and Z.W. Guan, *The perforation resistance of glass fibre reinforced PEKK composites*. Polymer Testing, 2018. **72**: p. 423-431.

7. Cortes, L.Q., A. Lonjon, E. Dantras, and C. Lacabanne, *High-performance thermoplastic composites poly(ether ketone ketone)/silver nanowires: Morphological, mechanical and electrical properties*. Journal of Non-Crystalline Solids, 2014. **391**: p. 106-111.
8. Converse, G.L., T.L. Conrad, C.H. Merrill, and R.K. Roeder, *Hydroxyapatite whisker-reinforced polyetherketoneketone bone ingrowth scaffolds*. Acta Biomater, 2010. **6**(3): p. 856-63.
9. White, K.L., L. Jin, N. Ferrer, M.H. Wong, T. Bremner, and H.J. Sue, *Rheological and thermal behaviors of commercial poly(aryletherketone)s*. Polymer Engineering and Science, 2013. **53**(3): p. 651-661.
10. Ashby, M.F., *The properties of foams and lattices*. Philos Trans A Math Phys Eng Sci, 2006. **364**(1838): p. 15-30.
11. Verdejo, R., P. Werner, J. Sandler, V. Altstädt, and M.S.P. Shaffer, *Morphology and properties of injection-moulded carbon-nanofibre poly(etheretherketone) foams*. Journal of Materials Science, 2009. **44**(6): p. 1427-1434.
12. Siddiq, A.R. and A.R. Kennedy, *Porous poly-ether ether ketone (PEEK) manufactured by a novel powder route using near-spherical salt bead porogens: characterisation and mechanical properties*. Mater Sci Eng C Mater Biol Appl, 2015. **47**: p. 180-8.
13. Akartuna, I., E. Tervoort, J.C.H. Wong, A.R. Studart, and L.J. Gauckler, *Macroporous polymers from particle-stabilized emulsions*. Polymer, 2009. **50**(15): p. 3645-3651.
14. Sonnenschein, M.F., *Hollow fiber microfiltration membranes from poly(ether ether ketone) (PEEK)*. Journal of Applied Polymer Science, 1999. **72**(2): p. 175-181.
15. Converse, G.L., T.L. Conrad, and R.K. Roeder, *Mechanical properties of hydroxyapatite whisker reinforced polyetherketoneketone composite scaffolds*. J Mech Behav Biomed Mater, 2009. **2**(6): p. 627-35.
16. Matsuyama, H., S. Berghmans, and D.R. Lloyd, *Formation of anisotropic membranes via thermally induced phase separation*. Polymer, 1999. **40**(9): p. 2289-2301.
17. van de Witte, P., P.J. Dijkstra, J.W.A. van den Berg, and J. Feijen, *Phase separation processes in polymer solutions in relation to membrane formation*. Journal of Membrane Science, 1996. **117**(1-2): p. 1-31.
18. Lloyd, D.R., K.E. Kinzer, and H.S. Tseng, *Microporous membrane formation via thermally induced phase separation. I. Solid-liquid phase separation*. Journal of Membrane Science, 1990. **52**(3): p. 239-261.
19. Kim, J.F., J.H. Kim, Y.M. Lee, and E. Drioli, *Thermally induced phase separation and electrospinning methods for emerging membrane applications: A review*. AIChE Journal, 2016. **62**(2): p. 461-490.
20. Önder, Ö.C., E. Yilgör, and I. Yilgör, *Fabrication of rigid poly(lactic acid) foams via thermally induced phase separation*. Polymer, 2016. **107**: p. 240-248.
21. Rusakov, D., A. Menner, and A. Bismarck, *High-Performance Polymer Foams by Thermally Induced Phase Separation*. Macromol Rapid Commun, 2020. **41**(11): p. e2000110.
22. Rusakov, D., A. Menner, F. Spieckermann, H. Wilhelm, and A. Bismarck, *Morphology and properties of foamed high crystallinity PEEK prepared by high temperature thermally induced phase separation*. Journal of Applied Polymer Science. **139**(1): p. 51423.
23. Goh, Y.Q. and C.P. Ooi, *Fabrication and characterization of porous poly(L-lactide) scaffolds using solid-liquid phase separation*. J Mater Sci Mater Med, 2008. **19**(6): p. 2445-52.
24. Yang, F., X. Qu, W. Cui, J. Bei, F. Yu, S. Lu, and S. Wang, *Manufacturing and morphology structure of polylactide-type microtubules orientation-structured scaffolds*. Biomaterials, 2006. **27**(28): p. 4923-33.
25. Kalika, D.S., D.G. Gibson, D.J. Quiram, and R.A. Register, *Relationship between morphology and glass transition temperature in solvent-crystallized poly(aryl ether ketones)*. Journal of Polymer Science Part B: Polymer Physics, 1998. **36**(1): p. 65-73.
26. Gardner, K.H., B.S. Hsiao, R.R. Matheson, and B.A. Wood, *Structure, crystallization and morphology of poly (aryl ether ketone ketone)*. Polymer, 1992. **33**(12): p. 2483-2495.
27. Coulson, M., L. Quiroga Cortés, E. Dantras, A. Lonjon, and C. Lacabanne, *Dynamic rheological behavior of poly(ether ketone ketone) from solid state to melt state*. Journal of Applied Polymer Science, 2018. **135**(27): p. 46456.

28. Ma, P.X. and R. Zhang, *Microtubular architecture of biodegradable polymer scaffolds*. Journal of Biomedical Materials Research, 2001. **56**(4): p. 469-477.
29. ALothman, Z.A., *A Review: Fundamental Aspects of Silicate Mesoporous Materials*. Materials, 2012. **5**(12): p. 2874-2902.
30. Thommes, M., *Physical Adsorption Characterization of Nanoporous Materials*. Chemie Ingenieur Technik, 2010. **82**(7): p. 1059-1073.

High porosity poly (ether ketone ketone): Influence of solvents on foam properties

Dmitrii Rusakov¹, Innozenz Steffny², Florian Spieckermann³, Angelika Menner¹ and Alexander Bismarck^{1,4}

¹ Polymer and Composite Engineering (PaCE) Group, Institute of Materials Chemistry, Faculty of Chemistry, University of Vienna, Währinger Str. 42, 1090 Vienna, Austria.

² Erich Schmid Institute of Materials Science of the Austrian Academy of Sciences, Jahnstrasse 12/I, 8700 Leoben, Austria.

³ Chair of Materials Physics, Department of Materials Science, Montanuniversität Leoben, Jahnstrasse 12/I, 8700 Leoben, Austria.

⁴ Department of Chemical Engineering, Imperial College London, South Kensington Campus, London, SW7 2AZ, UK.

Supporting Information

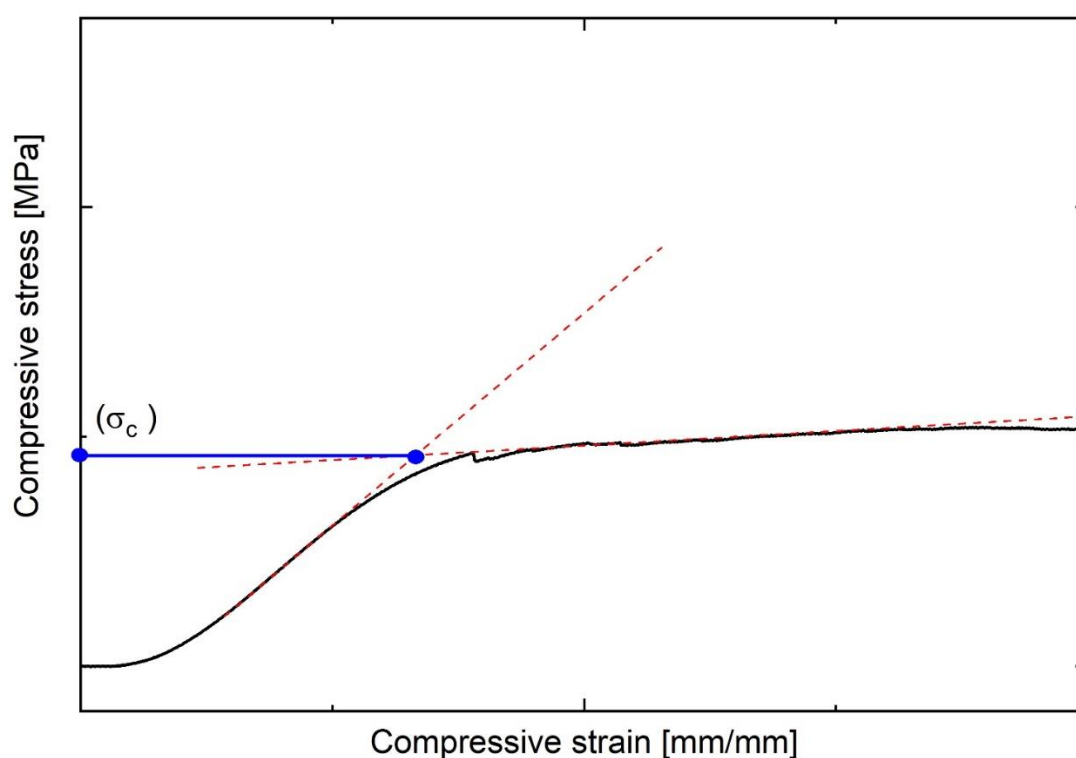


Fig. S1. Illustration of the determination of crush strength (σ_c) porous PEKK samples

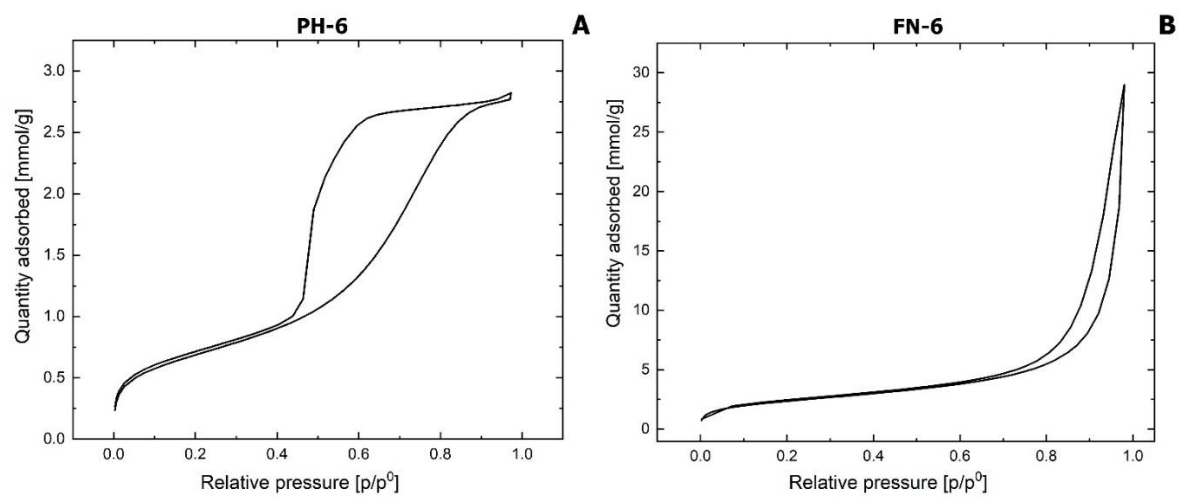


Fig. S2. Characteristic nitrogen ad/desorption isotherms of porous PEKK PH-6 (**A** - 4PPH, 1°C/min, 20 wt%) and FN-6 (**B** - 9FN, 1°C/min, 20 wt%).

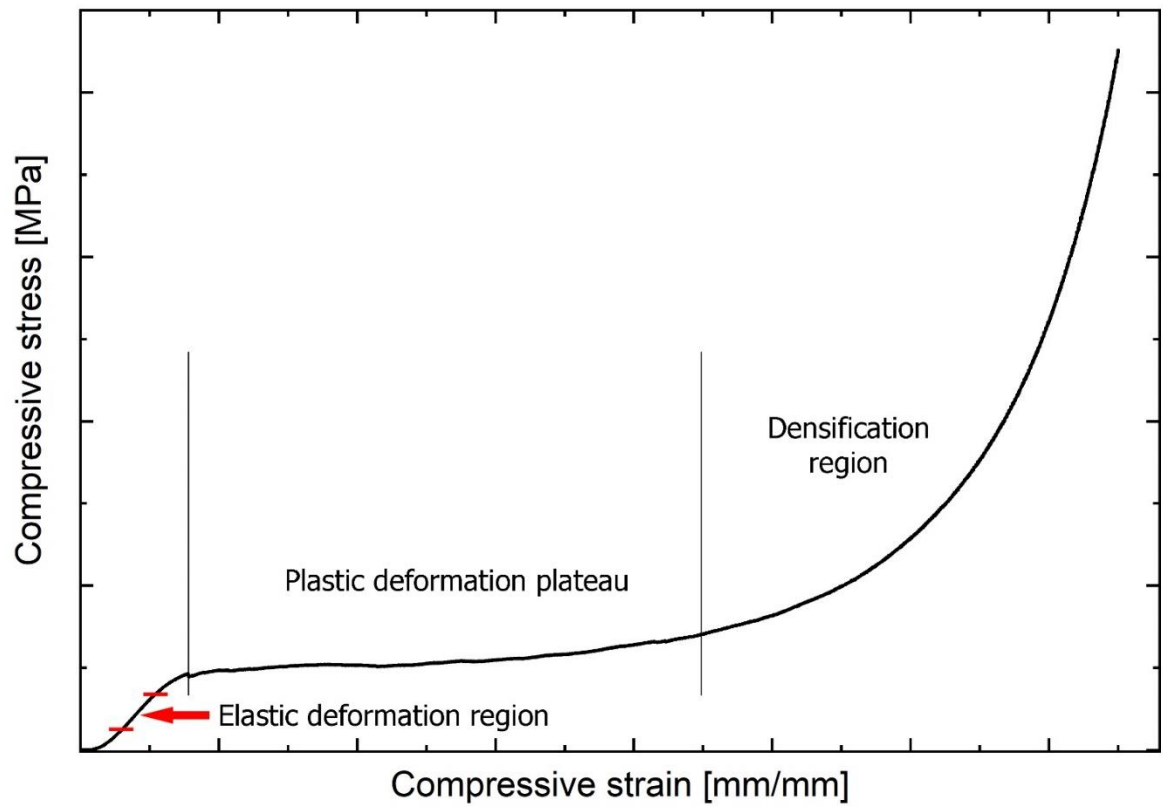


Fig. S3. Typical compression stress-strain curve of porous PEKK produced from 20 wt.% PEKK in 4PPH or 9FN solution.

Table S1. *Mechanical properties of the porous PEKK samples obtained from 20 wt% PEKK concentrations in 4PPH or 9FN as solvents and cooling rates 0.5 and 1 °C/min.*

Sample name	Porosity [%]	E-moduli [MPa]	Crush strength [MPa]
PH-5	76 ± 5	35 ± 11	2.1 ± 0.6
PH-6	78 ± 4	34 ± 17	1.9 ± 1
FN-5	78 ± 3	86 ± 19	4.3 ± 0.3
FN-6	79 ± 4	98 ± 24	4.8 ± 0.7